RL-TR-96-236
Final Technical Report
February 1997

C-BAND RADAR TESTING OF THE MULTICHANNEL ADAPTIVE OPTICAL PROCESSOR

Dynetics, Inc.

R.J. Berinato, D. Elmore, P.S. Julino, and M.C. Budge, Jr.

APPROVED FOR PUBLIC RELEASE; DISTRIBUTION UNLIMITED.

Rome Laboratory
Air Force Materiel Command
Rome, New York

This report has been reviewed by the Rome Laboratory Public Affairs Office (PA) and is releasable to the National Technical Information Service (NTIS). At NTIS it will be releasable to the general public, including foreign nations.

RL-TR-96-236 has been reviewed and is approved for publication.

APPROVED:

JEFFREY LUTSKO, Lt, USAF
Project Engineer

FOR THE COMMANDER:

DONALD W. HANSON, Director
Surveillance & Photonics Directorate

If your address has changed or if you wish to be removed from the Rome Laboratory mailing list, or if the addressee is no longer employed by your organization, please notify RL/OCPC, 25 Electronic Pky, Rome, NY 13441-4514. This will assist us in maintaining a current mailing list.

Do not return copies of this report unless contractual obligations or notices on a specific document require that it be returned.

REPORT DOCUMENTATION PAGE

Form Approved
OMB No. 0704-0188

1. AGENCY USE ONLY *(Leave blank)*	2. REPORT DATE	3. REPORT TYPE AND DATES COVERED
	February 1997	**FINAL, May 95 - May 96**

4. TITLE AND SUBTITLE
C-BAND RADAR TESTING OF THE MULTICHANNEL ADAPTIVE OPTICAL PROCESSOR

5. FUNDING NUMBERS
C - F30602-95-C-0077
PE - 62702F
PR - 4600
TA - P2
WU - PT

6. AUTHOR(S)
R.J. Berinato, D. Elmore, P.S. Julino, M.C. Budge, Jr.

7. PERFORMING ORGANIZATION NAME(S) AND ADDRESS(ES)
Dynetics, Inc.
P.O. Drawer B
Huntsville AL 35814-5050

8. PERFORMING ORGANIZATION REPORT NUMBER
N/A

9. SPONSORING / MONITORING AGENCY NAME(S) AND ADDRESS(ES)
Rome Laboratory/OCPC
25 Electronic Pky
Rome NY 13441-4515

10. SPONSORING / MONITORING AGENCY REPORT NUMBER
RL-TR-96-236

11. SUPPLEMENTARY NOTES
Rome Laboratory Project Engineer: Lt. Jeffrey Lutsko OCPC, (315) 330-7683

12a. DISTRIBUTION AVAILABILITY STATEMENT
Approved for Public Release; Distribution Unlimited

12b. DISTRIBUTION CODE

13. ABSTRACT *(Maximum 200 words)*

The final report documents the continued design, hardware implementation, and testing of an acousto-optic (AO) multichannel adaptive optical processor (MADOP) for application to the cancellation of multipath jamming interference in advanced surveillance applications. The work described in this report was performed for the Photonics Center at Rome Laboratory (RL) and represents the fourth year of Dynetics support on this project. The key program objective of this effort was to enhance the performance of the MADOP hardware as demonstrated with the C-band radar testbed at the RL Surveillance and Photonics Directorate. The successful integration of the MADOP with the C-band radar testbed was achieved, and testing of jammer cancellation in a number of configurations was performed, including multipath scenarios. Performance results included consistent signal to jammer (S/J) improvement of 30 dB or greater for narrowband tone jammers and 15 to 20 dB for wideband (8-MHz) noise jammers. Results for multipath were on the order of 10-dB S/J improvement for wideband noise jamming with approximately a 110-ns multipath delay and a 1.13° angular separation between the direct and multipath jamming signals.

14. SUBJECT TERMS
adaptive processing, acousto-optics, optical signal processing

15. NUMBER OF PAGES
138

16. PRICE CODE

17. SECURITY CLASSIFICATION OF REPORT	18. SECURITY CLASSIFICATION OF THIS PAGE	19. SECURITY CLASSIFICATION OF ABSTRACT	20. LIMITATION OF ABSTRACT
UNCLASSIFIED	**UNCLASSIFIED**	**UNCLASSIFIED**	**UNLIMITED**

NSN 7540-01-280-5500

Standard Form 298 (Rev. 2-89)
Prescribed by ANSI Std. Z39-18
298-102

ABSTRACT

This final report documents the continued design, hardware implementation, and testing of an acousto-optic (AO) multichannel adaptive optical processor (MADOP) for application to the cancellation of multipath jamming interference in advanced surveillance applications. The work described in this report was performed for the Photonics Center at Rome Laboratory (RL) and represents the fourth year of Dynetics' support on this project. The key program objective of this effort was to enhance the performance of the MADOP hardware as demonstrated with the C-band radar testbed at the RL Surveillance and Photonics Directorate. The successful integration of the MADOP with the C-band radar testbed was achieved, and testing of jammer cancellation in a number of configurations was performed, including multipath scenarios. Performance results included consistent signal-to-jammer (S/J) improvement of 30 dB or greater for narrowband tone jammers and 15 to 20 dB for wideband (8-MHz) noise jammers. Results for multipath were on the order of 10-dB S/J improvement for wideband noise jamming with approximately a 110-ns multipath delay and a 1.13° angular separation between the direct and multipath jamming signals.

TABLE OF CONTENTS

LIST OF ILLUSTRATIONS

LIST OF ILLUSTRATIONS (Continued)

LIST OF ILLUSTRATIONS (Concluded)

LIST OF TABLES

LIST OF ABBREVIATIONS

2-D	two-dimensional
A/D	analog-to-digital
AFG	arbitrary function generator
AO	acousto-optic
AOSLM	acousto-optic spatial light modulator
AOTDL	acousto-optic tapped delay line
BAW	bulk acoustic wave
BPF	bandpass filter
BW	bandwidth
CCD	charged coupled device
CCPD	charged coupled photo detector
CW	continuous wave
dc	direct current
DMD	deformable mirror devices
ESE	Expert in Science and Engineering
FFT	fast Fourier transform
FIR	finite impulse response
GPIB	general-purpose interface bus
I&Q	in-phase and quadrature
IF	intermediate frequency
IFFT	inverse fast Fourier transform
IIR	infinite impulse response
LHC	left-hand circular
LMS	least mean squared
LO	local oscillator
LPF	low-pass filter
MADOP	multichannel adaptive optical processor
MSE	mean-squared-error
PC	personal computer
PRI	pulse repetition interval
RF	radio frequency
RHC	right-hand circular
RL	Rome Laboratory
RMS	root mean square
S/J	signal-to-jammer
USAF	U.S. Air Force
VCSEL	vertical cavity surface emitting laser
VSWR	voltage standing wave ratio

Units of Measure

dB	decibels
dBi	decibels above an isotropic radiator
dBm	decibels above, or referred to, one milliwatt
°, deg	degrees
ft	feet
GHz	gigahertz
in.	inches
kHz	kilohertz

km	kilometers
kW	kilowatts
MB	megabytes
MHz	megahertz
mm	millimeters
ms	milliseconds
mW	milliwatts
m/s	meters per second
μm	micrometers
μs	microseconds
μV	microvolts
μW	microwatts
nm	nanometers
ns	nanoseconds
Ω	ohms
pJ	picojoules
%	percent
s	seconds
V	volts
W	watts

1. INTRODUCTION

This final report documents the continued design, hardware implementation, and testing of an acousto-optic (AO) multichannel adaptive optical processor (MADOP) for application to the cancellation of multipath jamming interference in advanced surveillance applications. This Expert in Science and Engineering (ESE) effort is a continuation of an ongoing program within the Rome Laboratory (RL) Photonics Center (References 1 through 10). Approximately half of the Dynetics effort was performed onsite at RL, Griffiss Air Force Base, NY. This work was accomplished in conjunction with Photonics Center personnel Lt. M. Turbyfill, Lt. J. Lutsko, and E. Walge, and Surveillance Directorate personnel M. Rudd, D. Mokry, and P. Stone under the in-house Project 4600P107. All work described in this report was performed under ESE Contract F30602-95-C-0077 during the period of 15 May 1995 to 14 May 1996.

The U.S. Air Force (USAF) has a requirement to effectively operate surveillance radars in the presence of hostile jammers and other interference sources, including multipath. The signal environment of the future is becoming increasingly dense, including the appearance of more wideband emitters that add to the complexity of the problem. Meeting this requirement demands a capability to cancel this interference in order to improve target detectability and track performance. Optical signal processing technology offers a possible solution to this demanding signal cancellation problem. This advanced technology has been pursued within the RL Photonics Center to address such USAF problems. The MADOP system has been part of this technology development over the past 5 years and appears to offer an attractive solution to future USAF surveillance missions in the presence of complex interference environments.

The key program objective of this effort was the enhancement of the MADOP hardware in order to improve the integration and testing of the system with the C-band radar testbed at the RL Surveillance and Photonics Directorate. To meet this objective, three activities were pursued: 1) the enhancement of the electronic canceller circuit to attain greater notch depths, 2) the improvement of the AO correlator subsystem to achieve greater stability in the C-band radar laboratory, and 3) the testing of the MADOP in the C-band radar testbed, including multipath jamming tests. The enhancements to the electronic canceller circuit were achieved by removing attenuators and path length from the feedback loop and adding diode limiters at the front of the phase comparator component to keep the signal levels below the damage threshold. Two alternatives to the Mach-Zehnder configuration of the AO correlator were considered in this effort. An in-line system that employs one AO cell and a modulated laser diode was fabricated and tested during on-site support period two. In addition, during on-site support period three, the RL-developed almost-common path AO correlator that employs a dove prism between two AO cells was used in the C-band radar testing.

We believe that this architecture will offer the greatest long-term potential for an optical correlator solution. During on-site support periods one and three, significant testing occurred with the C-band radar testbed, culminating in the successful testing of the MADOP in a challenging multipath scenario.

The key program objective was met during this program by integrating the MADOP with the C-band radar testbed at the 80-MHz system intermediate frequency (IF) (over the 8-MHz testbed bandwidth) and testing the cancellation performance in several configurations using narrowband tone and wideband noise jammers. Performance results included consistent signal-to-jammer (S/J) improvement of 30 dB or greater for narrowband tone jammers and 15 to 20 dB for wideband (8-MHz) noise jammers. Results for multipath were on the order of 10-dB S/J improvement for wideband noise jamming with approximately a 110-ns multipath delay and a 1.13° angular separation between the direct and multipath jamming signals. This integration and multipath testing represents a significant milestone in the long-term development of the MADOP system.

This technical report is organized as follows. After this introduction, the adaptive cancellation algorithm implemented by the MADOP hardware is described in Section 2, with continued emphasis on some of the challenges to be faced with testing in more complex signal environments. This section is only slightly modified from an earlier report and is included to provide perspective on the test results that follow. Section 3 provides an overview of the MADOP hardware configuration and details the improvements made to both the optical and electronic subsystems. MADOP system testing with laboratory signals and with the C-band radar testbed are then addressed in Section 4, followed by conclusions and recommendations in Section 5.

2. MADOP ALGORITHM OVERVIEW

The MADOP has been designed to achieve time-domain cancellation of multiple wideband interferers. As designed, the system will be able to cancel four independent interference sources, with each source having up to a 10-MHz bandwidth. The initial implementation emphasizes two channels. The key advantage of the optical approach over current state-of-the-art digital and analog electronic implementations is the ability to cancel wideband interference by using multiple tap weights per channel. The fact that the canceller employs time-domain cancellation also allows considerable latitude in the separation between the main antenna and the auxiliary channel antennas. Furthermore, the ability to implement multiple tap weights in the time-domain canceller provides the potential for jammer cancellation in the presence of multipath in the main and auxiliary channels. The discussion below contains an overview of the MADOP and its implementation within a radar. Cancellation in the presence of multipath is also addressed.

2.1 PROBLEM DEFINITION

Figure 2-1 presents an illustrative summary of the scenario being addressed. In this figure, two independent interference sources, $n_1(t)$ and $n_2(t)$, with spectral content in the radar system passband, contaminate the directional main antenna target return, s(t), through the sidelobes. The multipath versions of the two interference sources also contribute a significant noise term to the main channel signal resulting in the reception of:

$$d(t) = s(t) + \sum_{n=1}^{P1} a_{1n} n_1(t-\tau_{1n}) + \sum_{m=1}^{Q1} a_{2m} n_2(t-\tau_{1n}) \qquad (2\text{-}1)$$

where a_{1n} and a_{2m} represent relative attenuations due to multipath losses together with antenna sidelobe gain relative to mainlobe gain, and τ_{1n} and τ_{2m} represent the signal delays. The direct-path interference is given for n = 1 and m = 1. It is assumed that the interference is on the order of, or much larger than, the target return, s(t), resulting in a low S/J ratio in the main antenna. The two auxiliary antennas receive the interference, but the target return entering these antennas is negligible because of the low main-channel S/J assumption. Thus, the two auxiliary antennas receive the signals:

$$N_1(t) = \sum_{n=1}^{P2} a_{1n} n_1(t-\tau_{1n}) + \sum_{m=1}^{Q2} a_{2m} n_2(t-\tau_{2m}),$$

$$N_2(t) = \sum_{n=1}^{P3} a_{1n} n_1(t-\tau_{1n}) + \sum_{m=1}^{Q3} a_{2m} n_2(t-\tau_{2m}) . \qquad (2\text{-}2)$$

In addition to these correlated noises, uncorrelated receiver noise is present at each antenna. In general, P1, P2, P3, Q1, Q2, and Q3 can be different.

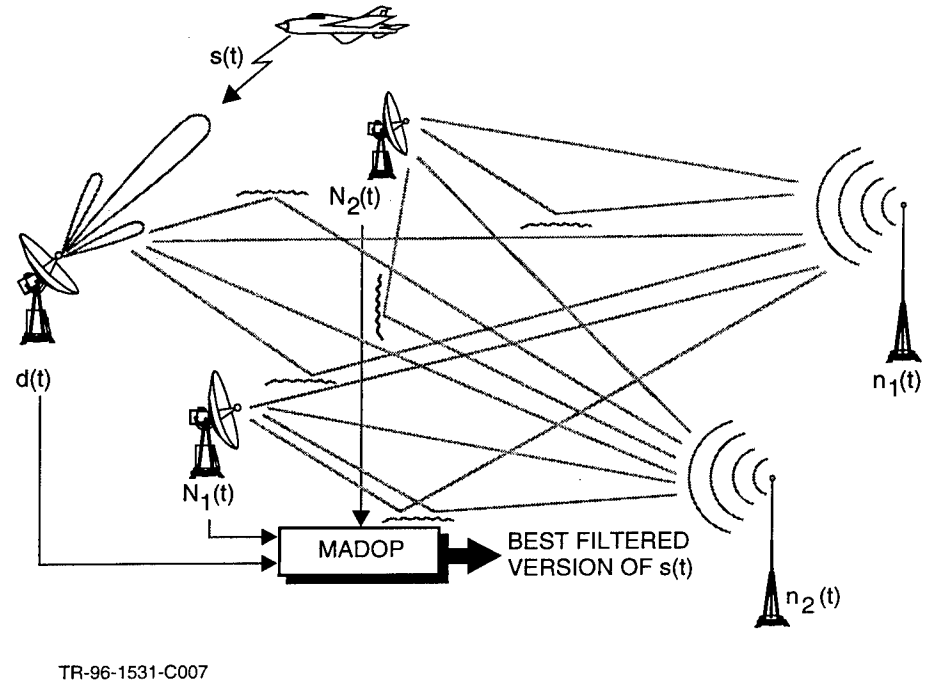

Figure 2-1. Two-Dimensional Operational Scenario for MADOP

Figure 2-2 shows a simplified block diagram of a typical surveillance radar that may benefit from the MADOP. This diagram is not intended to represent a specific radar system. The MADOP is shown in the radar IF after downconversion from the radio frequency (RF) carrier (3 or 10 GHz for example). The waveform generator provides the signal to be transmitted and also provides the matched filter to the signal processor to allow for pulse compression and pulse integration/Doppler filtering. The antenna system, whether phased array or dish, forms a beam (or multiple independent beams, as possible with a phased-array antenna) that illuminates the target in the presence of interference. The target reflection, contaminated by interference, is received in the main channel, while the interference is also received in auxiliary antenna channels (which can be portions of a single phased array). All signals are downconverted to the IF and input into the MADOP. The output of the MADOP is the desired signal with the interference suppressed. This signal then enters the coherent

pulse compression and Doppler filtering system, which is often implemented digitally following analog-to-digital (A/D) conversion of in-phase and quadrature (I&Q) channels. After this signal processing, the data processor performs such operations as target detection and tracking, beam scheduling, system control, and interface to the display.

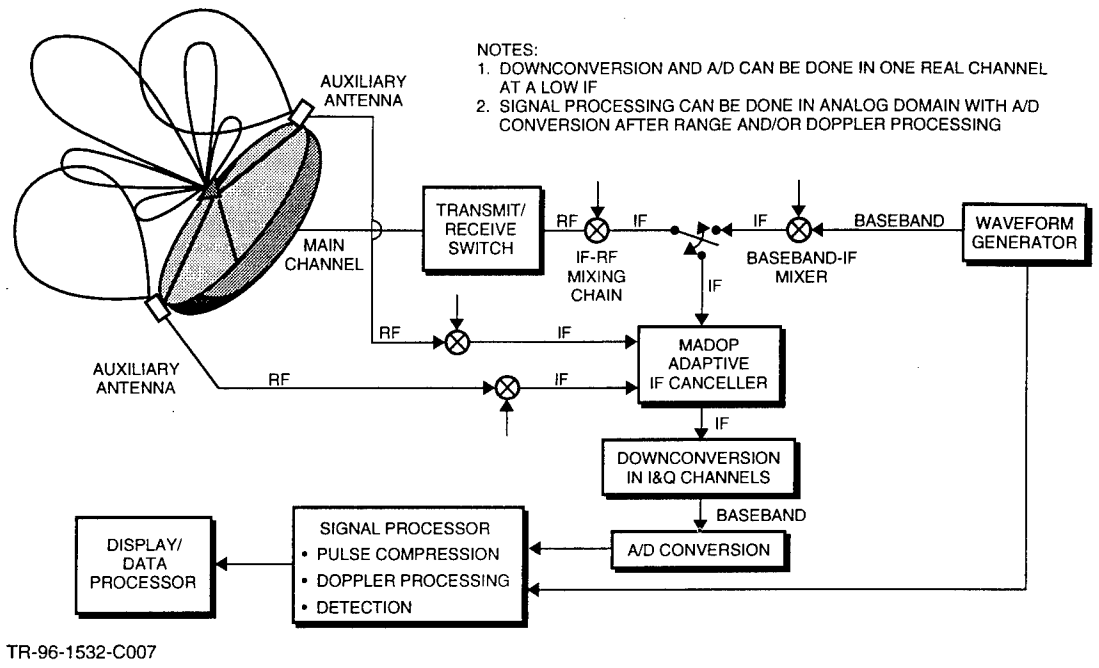

Figure 2-2. Surveillance Radar Simplified Schematic With Adaptive IF Processing

As stated above, the goal of the adaptive processor is to react to the interference environment in such a way that the main antenna interference is cancelled, resulting in a satisfactory S/J for further processing. The algorithm for achieving this objective is described below. The goals for this feasibility demonstration program, as coordinated with personnel in the Surveillance Technology Division of the Surveillance and Photonics Directorate (OCTS), are shown in ***Table 2-1***. It is recognized that, although the loop lock time (time to reach steady state) is critical in system applications (500 μs is desirable), the personal computer (PC) interface in the digital subsystem used in the current implementation makes practical loop lock times unachievable. The development of real-time, special-purpose digital interfaces will greatly increase system speed.

Table 2-1. Feasibility Demonstration Goals

System Bandwidth (MHz)	10
Number of Interference Sources	4 (initial demo will accommodate 2)
Maximum Multipath Delay (μs)	5 (corresponds to 1.5-km differential path)
Interference Cancellation Ratio (dB)	30
Number of Multipath Delays	>4
Loop Lock Time (ms)	5
Processor IF (MHz)	80

2.2 ADAPTIVE CANCELLATION ALGORITHM

Before considering the detailed math behind the adaptive cancellation algorithm, it is useful to consider the similarity between the MADOP and a traditional radar sidelobe canceller. The MADOP can be viewed as consisting of two subsystems, namely the long delay window AO tapped delay line (AOTDL) filter (driven by the AO correlator output) and the electronic canceller. The electronic canceller serves to lock the phase of the output from the AOTDL to the phase of the main-channel return. When these phases are matched, subtraction of the jamming signal can be performed. This is the function of a sidelobe canceller, which assumes no delay of the envelope of the jamming signal but rather just a phase shift of the carrier. The power of the MADOP system resides in its additional capability to estimate the delay of multipath components in the received jamming signal and to use these estimates to form an estimate that has an envelope that may in fact be quite different from the auxiliary channel output. The challenges of this cancellation problem in the presence of multipath is the motivation for continued pursuit of this processor.

The standard multidimensional tapped delay line implementation of the least mean squared (LMS) algorithm is shown in ***Figure 2-3***. Note that the LMS algorithm is based on steepest descent techniques, where the weight function is updated in the direction opposite the gradient at the current weight value. This will cause the weights to move in such a way as to reduce the mean-squared-error (MSE) along the steepest gradient. The input signals from the auxiliary antennas $N_i(t)$ are convolved with the weight functions $w_i(t;\tau)$, which are functions of time, t, and delay, τ, to yield an estimate $d_{est}(t)$ of the main channel signal:

$$d_{est}(t) = \sum_{i=1}^{P} \int_{\frac{-T_a}{2}}^{\frac{T_a}{2}} w_i(t;\tau) N_i(t-\tau) d\tau \qquad (2\text{-}3)$$

where P is the number of auxiliary antennas and T_a is the length of each tapped delay line. This estimate is subtracted from the main channel signal d(t) to form an error signal e(t). The weights are then updated according to the degree of correlation between this error and the auxiliary channel inputs. The i^{th} weight function is represented mathematically as:

$$w_i(t;\tau) = w_i(0;\tau) + \int_0^t \alpha(t)e(t)\, N_i^*(t-\tau)dt \qquad (2\text{-}4)$$

where $\alpha(t)$ is a time-varying (in general) acceleration parameter. As this process continues in time, the adaptively changing weights converge to a steady-state solution (if the signal environment is stationary). This cancels the interference in the main channel, which equivalently yields the minimum MSE and maximum output S/J ratio.

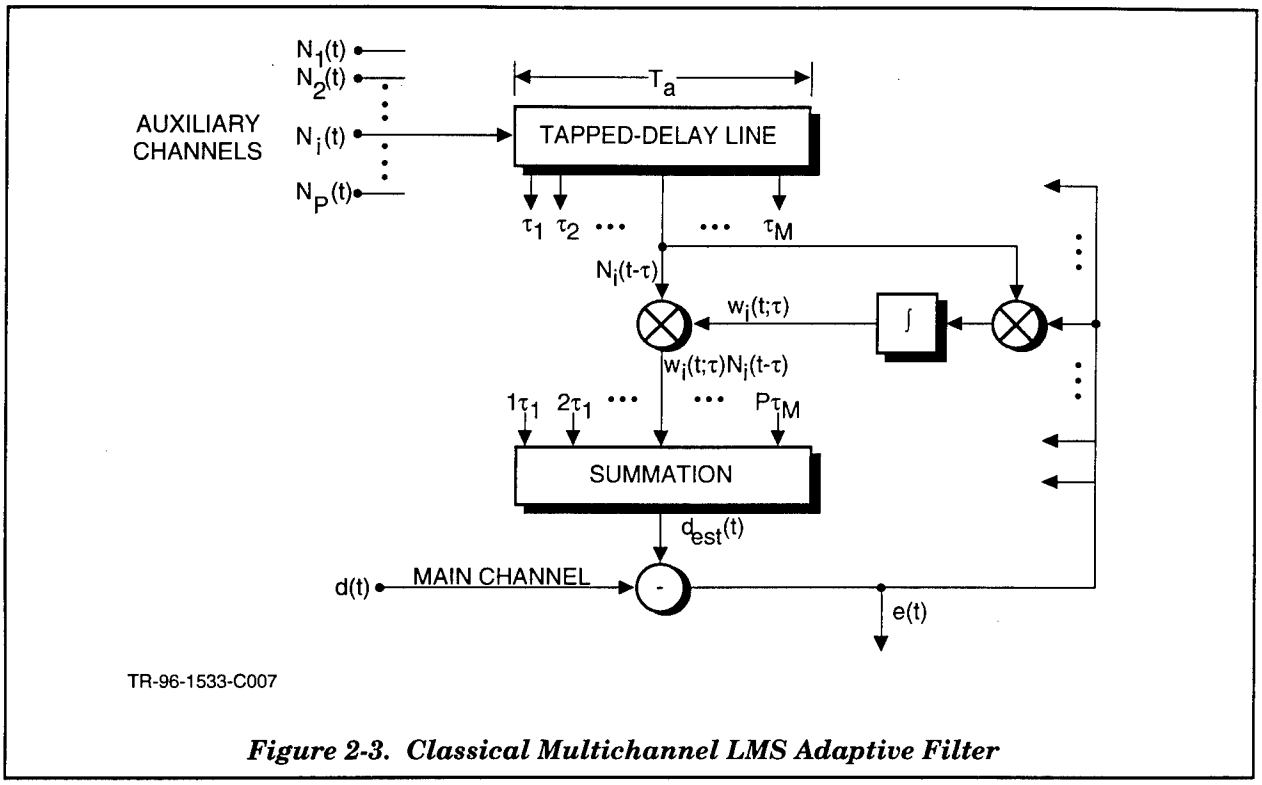

Figure 2-3. Classical Multichannel LMS Adaptive Filter

The classical LMS algorithm performs a weight update at each point in time. If a discrete algorithm is employed, the weight update is achieved at each time step, which must be at a frequency greater than twice the widest bandwidth to be processed. Thus, for 10-MHz bandwidth signals, the time step and weight update occur every 50 ns. ***Figure 2-3*** implies that taps must be positioned every

50 ns if discrete taps are employed. The integration shown in Equation 2-4 occurs over the entire observation period, resulting in a continuous weight update. In addition, as the weights are updated, the error continues to be reduced, which then feeds back into the weight calculation integration.

In the current implementation of the MADOP, the weight computations are performed by a digital computer, which means that the weights cannot be updated at the rate indicated above. Because of this, an alternative to the classical LMS algorithm is currently implemented in the MADOP. For our system, the correlation is performed, in the AO time-integrating correlator, over a longer window of time (T) during which the weight functions do not change. This time window has typically been greater than 2 ms. After the correlation has been obtained, the results are used to update the weight functions, a process that is performed in the digital computer and takes an additional increment of time (t_u). In the current implementation of the MADOP, t_u is approximately 1 s.

Because of the longer correlation time, the weights computed in a single step are very close to the final weights that would result after several iterations of the classical LMS algorithm. As a result, it is no longer necessary to use the error signal (e(t) in ***Figure 2-3***) to update the weights. Instead, the weights can be computed by directly correlating the main and auxiliary channel signals. This difference is similar to the two adaptive beamforming approaches: 1) iterative schemes that converge to the desired result and 2) direct matrix inversion of the correlation/covariance matrix that is formed through integration of the received signals over some relatively long time window. This longer integration is the basis for what has been implemented in the current MADOP system.

The windowed algorithm described above is similar to the block adaptive filtering approach that has been increasingly researched in the digital adaptive filtering community (References 11 through 13). The primary motivation for this interest is the compatibility of block routines with fast convolution algorithms that employ fast Fourier transforms (FFTs). In these adaptive filters, the weights are updated based on a window of data, rather than at each time step. An interesting result related to these block routines is that the convergence generally proceeds much faster than for the classical LMS routine due to the reduction in the gradient estimate noise. Also, highly correlated input data, resulting in a high correlation matrix condition number and generally slow convergence, are better processed through block techniques.

2.3 MULTIPATH CONSIDERATIONS

The cancellation of interference containing multipath returns has been very difficult for conventional sidelobe cancellers because the cancellation is based on adjusting the amplitude and phase of the auxiliary channel signal and subtracting it from the main channel signal. Such an

approach does not allow a means of accounting for delays caused by the multipath. Digital approaches have been implemented with some success.

In contrast to conventional sidelobe cancellers, the MADOP effects cancellation by delaying and adjusting the amplitude of the auxiliary channel signal and subtracting it from the main channel signal. Furthermore, the MADOP can apply multiple delays and amplitude weights to cancel the multiple returns caused by multipath.

As an example, let the signal in the auxiliary channel be:

$$N_1(t) = bn(t) \tag{2-5}$$

where n(t) is the interference signal and b accounts for the auxiliary channel antenna pattern and receiver characteristics. The range delay of n(t) and its delay through the receiver are set to zero without loss of generality for this analysis.

Let the main channel signal be given by:

$$d(t) = s(t) + a_d n(t-\tau_d) + a_m n(t-\tau_m) \tag{2-6}$$

where s(t) is the desired signal. The two interference terms represent the direct path (d subscript) and the multipath (m subscript) components, a_i is the relative amplitude, and τ_i is the delay relative to the auxiliary channel interference signal.

For these main and auxiliary channel signals, the AOTDL of the MADOP would ideally be configured (by the weight computation algorithm) to have two delays with weights of a_d/b and a_m/b. The result would be a cancellation signal of:

$$d_{est}(t) = a_d/bN_1(t-\tau_d) + a_m/bN_1(t-\tau_m) = a_d n(t-\tau_d) + a_m n(t-\tau_m)\,. \tag{2-7}$$

The resultant output of the MADOP would be:

$$e(t) = d(t) - d_{est}(t) = s(t)\,. \tag{2-8}$$

The key point above is the ability of the AOTDL to implement multiple time delays with multiple weights.

The above discussion was based on the premise that the main channel receives multipath returns, while the auxiliary channel receives only direct-path returns. A more realistic scenario involves the case where both the main and auxiliary channels receive multipath signals. In this case,

the ability to cancel the interference signal becomes more questionable. However, given the ability of the AOTDL of the MADOP to implement multiple delays and weights, it still may be possible to effect significant interference cancellation.

To discuss how the MADOP might be configured to handle multipath signals in the main and auxiliary channels, we consider the same problem in the sampled data domain and make use of z-transforms. In this context, let the auxiliary channel signal be:

$$N_1(k) = b_d n(k-l_d) + b_m n(k-l_m) \tag{2-9}$$

and the main channel signal be:

$$d(k) = s(k) + a_d n(k-k_d) + a_m n(k-k_m) = s(k) + N_{main}(k) . \tag{2-10}$$

The MADOP implements the equation

$$e(k) = d(k) - w(k) * N_1(k) \tag{2-11}$$

where w(k) represents the delay and weighting characteristics of the AOTDL and * denotes convolution.

Substituting for d(k) results in:

$$e(k) = s(k) + N_{main}(k) - w(k) * N_1(k) . \tag{2-12}$$

Ideally, we want e(k) = s(k), which leads to the requirement that:

$$N_{main}(k) - w(k) * N_1(k) = 0 . \tag{2-13}$$

The above says that we want to find w(k) such that the above equality is valid.

We can further examine the calculation of w(k) by transforming the above to the z-domain. Specifically, Equation 2-13 can be written in the z-domain as:

$$N_{main}(z) - W(z)N_1(z) = 0 \tag{2-14}$$

where $N_{main}(z)$, W(z), and $N_1(z)$ are the z-transforms of $N_{main}(k)$, w(k), and $N_1(k)$, respectively.

Hence, the AOTDL delay and weighting needed to effect interference cancellation can be obtained as:

$$W(z) = \frac{N_{main}(z)}{N_1(z)} \quad . \tag{2-15}$$

This is an interesting result but is of little practical value since it requires knowledge of $N_m(z)$ and $N_1(z)$. A more practical result can be obtained by multiplying Equation 2-14 by $N_1^*(1/z)$ to yield:

$$N_{main}(z)N_1^*(1/z) - W(z)N_1(z)N_1^*(1/z) = 0 \tag{2-16}$$

or

$$W(z) = \frac{N_{main}(z)N_1^*(1/z)}{N_1(z)N_1^*(1/z)} \quad . \tag{2-17}$$

The act of multiplying $N_{main}(z)$ and $N_1(z)$ by $N_1^*(1/z)$ represents a correlation of $N_{main}(k)$ and $N_1(k)$ with $N_1(k)$. The correlation of $N_{main}(k)$ with $N_1(k)$ is currently the operation performed by the AO time-integrating correlator of the MADOP. More specifically, the correlator performs the operation:

$$\begin{aligned} d(k) \otimes N_1(k) &= [s(k) + N_{main}(k)] \otimes N_1(k) \\ &= s(k) \otimes N_1(k) + N_{main}(k) \otimes N_1(k) \\ &\approx N_{main}(k) \otimes N_1(k) \quad . \end{aligned} \tag{2-18}$$

The assumption that $s(k) \otimes N_1(k) \approx 0$ is a basic assumption of the MADOP and is based on the fact that $s(k)$ and $N_1(k)$ are uncorrelated.

For the case where there is no multipath in the auxiliary channel and N(k) is wideband:

$$N_1(k) \otimes N_1(k) \approx b^2\delta(k) \tag{2-19}$$

and

$$N_1(z)N_1^*(1/z) = b^2 \quad . \tag{2-20}$$

With this, W(z) and w(k) become:

$$W(z) = \frac{1}{b^2} N_{main}(z)N_1^*(1/z) \tag{2-21}$$

and

$$w(k) = \frac{1}{b^2} N_{main}(k) \otimes N_1(k) \approx \frac{1}{b^2} d(k) \otimes N_1(k) . \tag{2-22}$$

The latter equation represents the weight calculation as a block LMS algorithm and is the form currently implemented in the MADOP.

W(z) as given in Equation 2-21 is of the form:

$$W(z) = \sum_m c_m z^{-l_m} , \tag{2-23}$$

which means that the convolution of w(k) and d(k) can be performed in a finite impulse response (FIR) filter as is currently done in the AOTDL portion of the MADOP.

For the case where the interference in the main channel contains both direct-path and multipath signals, and the interference is wideband, the autocorrelation of $N_1(k)$ yields:

$$N_1(k) \otimes N_1(k) = \sum_n d_n \delta(k - k_n) , \tag{2-24}$$

thus,

$$N_1(z) N_1^*(1/z) = \sum_n d_n z^{-k_n} . \tag{2-25}$$

This means that W(z) will not be of the simple form of Equation 2-23, but will be the ratio of polynomials in z. That is:

$$W(z) = \frac{\sum_m c_m z^{-l_m}}{\sum_n d_n z^{-k_n}} . \tag{2-26}$$

The above form of W(z) implies that the convolution of d(k) and w(k) must be carried out by an infinite impulse response (IIR) filter. A method of implementing such a filter using AOTDLs was presented in the final report for the second ESE effort (Reference 2).

A block diagram of a modified MADOP that would implement the above algorithm is contained in ***Figure 2-4***. It differs from the current configuration by the addition of another AO time-integrating correlator to form the autocorrelation of $N_1(t)$ and another AOTDL to implement the IIR filter.

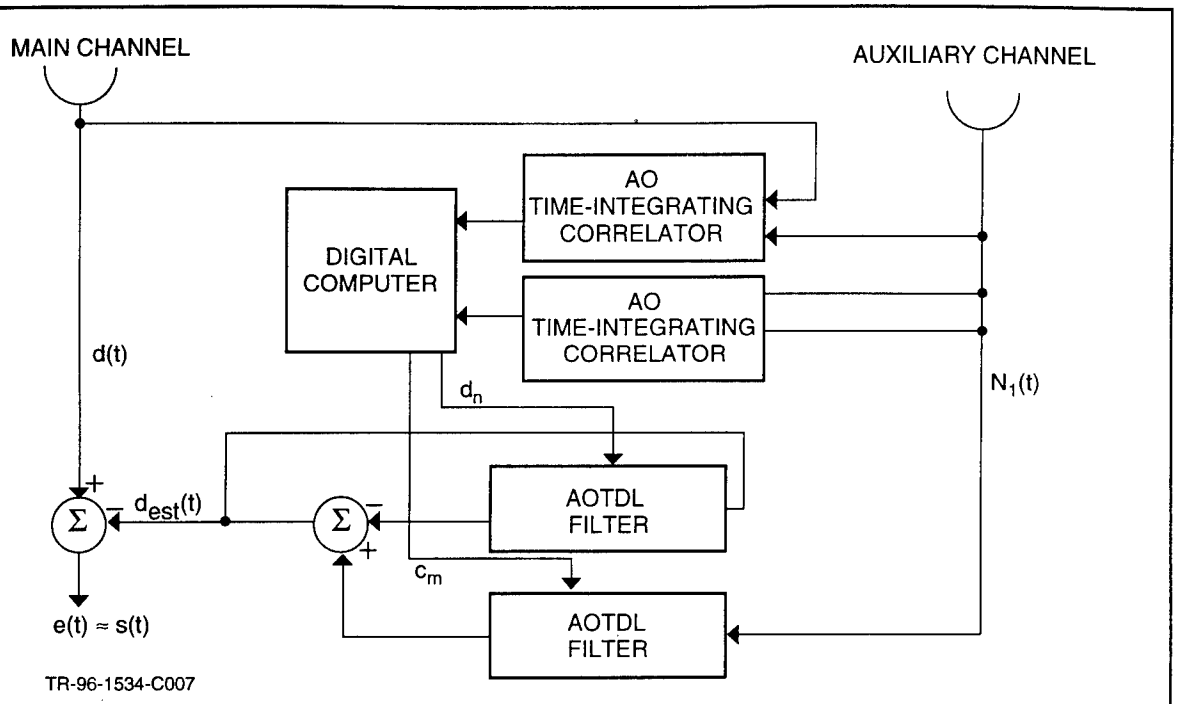

Figure 2-4. MADOP Configuration for Implementing an IIR Filter

The implementation of the MADOP indicated in ***Figure 2-4*** is considerably more complex than the original MADOP configuration. In addition, as indicated in Reference 2, there is a potential problem with the stability of the IIR filter. Because of this, this method of implementing the MADOP should be carefully investigated before it is pursued further. Preliminary investigations conducted during the previous ESE effort indicate that the original, adaptive LMS implementation of the MADOP may be able to compensate for multipath by providing an FIR approximation to the IIR filter. This is an area that warrants further investigation.

3. MADOP HARDWARE CONFIGURATION

During the performance of this effort, the optical and electronic subsystems of the MADOP were further developed and tested. Previous test results and detailed theoretical development are contained in References 1, 2, and 3.

3.1 OVERVIEW OF THE ARCHITECTURE

The MADOP subsystems and their relevant inputs and outputs are shown in ***Figure 3-1***. This figure shows two auxiliary antenna inputs together with the main channel received signal. The AO time-integrating correlator accepts the main channel signal and the auxiliary channel signals and forms the appropriate cross-correlations. This cross-correlation information contains the information needed to select, through the PC interface, the weights to be applied to the AOTDL filter. This AOTDL filter convolves the auxiliary channel inputs with the weights and sums the resultant channels to obtain an estimate for the jamming signal in the main channel. This estimate was originally subtracted from the main channel to generate the error signal. After development of the system, it was noted that the system maintains a stable tap position relative to the envelope of the modulation, but relative to the 80-MHz IF there is phase drift. Therefore, the single-loop electronic canceller was fabricated and inserted into the system at the output of the AOTDL filter to, in effect, lock the carrier of the AOTDL filter output to the main channel signal to achieve effective cancellation.

Each of the following subsections will describe the further development and testing of the individual subsystems, namely the AO time-integrating correlator, the AOTDL filter, the single-loop electronic canceller circuit, and the PC interface.

3.2 TIME-INTEGRATING CORRELATOR FOR WEIGHT FUNCTION CALCULATION

The work performed on the time-integrating correlator under this effort included: 1) alignment and optimization of the Mach-Zehnder AO correlator during on-site support period one; 2) development and testing of an in-line architecture that employs a laser diode and multichannel AO cell during on-site support period two; and 3) alignment and use of the RL-developed almost-common path in-line AO correlator that uses a dove prism between two multichannel AO cells. Items 2 and 3 represent new architectures that are described in more detail in the following subsections.

3.2.1 In-Line Time-Integrating Correlator

Prior efforts (References 1, 2, and 3) had considered the in-line time-integrating correlator architecture, but it was decided during these previous contracts that the Mach-Zehnder architecture

was preferable. During this effort, the correlator architectures were reconsidered in the light of new concerns for stability within the C-band radar test environment.

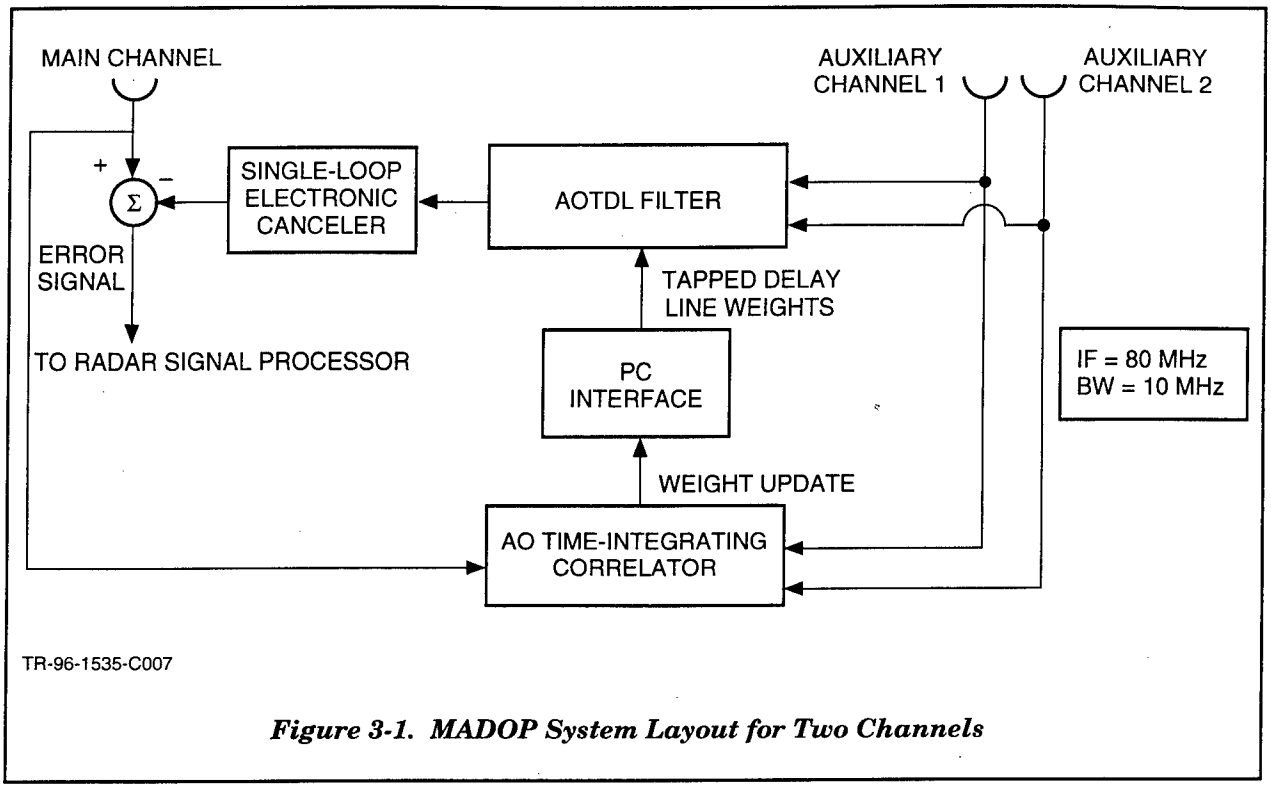

Figure 3-1. MADOP System Layout for Two Channels

During on-site support period two, Dynetics fabricated and tested an in-line time-integrating correlator based on direct modulation of a GALA model 075-04-04 laser diode emitting at a wavelength of 750 nm. The hardware implementation was performed using RL equipment. ***Figure 3-2*** illustrates the optical layout of the in-line time-integrating correlator architecture. The output of a modulated laser diode is collimated and expanded to fill the multichannel AO device. For testing purposes, the entire multichannel AO cell was illuminated however only a single channel was used for correlation processing. To detect and integrate the correlation output, a linear 512-pixel charge coupled device (CCD) array was used.

Mathematically, the operation of the in-line architecture is as follows. The laser diode intensity modulation is given by:

$$I_1(t) = A_1[1 + m_1 \mathrm{Re}\{A_e(t)\exp[j\phi_e(t)]\exp[j2\pi f_0 t]\}] \qquad (3\text{-}1)$$

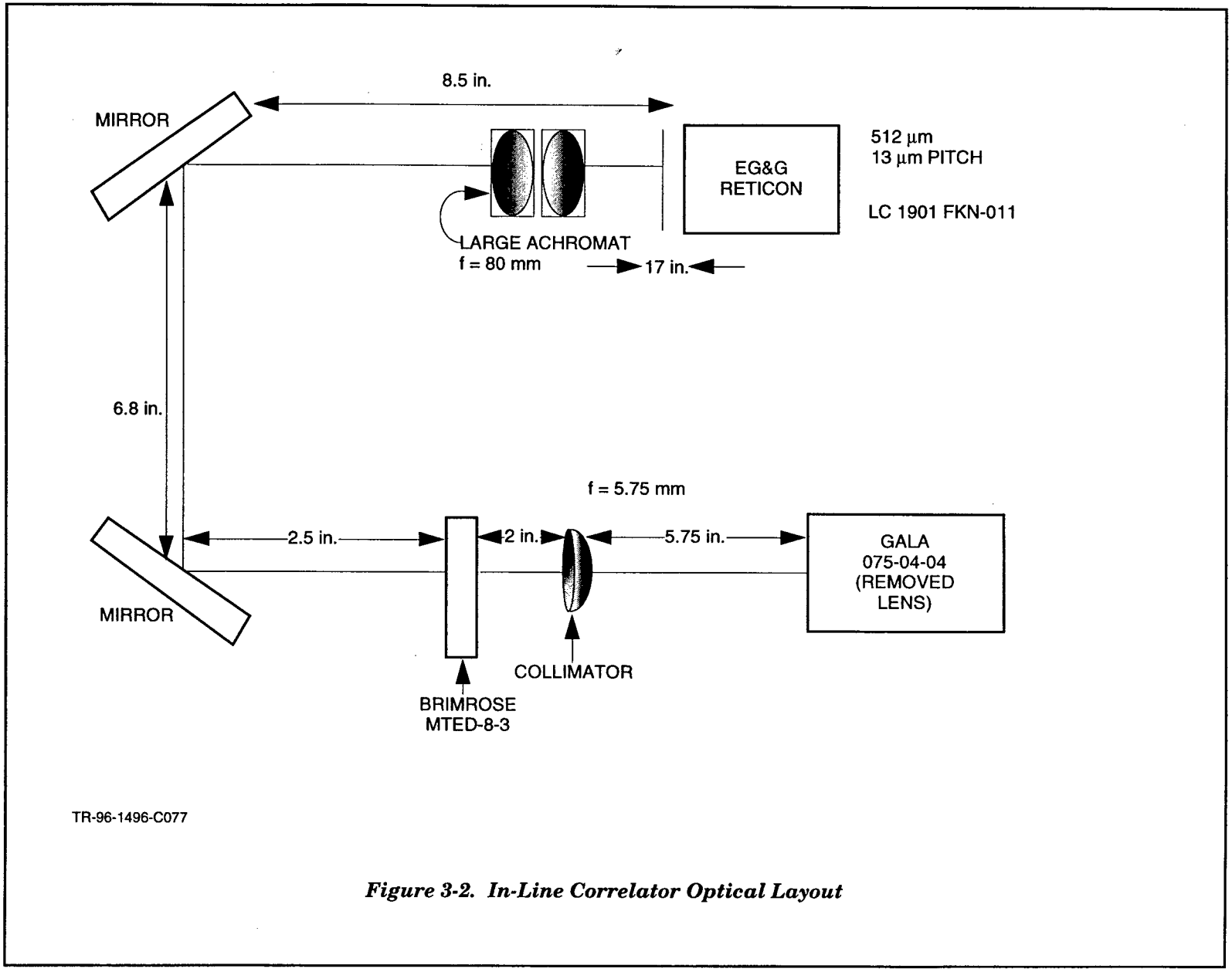

Figure 3-2. In-Line Correlator Optical Layout

where m_1 is the modulation depth, $A_e(t)\exp[j\phi_e(t)]$ is the complex baseband main-channel modulation, and f_0 is the laser diode carrier frequency. Each channel of the AO cell is amplitude modulated to provide the spatial and temporal signal:

$$A_2(t;\tau) = \sqrt{A_2}\{1 + m_2 A_N(t-\tau)\exp[-j\phi_N(t-\tau)]\exp[-j2\pi f_0(t-\tau)]\} \bullet \exp[-j2\pi f_c(t-\tau)] \tag{3-2}$$

where m_2 is the ratio of signal amplitude to reference oscillator amplitude, $A_N(t)\exp[j\phi_N(t)]$ is the complex baseband auxiliary-channel modulation, and f_c is the AO cell carrier frequency. Taking the squared magnitude of this amplitude and multiplying by the laser intensity modulation given above provides the detected intensity for the i^{th} correlation:

$$\begin{aligned} I_d(t;\tau) = {} & A_1A_2(1 + m_2^2A_N^2(t-\tau)) \\ & + A_1A_2m_1(1 + m_2^2A_N^2(t-\tau))\mathrm{Re}\{A_e(t)\exp[j\phi_e(t)]\exp[j2\pi f_0t]\} \\ & + A_1A_2 2m_2\mathrm{Re}\{A_N(t-\tau)\exp[-j\phi_N(t-\tau)]\exp[-j2\pi f_0(t-\tau)]\} \\ & + A_1A_2m_1m_2\mathrm{Re}\{A_e(t)\exp[j\phi_e(t)]A_N(t-\tau)\exp[-j\phi_N(t-\tau)]\exp[j2\pi f_0\tau]\} \\ & + A_1A_2m_1m_2\mathrm{Re}\{A_e(t)\exp[j\phi_e(t)]A_N(t-\tau)\exp[j\phi_N(t-\tau)]\exp[j2\pi(2f_0t - f_0\tau)]\}\,. \end{aligned} \tag{3-3}$$

The second, third, and fifth terms shown have a temporal modulation at frequency f_0 and will integrate to zero over typical detector integration times. The first term is low frequency in both space and time relative to the desired term, which simply results in an intensity bias. The fourth term in this equation is the desired term, which when integrated over time yields the carrier-modulated correlation. After detector readout, but before digitization, it is desirable to employ a bandpass filter (BPF) to eliminate both the low-frequency bias and the high-frequency clock noise.

An Excel spreadsheet was used to determine imaging requirements based on physical parameters of the components used. The spreadsheet allows various configurations to be examined, yet remains consistent with design goals and physical limitations. For example, the detector sampling requirement is calculated according to standard Nyquist sampling theory. First, consider the imaging of the 5-μs correlation window across the linear array. The highest temporal frequency (encoded spatially) for the numerical example above is 20 MHz (15-MHz center frequency with a 10 MHz bandwidth). One cycle at this frequency corresponds to 50 ns, which implies a required pixel spacing of 25 ns. Using this spacing over a 5-μs window requires a total of 200 pixels. Thus, the Nyquist sampling requirement will be satisfied with a standard 512-pixel array. If the carrier frequency is increased to greater than 15 MHz (by using a reference oscillator of less than 65 MHz), more than 200 pixels will be required. This shows why the use of the undiffracted beam as a reference oscillator

is impractical (the reference oscillator offset is 80 MHz requiring more than 800 pixels). The critical design parameters calculated by the spreadsheet for the in-line architecture constructed during the second on-site visit are given in ***Table 3-1***.

Table 3-1. Design Spreadsheet for In-Line AO Correlator

Parameter	Value	Entered/ Calculated
System Requirements		
System Bandwidth (MHz)	10.00	Entered
Time-Bandwidth Product (Number of Range Bins)	100.00	Calculated
Frequency Resolution (MHz)	0.10	
Spur Free Dynamic Range (3-Tone) (dB)	30.00	Entered
System IF (GHz)	0.08	Entered
Desired Roll-Off across Correlation Window (e^{-2})	1.00	Entered
Spot Size Increase Factor Over Rectangular	1.00	Entered
Integration Time (μs)	1000.00	Entered
Laser Diode Information		
Wavelength (nm)	750.00	Entered
Bias Optical Powee (mW)	2.00	Entered
Maximum Optical Signal Power (mW)	4.00	Entered
x-Axis Gaussian Beam Factor at AO Cell (mm^{-2})	0.00	Calculated
x-Axis e^{-2} Beam Size at AO Cell Diameter (mm)	21.00	Calculated
Desired y-Axis e^{-2} Beam Size at AO Cell (mm)	2.00	Transferred
Actual y-Axis e^{-2} Beam Size at AO Cell (mm)	2.00	Entered
y-Axis Gaussian Beam Factor (mm^{-2})	2.00	Calculated
x-Axis Error Function Parameter	1.41 Normalized	Calculated
y-Axis Error Function Parameter	2.00 Normalized	Calculated
Fraction of Power Used in x-Axis	0.84	Calculated
Fraction of Power Used in y-axis	0.95	Calculated
Required Time Delay (μs)	5.00	Calculated
Center Frequency (MHz)	12.50	Calculated
Maximum Frequency (MHz)	17.50	Calculated
Required Conversion from IF (MHz)	67.50	Calculated
AO Drive Information		
Signal-to-Tone Ratio	1	Entered
Tone Frequency (MHz)	67.5	Calculated

Table 3-1. Design Spreadsheet for In-Line AO Correlator (Continued)

Parameter	Value	Entered/ Calculated
Tone Power (dBm)	18.01	Calculated
Signal Power (dBm)	18.01	Calculated
Tone Diffraction Efficiency (%)	4.74	Calculated
Signal Diffraction Efficiency (%)	4.74	Calculated
Total AO Bandwidth (MHz)	17.5	Calculated
Signal Center Frequency (MHz)	80.0	Calculated
Required Downconversion from ESM (MHz)	0.0	Calculated
AO Cell Data		
Required Time Aperture (μs)	10.00	Calculated
Acoustic Velocity (m/s)	3960.00	Entered
Acoustic Aperture of Interest (mm)	39.60	Calculated
Acoustic Column Height (mm)	2.00	Entered
Bragg Angle at Center (deg)	0.41	Calculated
Diffraction Efficiency per RF Watt (Approximate) (%/W)	75.00	Entered
Diffraction Efficiency for Maximum Signal (Set by 3-Tone Intermodulation Products) (%)	9.49	Calculated
Maximum Drive Power for Input Signal (dBm)	21.02	Calculated
AO Center Frequency (MHz)	76.25	Entered
Diffracted Angular Spread (deg)	0.19	Calculated
Angular Separation ($f_{dc} - f_{low}$) (deg)	0.73	Calculated
Total Angular Spread ($f_{dc} - f_{max}$) (deg)	0.92	Calculated
Losses		
Optical Losses	0.50	Entered
Spatial Frequencies Before Magnification		
Spatial Frequency BW of Correlation (Maximum) (Abels)	2.53	Calculated
Highest Spatial Frequency (Abels)	4.42	Calculated
Imaging Optics		
Required Magnification of Optics	0.14	Calculated
Focal Length of Imaging Lens (mm)	80.00	Entered
Distance from AO to First Lens (mm)	637.01	Calculated
Distance from Lens to Detector Array (mm)	91.49	Calculated
Lens Aperture Required for dc + Diffracted (mm)	49.86	Calculated
Lens Aperture Required for Diffracted Only (mm)	41.71	Calculated
Required f/# for dc + Diffracted	1.60	Calculated

Table 3-1. Design Spreadsheet for In-Line AO Correlator (Continued)

Parameter	Value	Entered/ Calculated
Required f/# for Diffracted Only	1.92	Calculated
Vertical e^{-2} Diameter on Detector (mm)	0.29	Calculated
Cylindrical Lens - Not Used		
Focal Length (mm)	50.00	Entered
Approximate Distance from Detector (mm)	50.00	Calculated
Diameter at Lens (mm)	0.27	Calculated
Approximate e^{-2} Beam Size at Detector (μm)	193.43	Calculated
Vertical Gaussian Factor (mm^{-2})	213.81	Calculated
AO Intensities		
Percent in Tone (%)	4.74	Calculated
Percent in Signal Term (%)	4.74	Calculated
Percent in Squared Signal Term (%)	4.74	Calculated
Intensity Multiplication		
Power in Bias/dc Term (μW)	37.80	Calculated
Maximum Power in Signal Term (μW)	75.60	Calculated
Power in Squared Signal Term (μW)	37.80	Calculated
Spatial Frequency Content of Squared Term (Abels)	0.00	Calculated
Total Biases (μW)	75.60	Calculated
Contrast Ratio	1.00	Calculated
Detector Information		
Carrier Frequency Factor [N*(B/2)]	2.50	Entered
Number Detectors per Highest Frequency (f_{high})	2.50	Entered
Detector Spacing (μm)	13.00	Entered
Number of Detectors per Correlation Peak	4.38	Calculated
Peak Correlation Energy per Pixel (pJ)	172.81	Calculated
Peak Correlation Photon Counter per Pixel (photons)	6.52×10^{-8}	Calculated
Quantum Efficiency (electrons/photon)	0.10	Entered
Peak Correlation Electron Count per Pixel (electrons)	6.52×10^{-7}	Calculated
Maximum Allowable Electron Count (electrons)	1.50×10^{-6}	Entered
Peak-to-Maximum-Electron Ratio	43.4	Calculated
Amplifier Noise/Clock (electrons)	100.00	Entered
Dark Noise Rate (e/ms)	2000.00	Entered
Dark Noise (electrons)	2000.00	Calculated

Table 3-1. Design Spreadsheet for In-Line AO Correlator (Concluded)

Parameter	Value	Entered/ Calculated
Output Voltage Scale Factor (μV/electron)	2.00	Entered
RMS Noise Voltage (mV)	0.20	Calculated
Peak Output Voltage (V)	3.00	Calculated
Peak Correlation Signal Voltage (V)	3.00	Calculated
Peak Correlation Signal + Bias Voltage (V)	130.32	Calculated
Number of Detectors		
Calculated Number of Detectors	437.50	Calculated
Actual Number of Detectors	512.00	Entered

Coherent operation is achieved with the in-line architecture by adding a reference oscillator to the AO cell input to create a reference beam to spatially and temporally interfere with the information beam. The interference between the reference beam and the information beam at a relative angle will create the spatial fringe pattern described earlier. In addition, due to the different Doppler shifts induced by the AO cell, the fringe pattern will oscillate at the difference frequency between the reference frequency and the information frequency. Modulation of the laser diode cancels this beat frequency in order to freeze the fringe pattern and allow for time integration. The undiffracted beam can be used to interfere with the information beam, but the resulting spatial carrier frequency will be prohibitively high, requiring a very long detector array to adequately sample the carrier. Using the reference oscillator allows the user to set the output carrier at the desired frequency. The condition on this carrier is that the reference oscillator be at least 1.5 times the bandwidth away from the information center frequency. Thus, for an 80-MHz center and a 10-MHz bandwidth, the reference oscillator must be at a frequency of 65 MHz or less (or greater than 95 MHz). For this numerical example, with a 65-MHz reference oscillator resulting in a 15-MHz oscillator offset, the laser diode must be driven with the 10-MHz bandwidth signal on a 15-MHz carrier.

Figures 3-3 and 3-4 illustrate the design of the electronics used to generate the input signals to the laser diode and to the AO cell. Note that the direct current (dc) bias term for the laser diode input is generated internal to the GALA laser system. Also, the electronics design shown in these figures is configured for realizing an autocorrelation. Thus, s(t) represents the temporal signal to be autocorrelated. As shown in ***Figure 3-3***, the offset frequency, f_0, was chosen to be 12.5 MHz. The requirement on the tone separation depends on the bandwidth of information being input to the correlator and is given by:

$$f_0 \geq 1.5B. \tag{3-4}$$

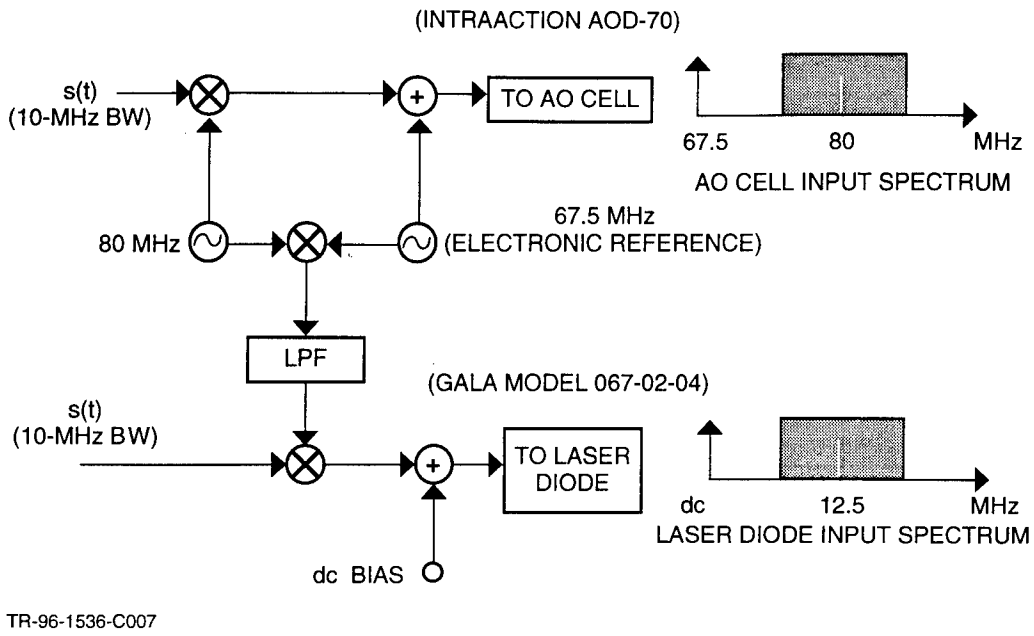

Figure 3-3. In-Line Correlator Design Input Spectra

Figure 3-3 illustrates the required signal spectrum inputs into the AO cell and laser diode. ***Figure 3-4*** shows the configuration of the RF drive electronics used for testing the operation and performance of the in-line correlator.

Tests were performed to determine the dynamic range of the laser diode to be used in the in-line correlator initial breadboard. Due to its immediate availability, a DO Industries GALA laser system (model 075-04-04, 750-nm, 4-mW maximum power) was chosen as the laser diode. A high-speed photodiode (Antel Corporation) was used to detect the temporal modulation of the laser diode. The output of the photodiode was observed on a Tektronix 11403 digitizing oscilloscope. The dynamic range was calculated in the following manner. A sinusoid was input to the laser diode. The signal power was set to correspond to the maximum output of the laser diode. After photodiode detection, the input signal to the laser diode was attenuated, and the corresponding results were observed on the oscilloscope. The maximum amount of attenuation that still allowed detection of the modulated waveform was used as an indication of the dynamic range. For the test, an 80-MHz sinusoid was input into the laser diode. As a result of the test, it was determined that the dynamic range of the laser diode was approximately 27 dB. Previous testing (Reference 3) of a GALA laser diode (model 067-02-04) indicated a dynamic range greater than 45 dB. This difference resulted from the use of a

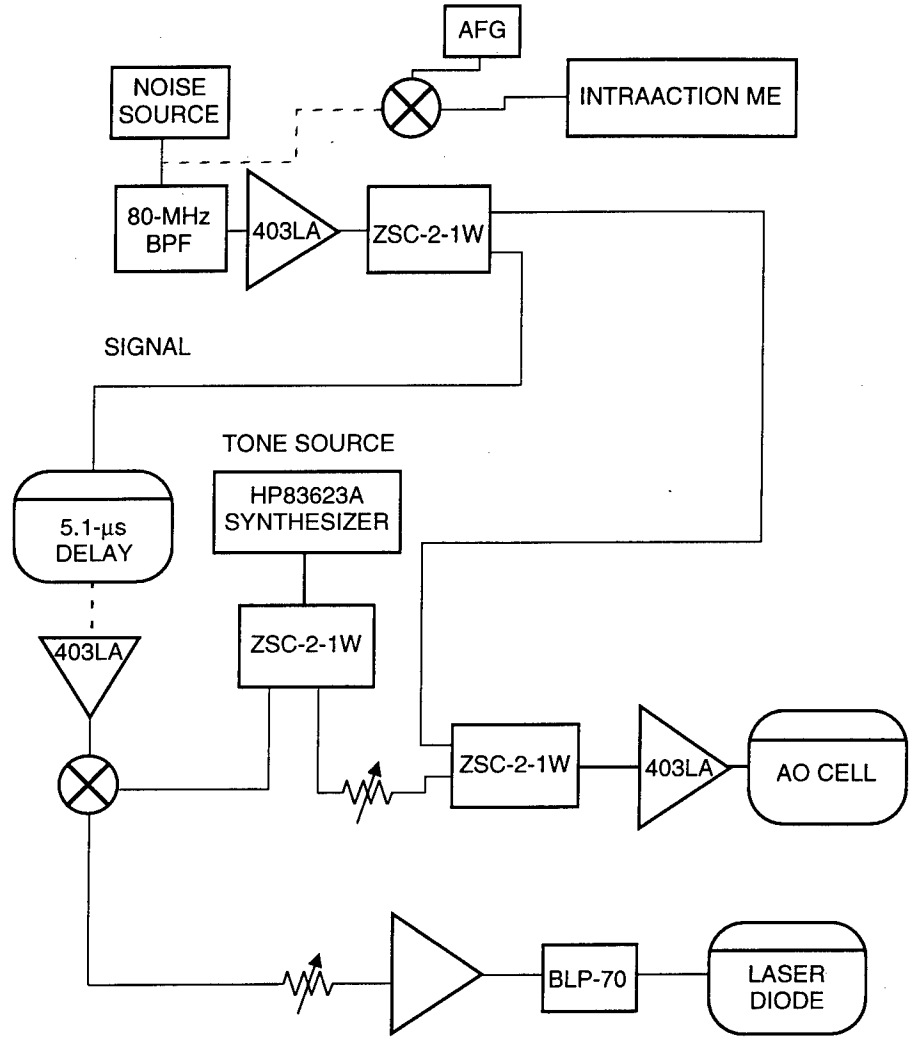

Figure 3-4. RF Drive Electronics Testing Configuration

different laser diode whose operation is not optimized for higher-frequency modulation. Additionally, the modulated output of the 750-nm laser diode was very noisy, showing strong spikes in the modulated signal.

The laser diode used in an in-line correlator architecture is critical to the overall achievable performance. A specially constructed high-bandwidth, high-optical-power laser diode should be considered for any further in-line designs.

Adjustments in AO cell position and imaging/focusing lens positions were made to optimize the uniformity of the correlation across the range window. An 80-MHz tone was input to each AO cell, resulting in the spatial carrier correlating across the charged coupled photo detector (CCPD) array. ***Figure 3-5*** shows the output from the linear CCD array. A two-dimensional (2-D) camera was used to aid initial AO cell alignment since the optical power of the laser diode at 750 nm was very small and falls at the edge of the human eye response. As can be observed from ***Figure 3-5***, the optical modulation depth is very good, using almost all of the dynamic range of the detector. However, the uniformity across the array window is rather poor. Pixel-to-pixel nonuniformities and gain imbalances between odd and even pixels also appear to contribute to the overall nonuniformities observed.

Correlation window centering was achieved through the use of a 10-MHz bandwidth noise signal into the AO cells. The CCD array was linearly translated along the AO aperture direction, until the correlation peak due to the noise was centered on the array. ***Figure 3-6*** shows the alignment results and the autocorrelation of a 10-MHz bandwidth noise source with the laser diode dc bias set to maximum. ***Figure 3-7*** shows the autocorrelation of a 10-MHz bandwidth noise source with the laser diode dc bias set to minimum. Each plot shows the nonuniformities across the window. Although the magnitude of the correlation is higher when the dc bias is maximum, the modulation depth of the correlation is greater with minimum dc bias.

The testing performed on the in-line correlator has provided much insight into the architecture setup, operation, capabilities, and limitations. A new laser diode should be considered to optimize the architecture. Further analysis/testing should be performed since operation and performance of the new components, such as the multichannel AO cell and CCD array, may differ from that of the current components in the preliminary setup. Tests that should be performed include further dynamic range characterization, linearity, delay window uniformity, and the effects of the post-detection processing algorithms on these measurements.

3.2.2 Almost-Common Path In-Line Time-Integrating Correlator

During the third on-site testing period, an almost-common path architecture, designed and fabricated by RL personnel, was transported to the radar facility, recalibrated after transportation,

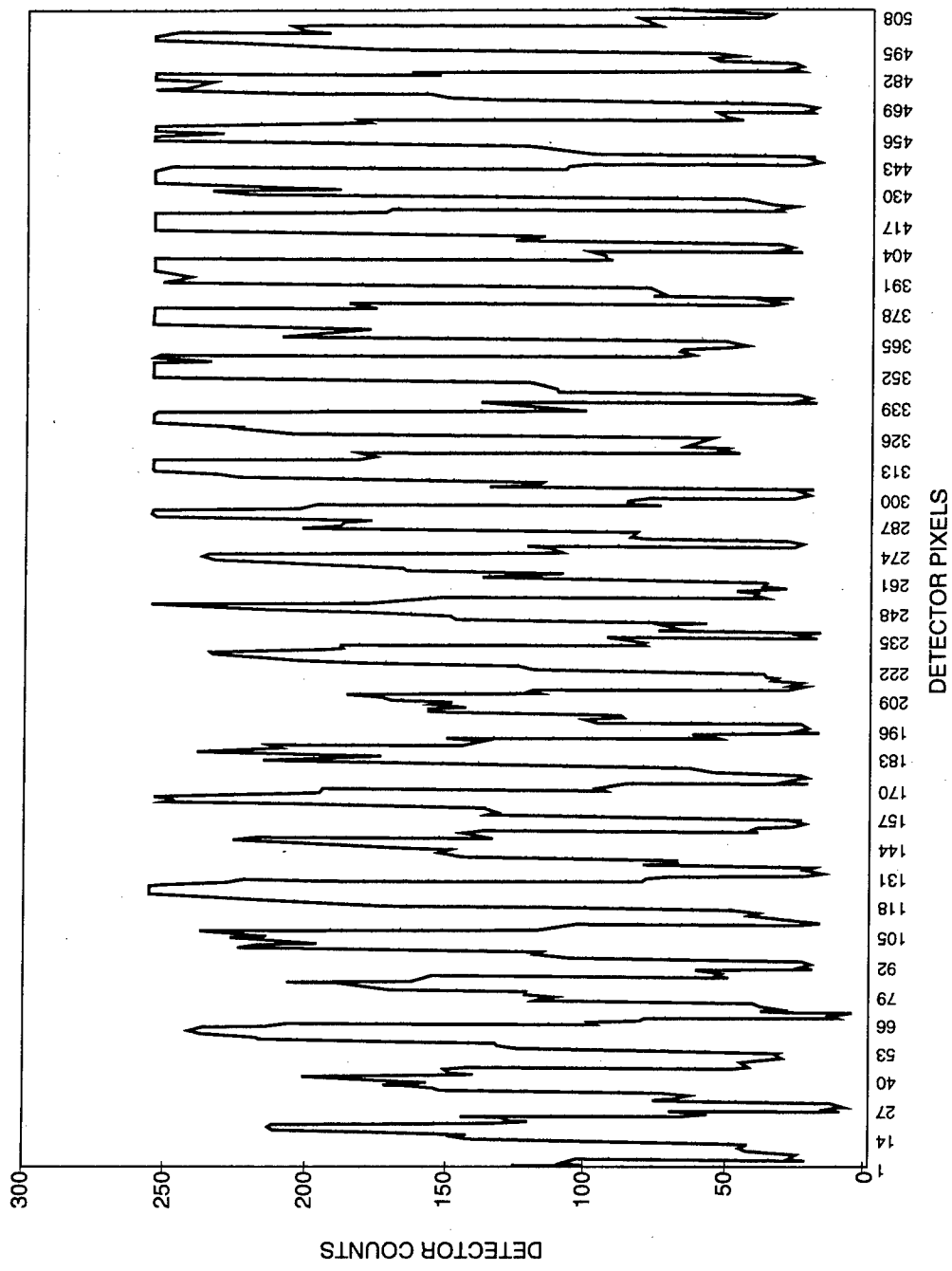

Figure 3-5. Autocorrelation of 80-MHz Tone

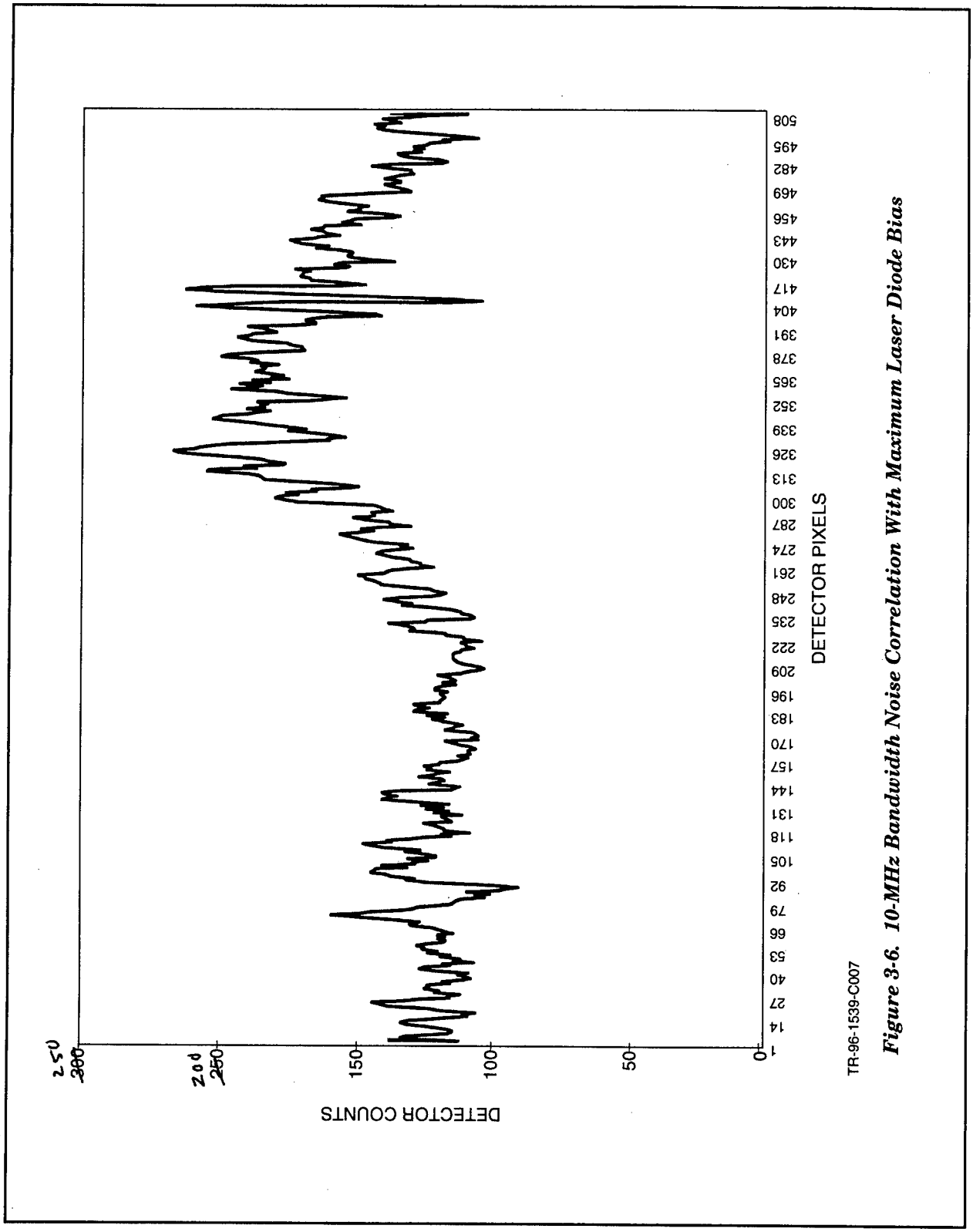

Figure 3-6. 10-MHz Bandwidth Noise Correlation With Maximum Laser Diode Bias

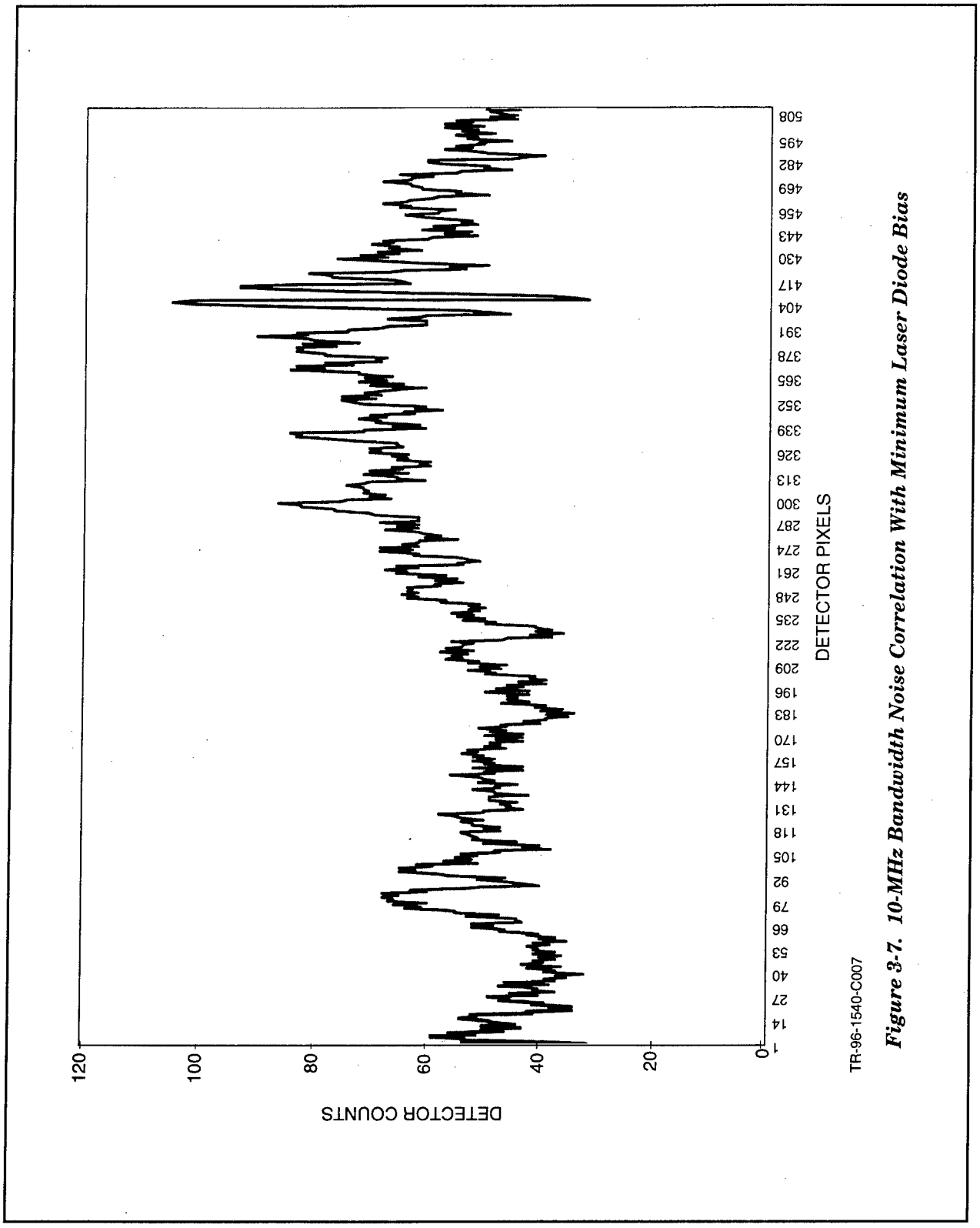

Figure 3-7. 10-MHz Bandwidth Noise Correlation With Minimum Laser Diode Bias

and tested. Hardware implementation was performed using RL equipment. During verification testing, it was discovered that components had shifted during transport. Minor realignment and performance verification testing was performed on the correlator. Performance of the correlator after realignment was assumed to be equivalent to that measured prior to breadboard transportation.

The almost-common path interferometric architecture tested during the third testing phase is illustrated in ***Figure 3-8***. This architecture was constructed previously by RL personnel (Reference 14) and is based on a modified architecture of Riza (Reference 15). The unique aspect of this architecture is the use of a dove prism, rather than a beam-splitter cube as in most interferometric architectures. A full discussion of the architecture theory is presented in References14 and 15.

Input test signals for the realignment included a broadband noise source with a 10-MHz bandpass centered at 80 MHz (NoiseCom), and tones generated by an HP6259A synthesizer. For realignment testing, the signals were input into a single channel of each of the multichannel AO cells. The output was detected by a 512-element EG&G CCD array.

By performing autocorrelation of tones at various frequencies and noting the minimum/maximum amplitudes of the resulting fringe pattern, it is possible to determine the frequency response of the AO correlator as shown in ***Figure 3-9***. Over the bandwidth of 70 to 90 MHz, the relative response of the correlator is approximately uniform.

Using the tone inputs, a frequency chirp across the array was observed. Initially, this pattern appeared to be the result of spherical aberrations in the system. However, it was noted that the chirping pattern could be changed by slight adjustments in the position of the diffracted beam at the dove prism, which should not introduce aberrations. The geometry of the focused diffracted beam needs to be reexamined to fully explain this phenomenon.

Figure 3-10 shows the raw output of the in-line architecture with a 10-MHz bandwidth noise source. The correlation spike shows good modulation depth. Sampling is slightly more than three fringes, with four detectors per fringe. Much of the unevenness in the output is attributable to scattered light and detector odd/even imbalances.

This architecture exhibited good mechanical stability while being operated in the C-band antenna room. Additionally, the alignment of the system appeared to be much more flexible than a conventional interferometric architecture with a beam splitter. Reducing the size of the assembly with fewer spring-loaded mounts would likely increase the stability.

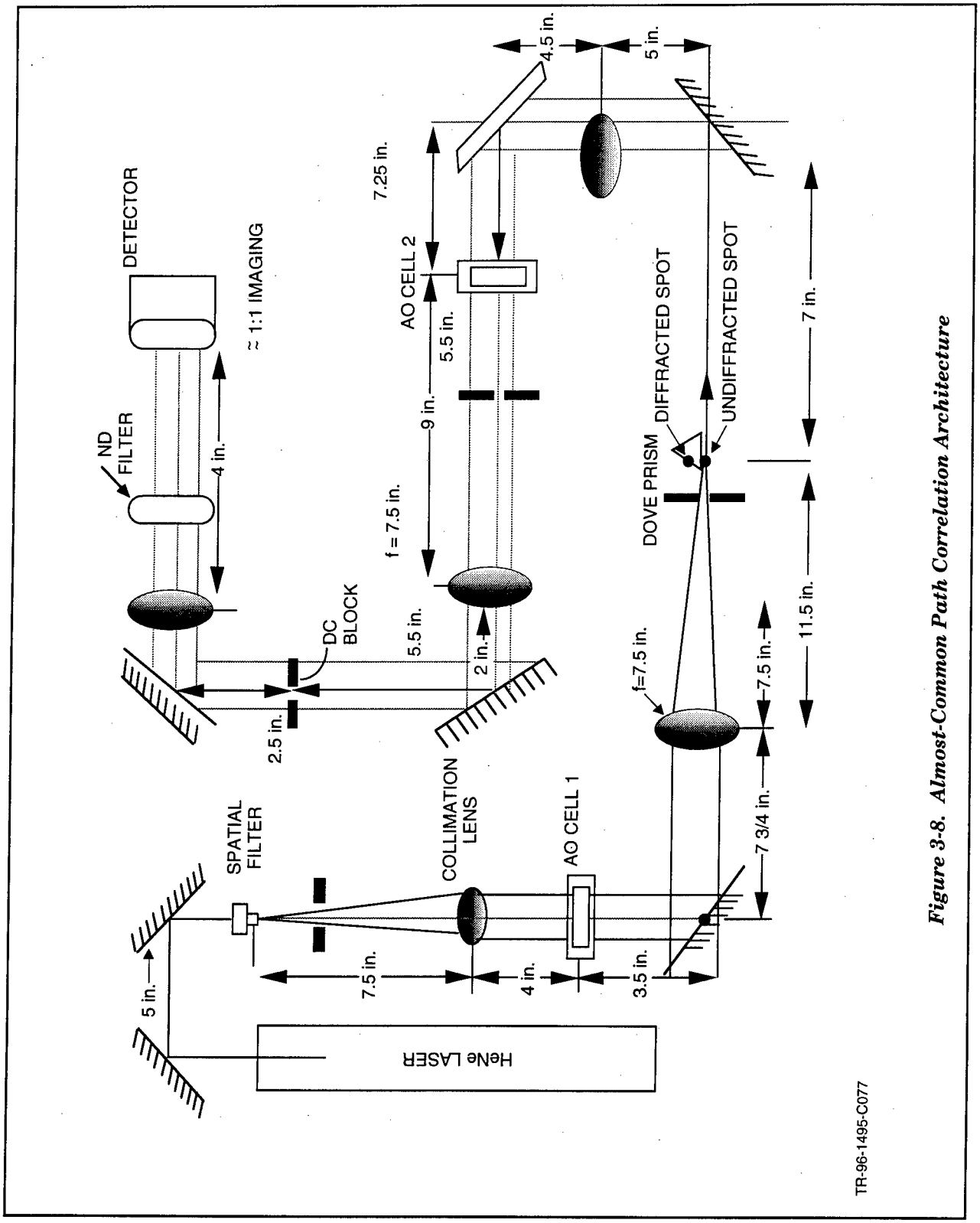

Figure 3-8. Almost-Common Path Correlation Architecture

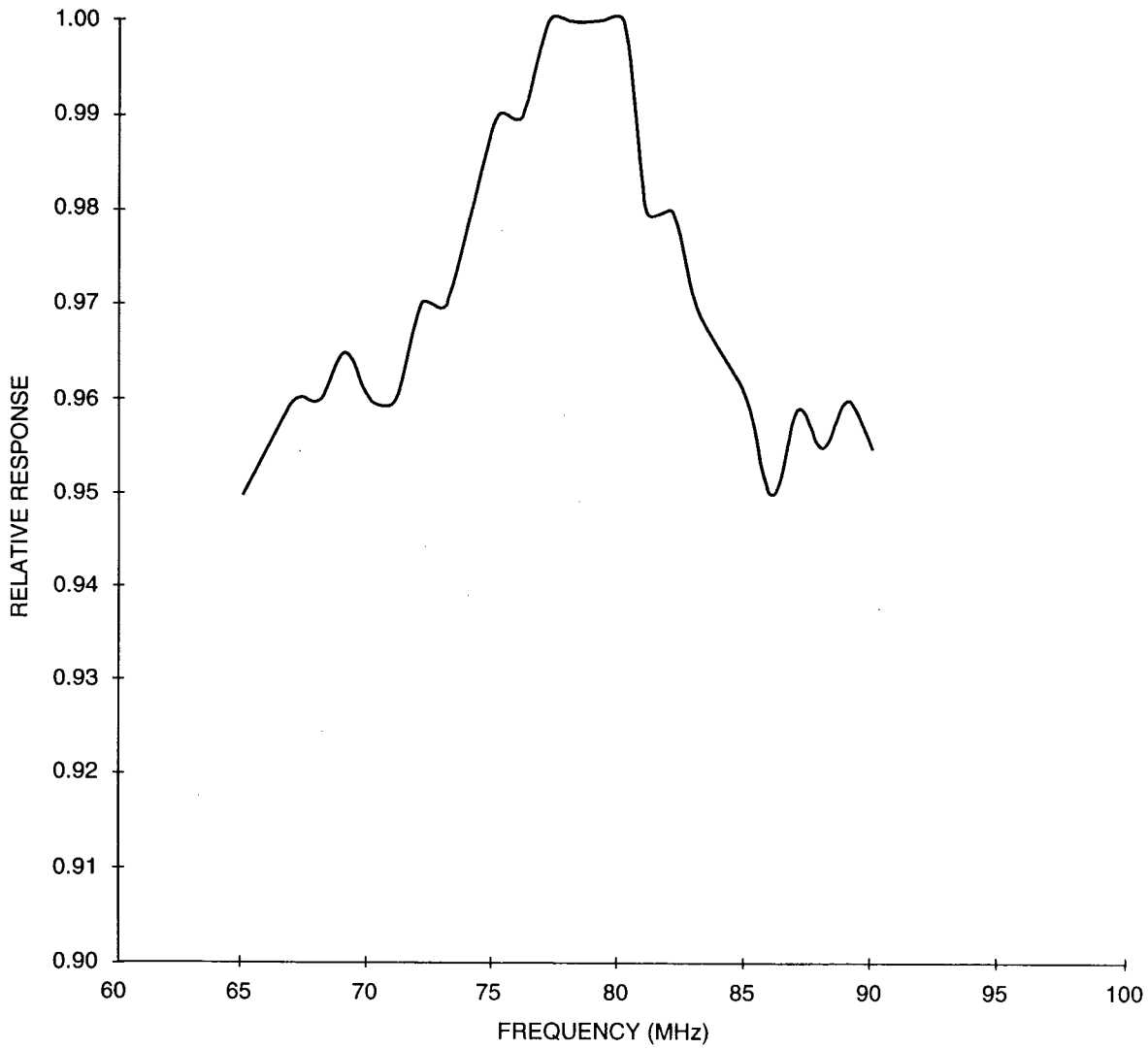

Figure 3-9. Relative Frequency Response of Almost-Common Path Correlator

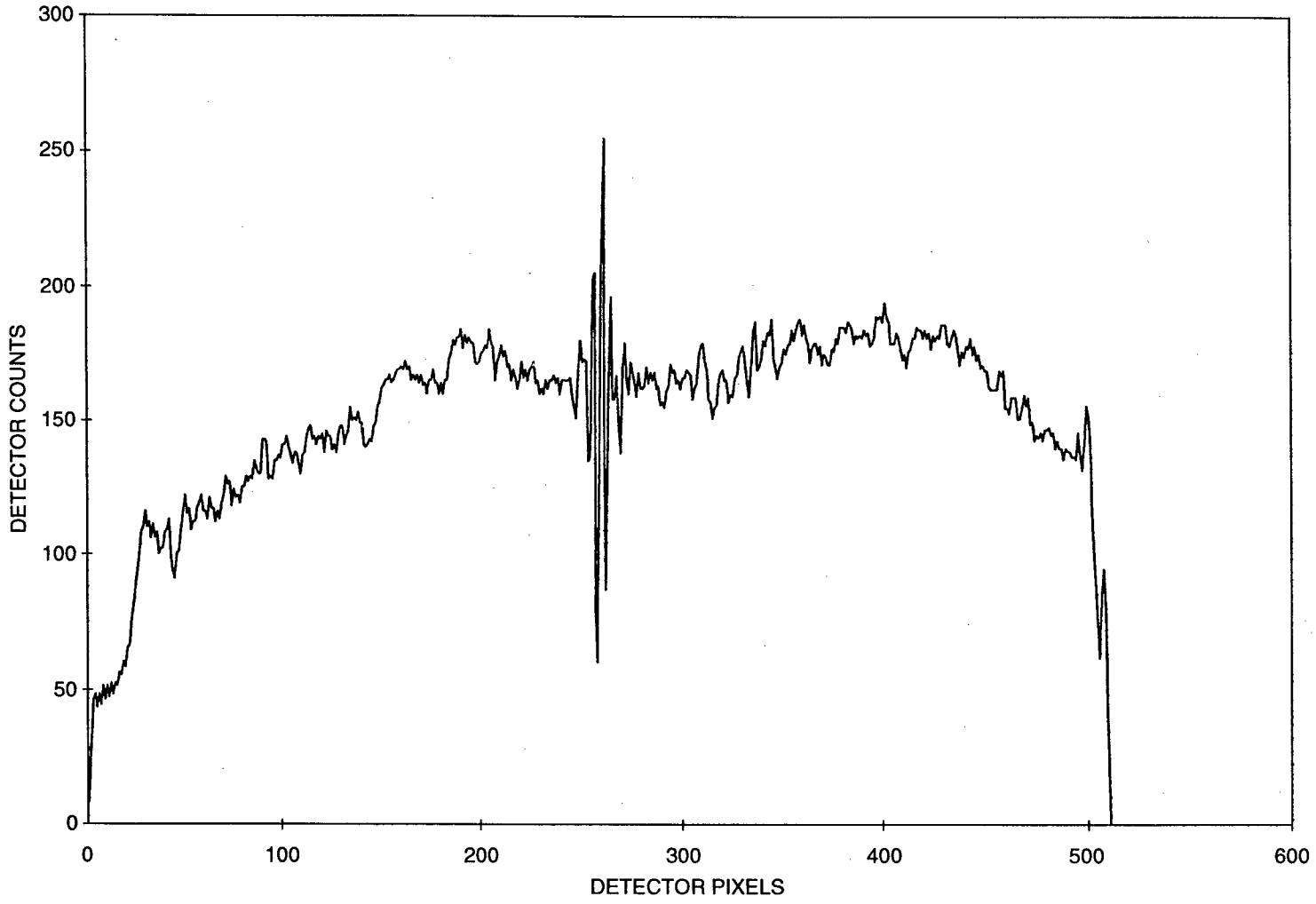

Figure 3-10. Autocorrelation of Wideband Noise

3.3 AOTDL FILTER

The AOTDL filter was not modified from its earlier design and hardware implementation, as provided in Reference 1. The primary activity with this subsystem was the extensive testing within the MADOP architecture as part of the C-band radar testbed. The combined cancellation performance of the AOTDL filter and the electronic canceller is described in Subsection 3.4.

3.4 SINGLE-LOOP ELECTRONIC CANCELLER

During the third period of on-site support, additional enhancements were made to the integrated MADOP system, and this new configuration was tested in the laboratory. The electronic canceller was at the focus of these design changes, and all modifications were tested in the laboratory using the HP4195A Network/Spectrum Analyzer. Once optimal canceller performance was obtained, characterization with the AOTDL and later with the RF electronics, which includes the bulk acoustic wave (BAW) delay lines and other components required to interface to the C-Band radar, was accomplished. The HP4195A Spectrum/Network Analyzer was used to establish system performance, to analyze test signals, and to provide test waveforms. The HP83623A synthesizer was used to select the tap frequency of the AOTDL.

The design changes to the electronic canceller significantly improved the bandwidth and depth of waveform cancellation. For comparison, ***Figure 3-11*** shows the electronic canceller frequency response obtained during on-site support period one. A number of the changes to the design were necessary due to impedance mismatches between certain components of the electronic canceller. Specifically, the BNC Tee's used in some areas of this system were replaced with power splitters specified to operate over the bandwidth of the canceller, an approach that provides a better match between devices. In addition, the PA-4 RF amplifier within the canceller was replaced with a model TW-1000 amplifier from Amplifier Research. This new amplifier provided better canceller performance because the group delay of this device was better suited to the rest of the canceller circuitry. In addition, 13 dB of attenuation was previously added to the local oscillator (LO) input to the phase comparator for the purpose of protecting this device from the high input power that can occur when the jammer signal is out of the frequency range of the canceller. To protect the phase comparator under these conditions, signal amplitude limiting devices were assembled to clamp the amplitude of the waveforms into both the RF and LO inputs. This allowed the removal of the 13 dB of attenuation on the LO input of the phase comparator, resulting in an additional 13 dB of signal cancellation. Lastly, the low-pass filter (LPF) in the error feedback path was moved to the output of the AOTDL detector. The frequency response of this new canceller configuration is shown in ***Figure 3-12*** and reflects a cancellation of over 60 dB for continuous wave (CW) tone waveforms over a passband from

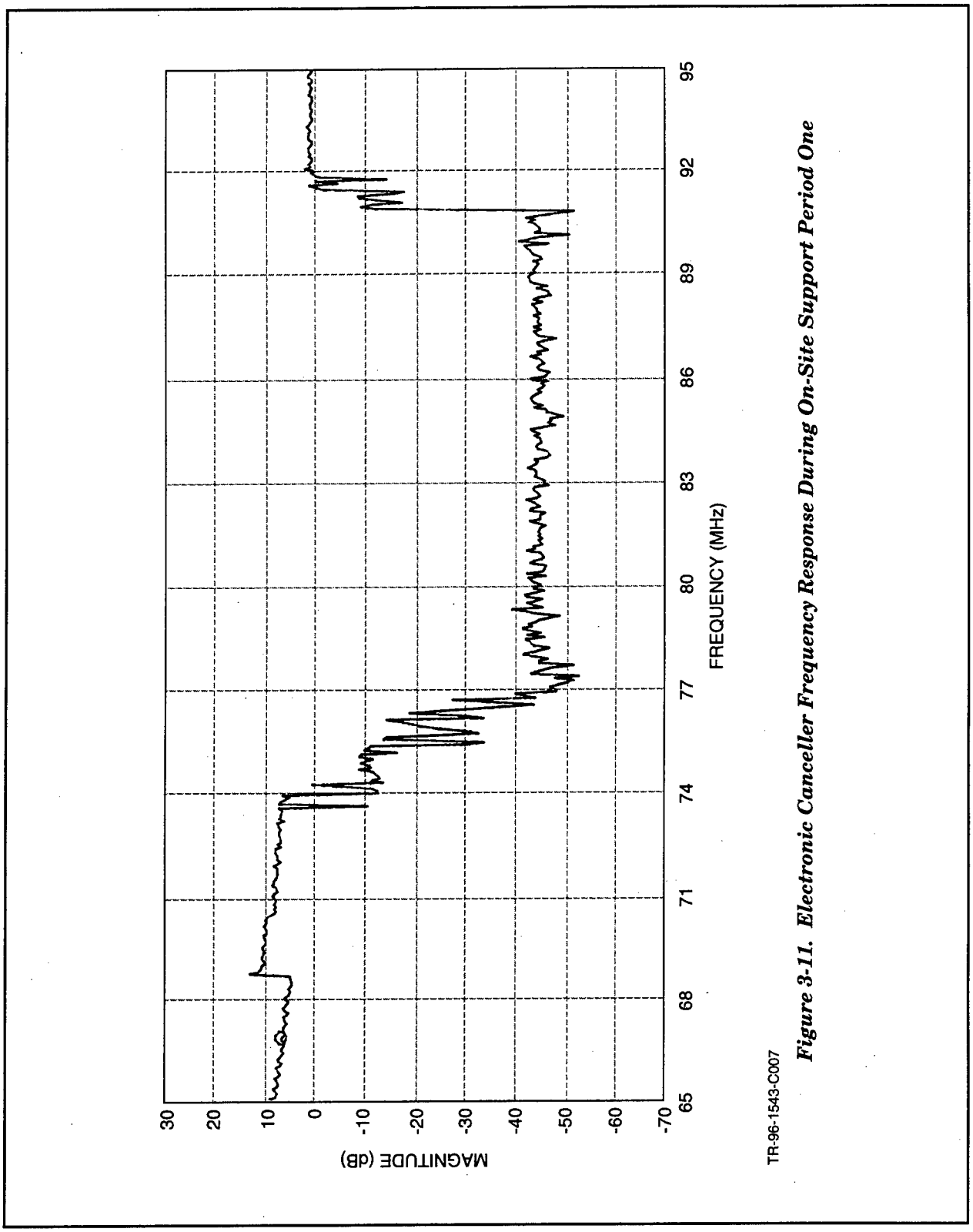

Figure 3-11. Electronic Canceller Frequency Response During On-Site Support Period One

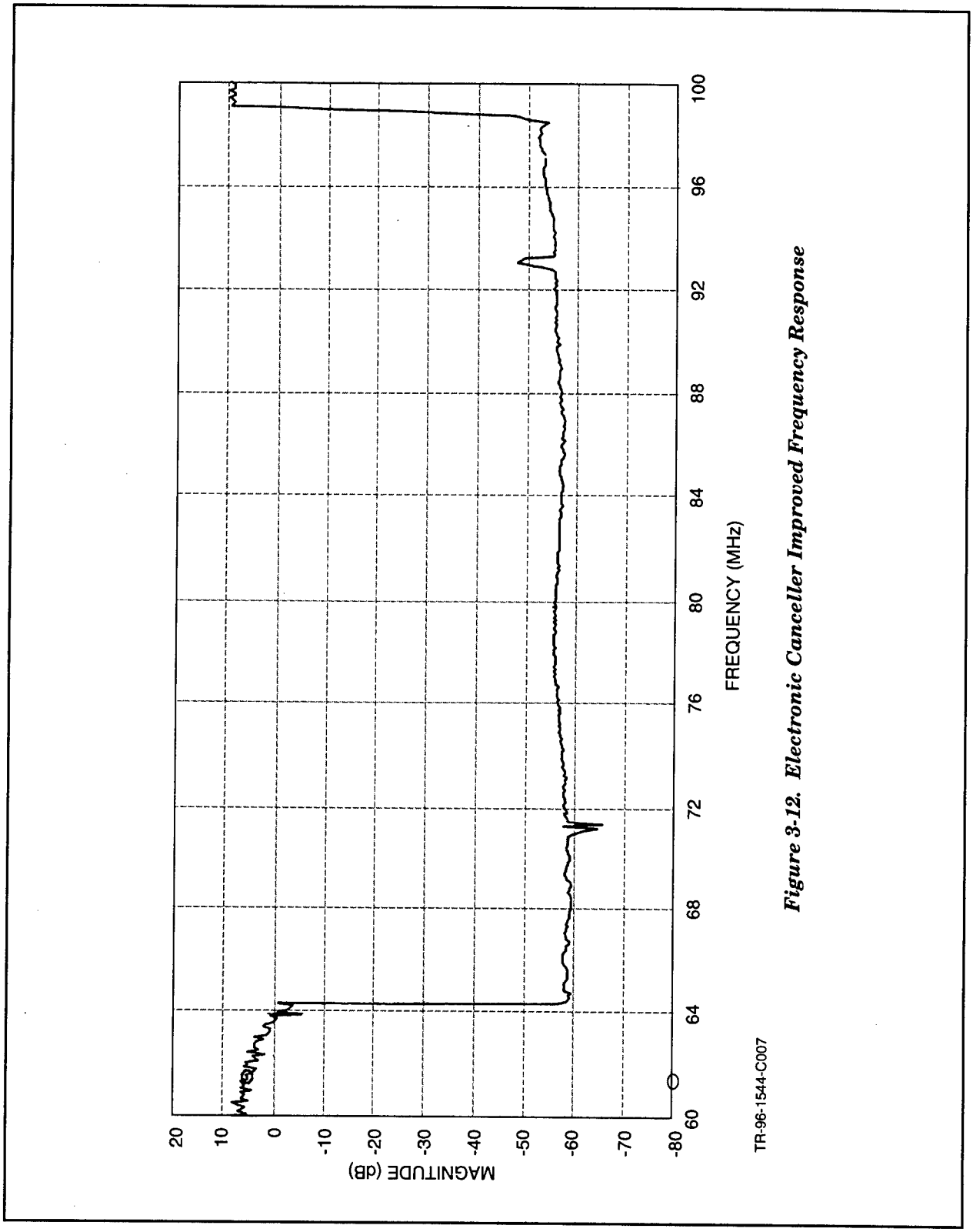

Figure 3-12. Electronic Canceller Improved Frequency Response

65 MHz to over 98 MHz. The block diagram of the new canceller configuration is provided in ***Figure 3-13***.

After the performance of the electronic canceller was optimized, the AOTDL was integrated into the system, and the system performance was again tested. The HP83623A synthesizer was used to select the appropriate tap of the AOTDL by tuning it to the appropriate frequency. Since the performance of the system was tested over a range of sinusoidal input frequencies, the HP83623A was tuned to select the zero tap frequency. Again, the HP4195A Spectrum/Network Analyzer was used to characterize the frequency response of the system. The resulting system response, including the AOTDL, is shown in ***Figure 3-14.*** This plot indicates a cancellation depth of approximately 45 dB over a bandwidth of 32 MHz from 65 MHz to 97 MHz. The dotted line in this figure is the level of the reference (main) channel into the canceller and represents 0 dB of cancellation. As can be seen, outside the frequency range of cancellation, the system provides approximately 15 dB of signal gain.

Lastly, the RF electronics was integrated into the system, and further testing was performed. ***Figure 3-15*** represents the total system frequency response, including the electronic canceller, AOTDL, and the RF electronics necessary to interface the system to the C-Band radar receiver. In this test, the tap frequency was determined manually. The dashed line in this figure again represents the level of the reference (main) channel into the canceller and represents 0 dB of cancellation. The slope of this line indicates the frequency response of the reference channel of the RF electronics and, particularly, the BAW delay line. ***Figure 3-16*** provides the total system frequency response with the AOTDL tap frequency determined by the computer. In this case, the frequency of the HP83623A synthesizer is under the control of the computer through the general-purpose interface bus (GPIB). This configuration results in a noisier appearance. The spikes in the plot are the result of the synthesizer being tuned over the required tap frequencies as the input frequency is swept. As ***Figures 3-15 and 3-16*** reveal, the cancellation depth of the system is at least 40 dB over a band from 64 MHz to 94 MHz. These results represent the degree of cancellation of the system against CW jammer sources since the sweep time of the network analyzer was set to 20 s (i.e., a slow frequency sweep). The configuration of the new system design is presented in the block diagram of ***Figure 3-17***, which shows the layout of the electronic canceller, the RF electronics, the interfaces between these subsystems, the AO time-integrating correlator, and the AOTDL.

3.5 DIGITAL COMPUTER INTERFACE

During this contract, a Pentium PC® was received, along with cards to interface the camera controller to the PC and to control the synthesizer for the AOTDL filter. Work on this portion of the system was initiated during on-site support periods one and two, but success was limited due to the complexity of the interfacing and the fact that the hardware was ordered by Capt. Andrews, who also

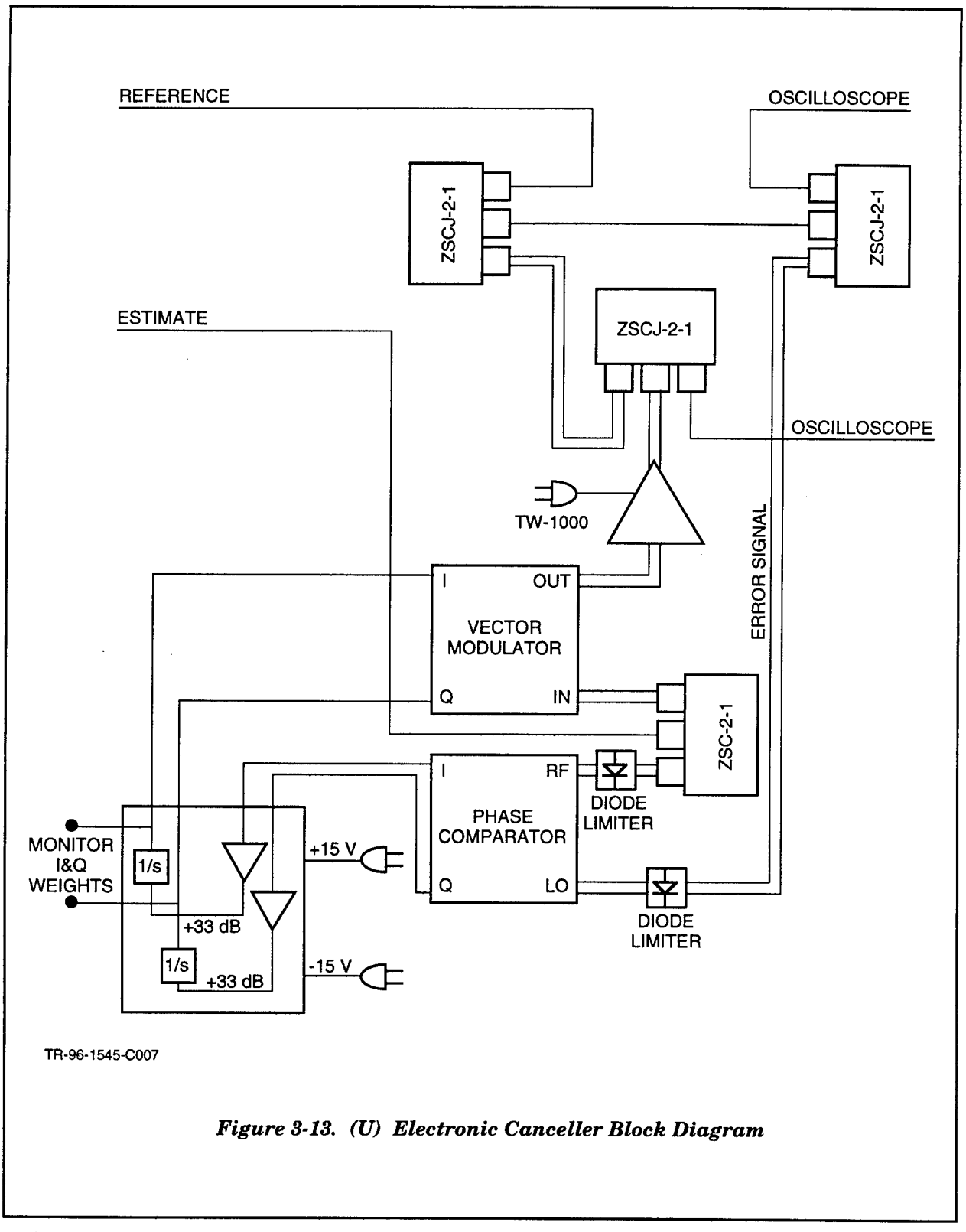

Figure 3-13. (U) Electronic Canceller Block Diagram

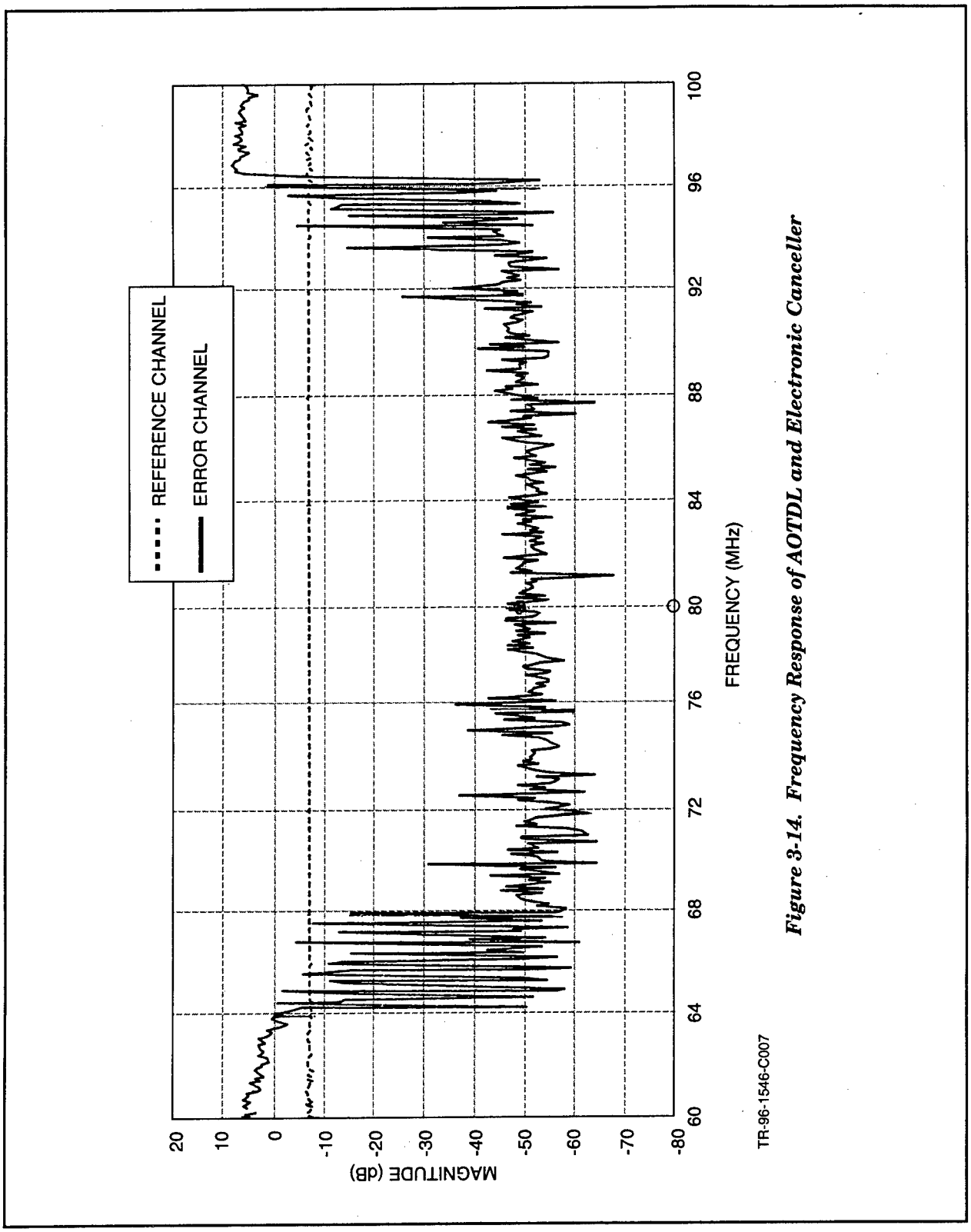

Figure 3-14. Frequency Response of AOTDL and Electronic Canceller

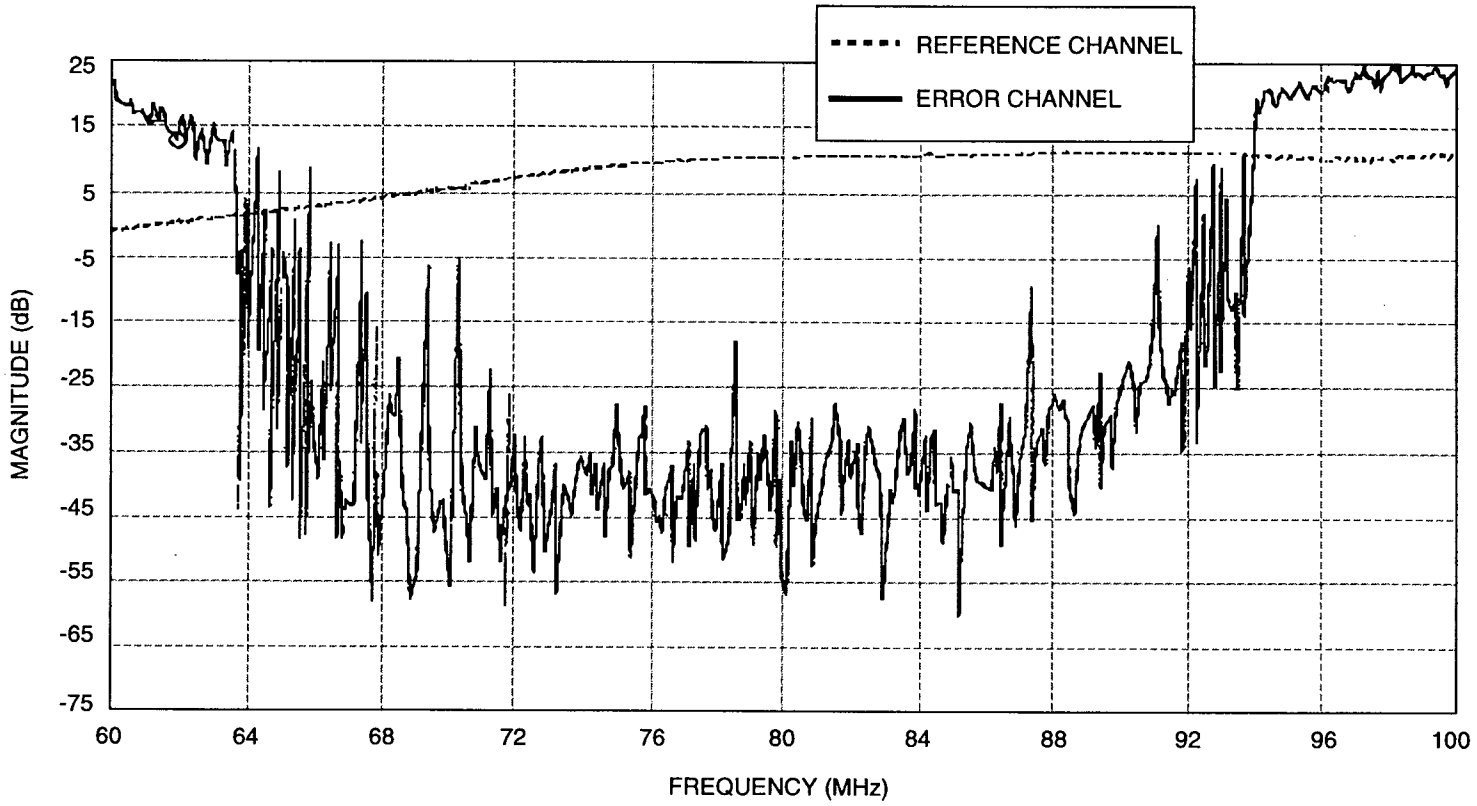

Figure 3-15. (U) Total System Frequency Response

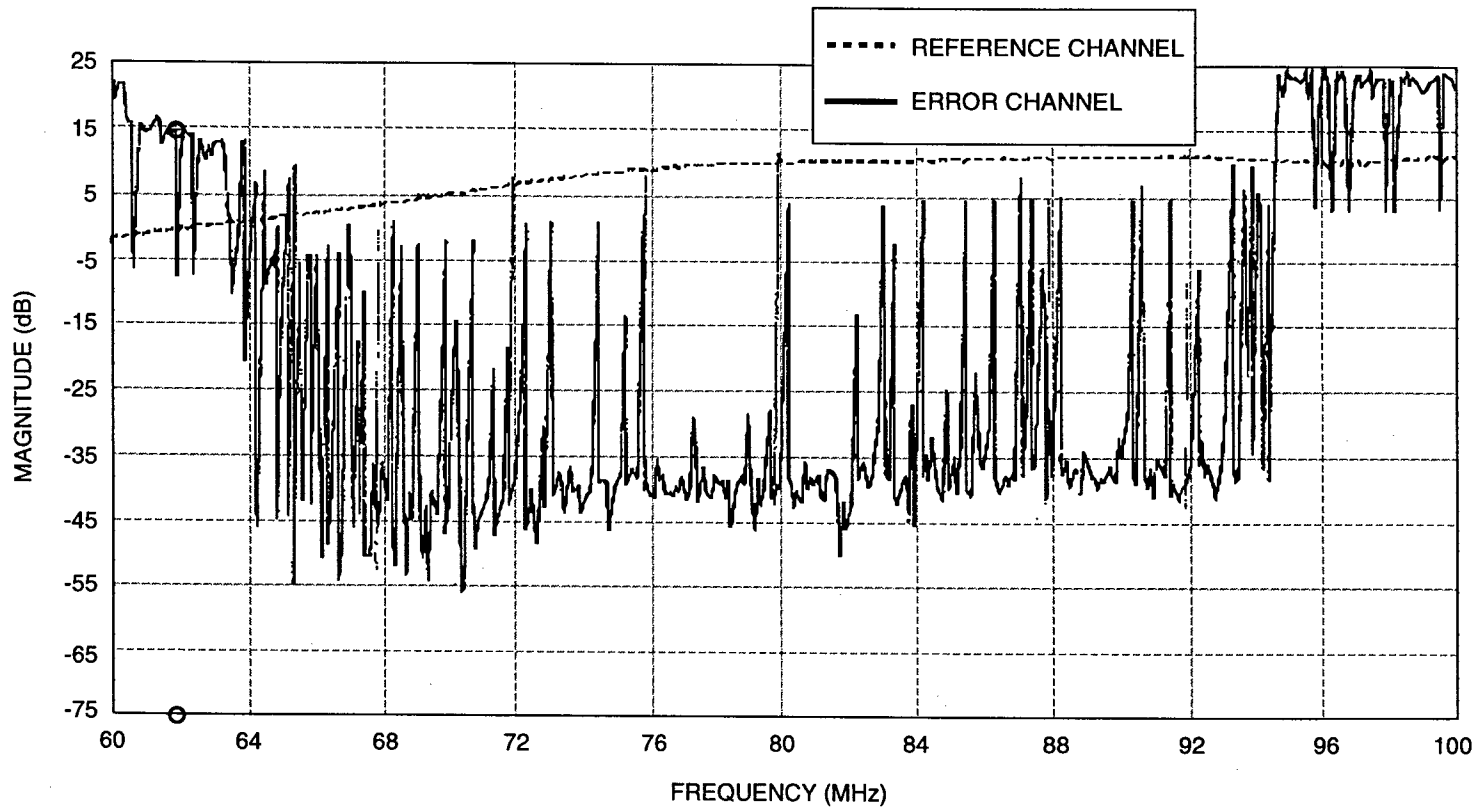

Figure 3-16. Total System Frequency Response With PC Control of Tap Frequency

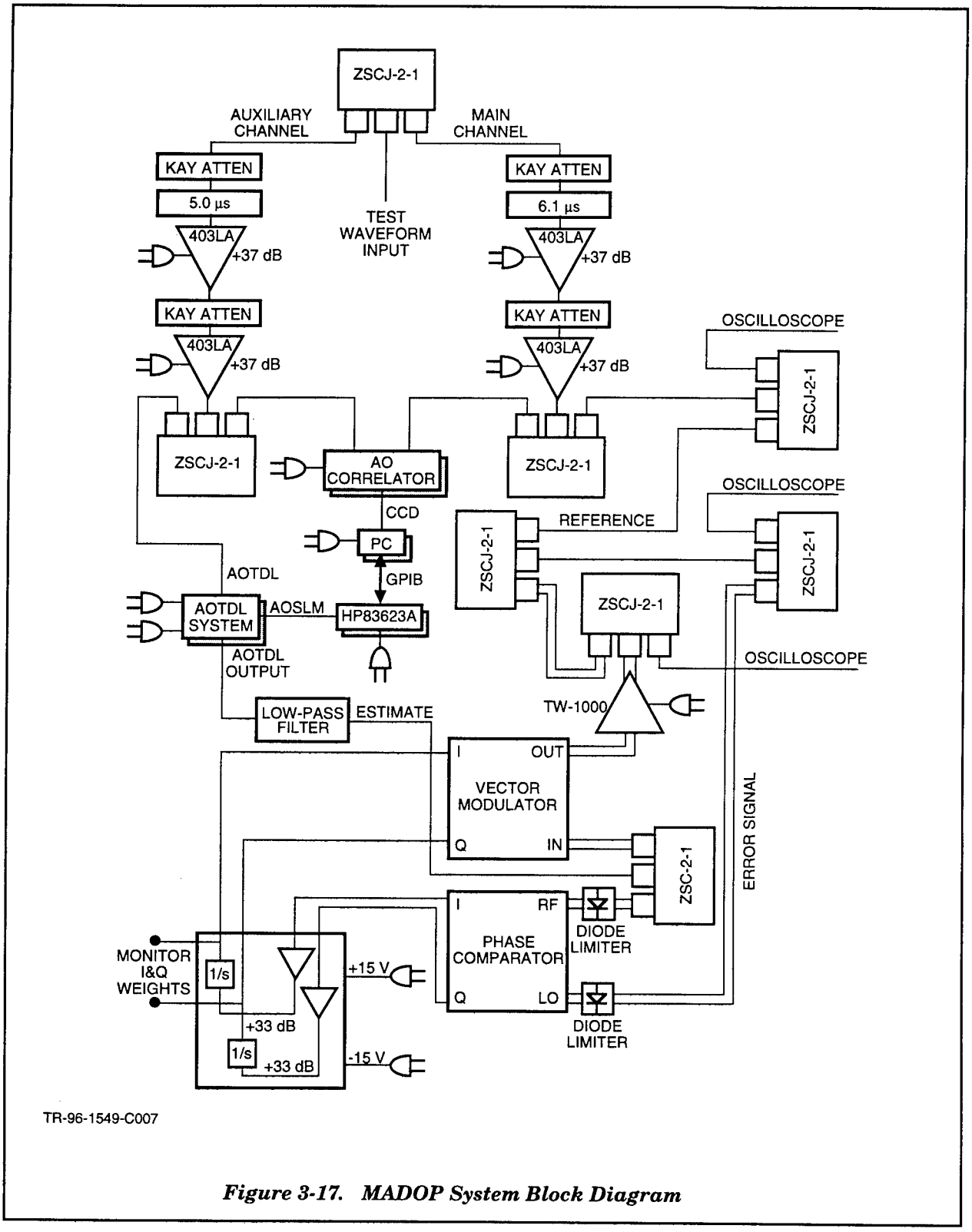

Figure 3-17. MADOP System Block Diagram

developed the PC software but is no longer at RL. Several conversations with Capt. Andrews took place, and progress was made, but more work in this area remains to be done.

During future MADOP test activities, it is recommended that the new Pentium® PC be configured and the software interface be improved, possibly through the use of LABVIEW® instrument control software and MATLAB signal processing software.

4. MADOP SYSTEM TESTING

A major emphasis in this program was the testing of the MADOP under laboratory conditions and while integrated within the C-band radar testbed. Results from the tests are presented in this section.

4.1 INTEGRATION WITH THE C-BAND RADAR TESTBED

The principal thrust of activities during on-site support periods one and three was to interface the MADOP to the RL C-band radar and test the performance of the MADOP using real radar signals. The C-band radar had been identified as a suitable testbed during previous on-site support trips because it possessed most of the features that were needed in the tests. Work under this effort benefitted from the previous C-band radar integration activity performed during August 1994 (see Reference 1).

The RL C-band radar is a phased-array radar that is located very close to the Photonics Laboratory. The antenna can be electronically scanned ±45° in azimuth and from –1° to 8° in elevation and can also employ a 360° mechanical scan. Vertical, horizontal, left-hand circular (LHC), or right-hand circular (RHC) antenna polarizations are supported. The antenna gain is 36 dBi on transmit and 32 dBi on receive. The antenna beamwidth, on both transmit and receive, is approximately 1° in azimuth and 2° in elevation.

The operating frequency of the radar is 5.65 to 5.9 GHz with a nominal value of 5.775 GHz. The transmit power is approximately 200 kW peak and operates at a 1.8% maximum duty cycle with pulsewidths up to 100 μs. The transmitter was not used during the tests of the MADOP because it was deemed inappropriate to attempt to track targets during this phase of testing.

The C-band receiver is full monopulse and also has provisions for eight auxiliary channels. Auxiliary channels are obtained from the eight subarrays of the antenna. The subarrays are formed by dividing the antenna into eight vertical sections as indicated in ***Figure 4-1***. Each subarray has the same elevation beamwidth as the entire array. The azimuth beamwidth is about eight times the array beamwidth (i.e., approximately 8°), and the subarray gain is about one-eighth of the entire array gain. The auxiliary channels of the radar could serve as the auxiliary channels needed by the MADOP.

Three downconversions and three IFs are utilized in the C-band receiver (see ***Figure 4-2***). The first IF is 1265 MHz, the second IF is 592 MHz, and the third IF is 80 MHz. The final bandwidth of the 80-MHz IF is 8 MHz. The sum and difference channels and the eight auxiliary channels have separate IF amplifiers. Furthermore, the outputs of these IF amplifiers are available through 50-Ω BNC connectors. The IF amplifiers are located in the C-band radar control room and are easily

accessible. Outputs from the sum channel and one of the auxiliary channels were used during MADOP testing.

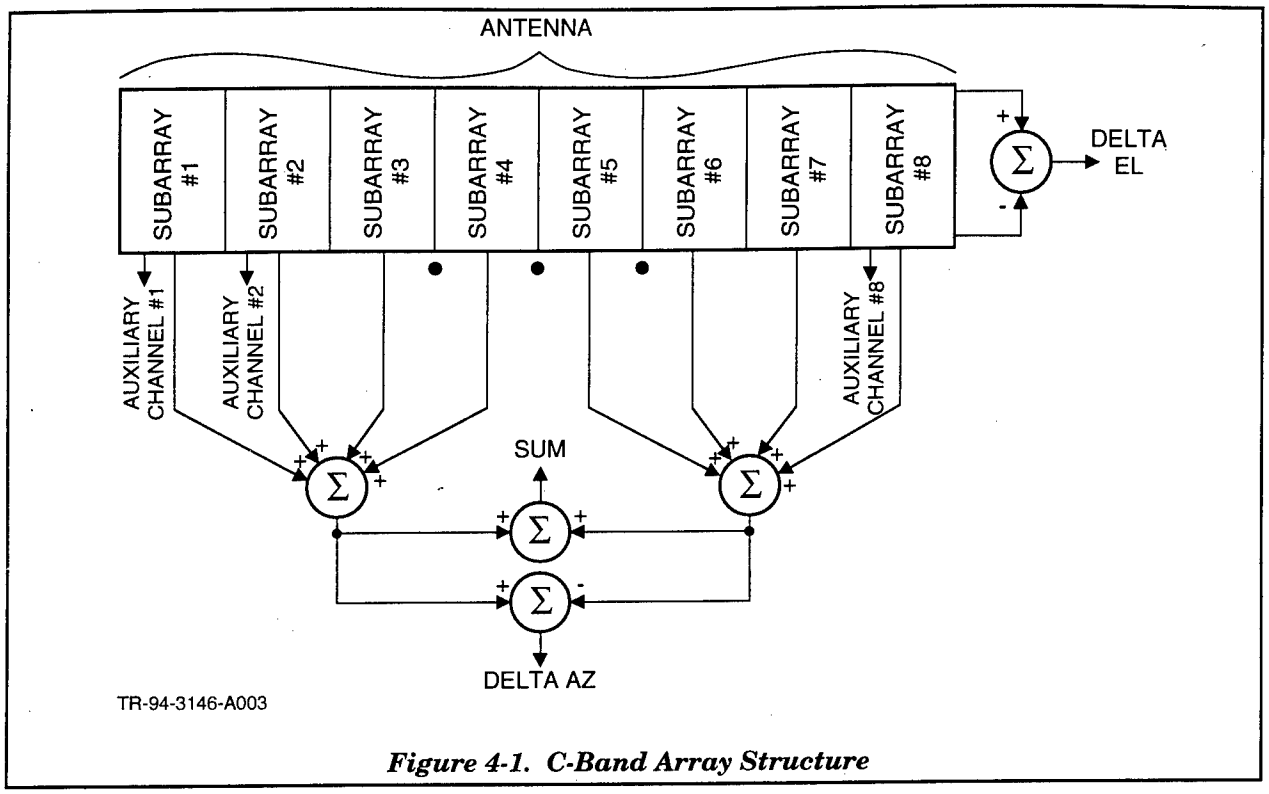

Figure 4-1. C-Band Array Structure

The characteristics of the C-band radar were almost a perfect match for the MADOP. The radar has an IF of 80 MHz and a bandwidth of 8 MHz, both of which are approximately the design parameters of the MADOP. (In fact, the 80-MHz IF used in the MADOP was chosen with the thought of interfacing the MADOP to the C-band radar.) The radar has the capability of supplying the main and auxiliary channels that would be needed by the MADOP, and these signals are easily accessible. Also, the C-band control room had space to accommodate the MADOP and the prime power needed to drive it.

There are two remote test signal sources associated with the C-band radar that can be used to generate the target and jammer signals that are needed to test the MADOP. These sources can be independently controlled and are able to generate CW, pulsed, and noise signals. A third antenna, normally used for the S-band radar, was converted to C-band to allow transmission from a greater angular separation. This third source provides only a CW signal, but can be fed with the signal from another of the C-band antennas. The sources are located about 6500 ft from the radar and are each separated by about 65 ft (see ***Figure 4-3***). This provides an azimuth angular separation of about 0.58°

between adjacent sources and 1.16° between the two antennas with widest separation. The C-band sources can be controlled from the C-band radar control room and can be synchronized with the radar timing signals. The converted S-band antenna is not controllable from the C-band radar control room.

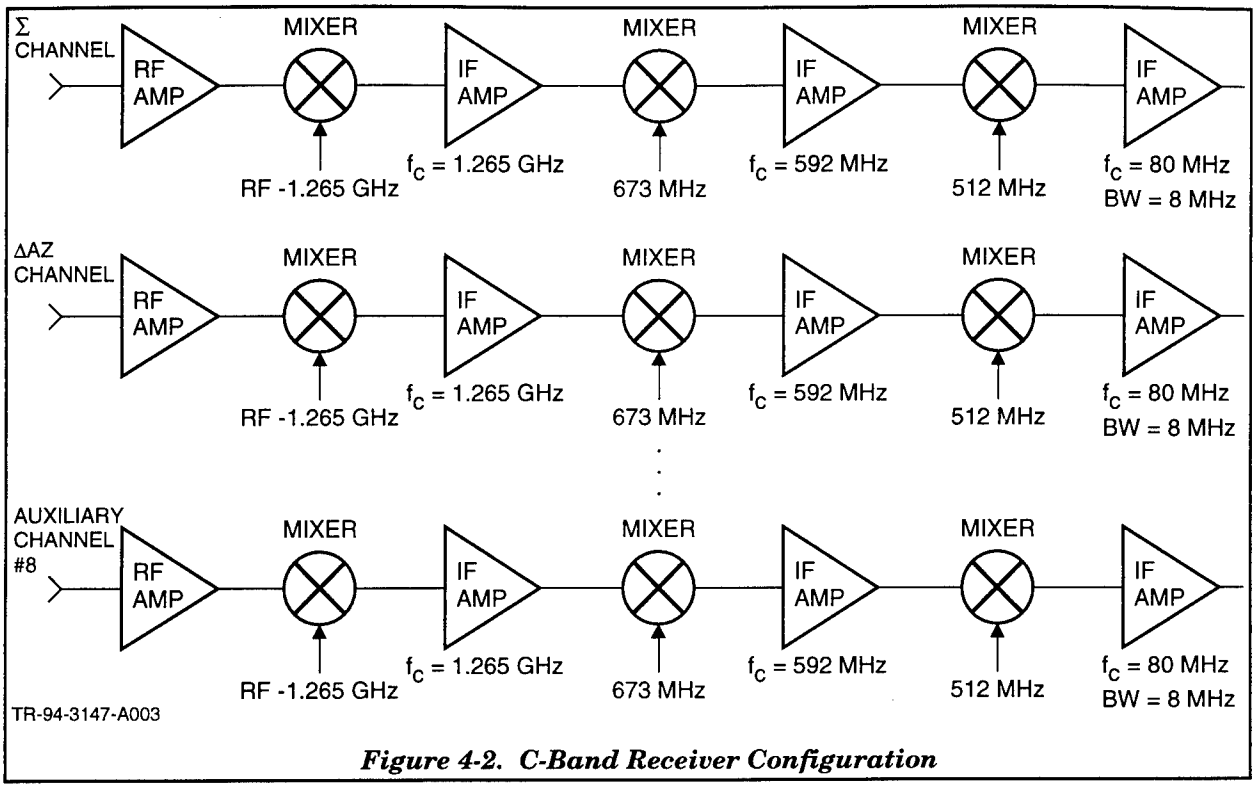

Figure 4-2. C-Band Receiver Configuration

4.2 C-BAND RADAR TESTING: ON-SITE SUPPORT PERIOD ONE

During on-site support period one, Dynetics worked with RL personnel to integrate the MADOP hardware and test instrumentation with the C-band radar testbed hardware for a second phase of testing (see Reference 1 for the first phase of C-band radar testing). The results of the testing are summarized below. During this testing, the Mach-Zehnder AO correlator architecture was employed, and full closed loop-operation was achieved. The hardware setup is shown in ***Figure 4-4***. Cancellation on the order of 25 to 30 dB for narrowband jamming and 10 to 15 dB for wideband jamming was achieved routinely. The test matrices for on-site support periods one and three are contained in Appendices A and B, respectively.

Figure 4-5 shows an example of a preliminary test using laboratory-generated signals. A 1-μs pulse with a 10-μs pulse repetition frequency (PRI) represented the radar target return, and a

tone jammer was inserted. ***Figure 4-6*** shows the resultant spectrum in the main channel. The auxiliary channel had negligible signal level, demonstrating about 15 dB of cancellation in this case. ***Figure 4-7*** shows each of these signals, plus the auxiliary channel tone signal. It is apparent from this figure that the MADOP processor was able to pull out the pulsed signal from the main channel jammed signal. ***Figures 4-8 through 4-10*** show a similar example with a 100-ns pulse and a 1-μs PRI. The S/J improvement in this case was approximately 28 dB.

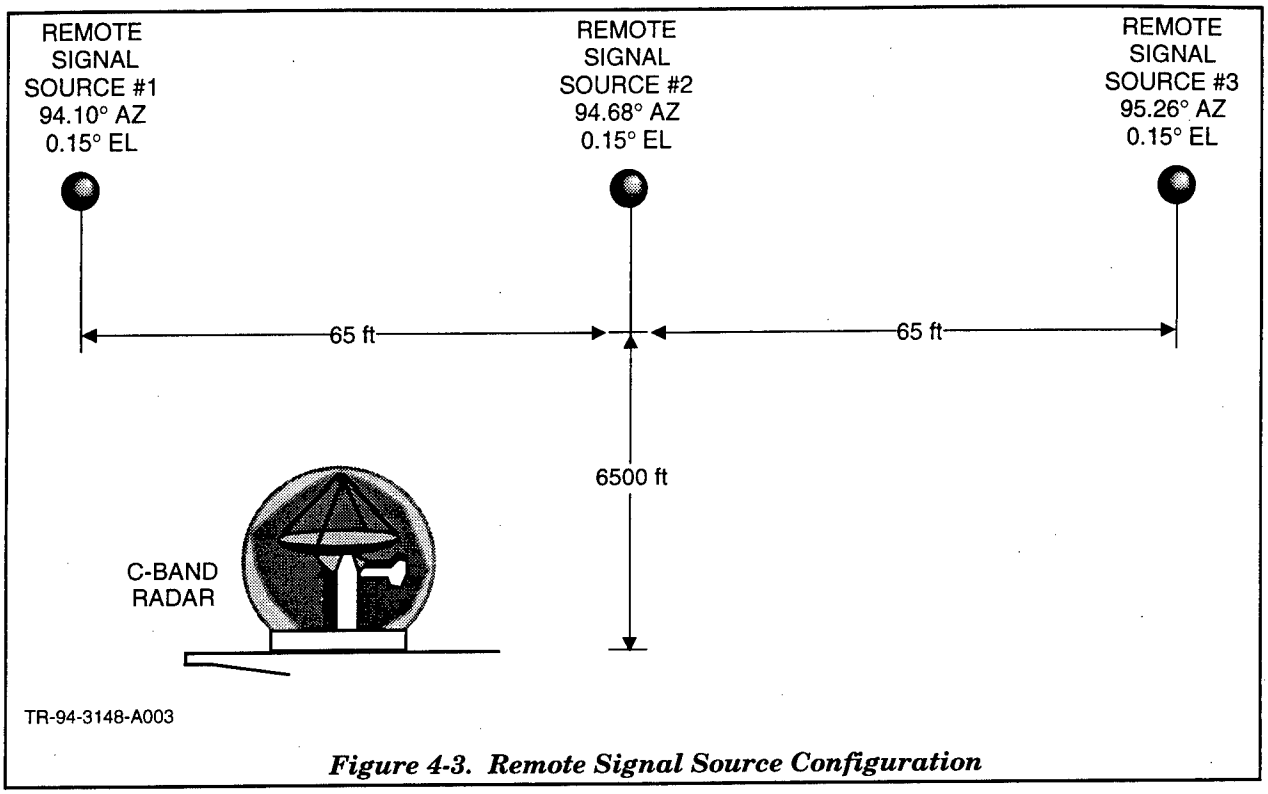

Figure 4-3. Remote Signal Source Configuration

Cancellation of wideband noise was also performed with laboratory signals, as shown in ***Figures 4-11 through 4-13***. For this case, computer control of the HP83623A synthesizer was used to place the tap at the appropriate delay. The frequency was selected as a function of pixel location according to the equation:

$$f = 60 \text{ MHz} + 0.02 \text{ MHz/pixel} * \text{pixel location.} \quad (4\text{-}1)$$

The frequency offset and rate were selected to match the correlator window to the AOTDL window. The main channel signal is shown in ***Figure 4-11***, where it can be seen that the desired pulsed signal is obscured. After cancellation, the pulse emerges in the spectrum shown in ***Figure 12***, and is easily found in the time-domain displays of ***Figure 4-13***. The S/J improvement in this case was approximately 20 dB.

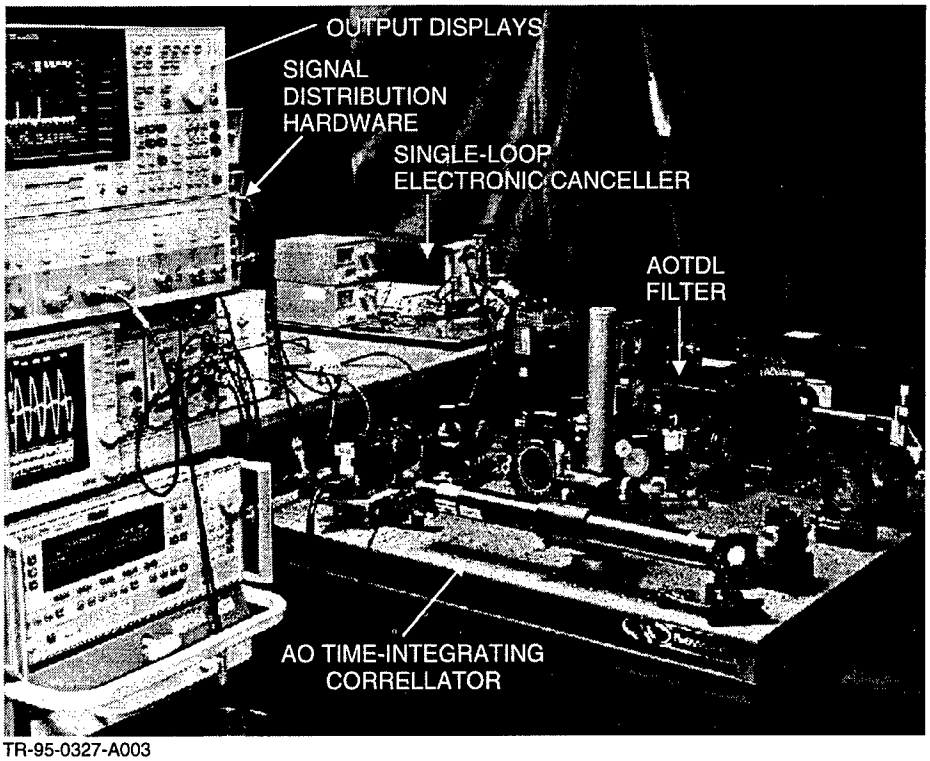

TR-95-0327-A003

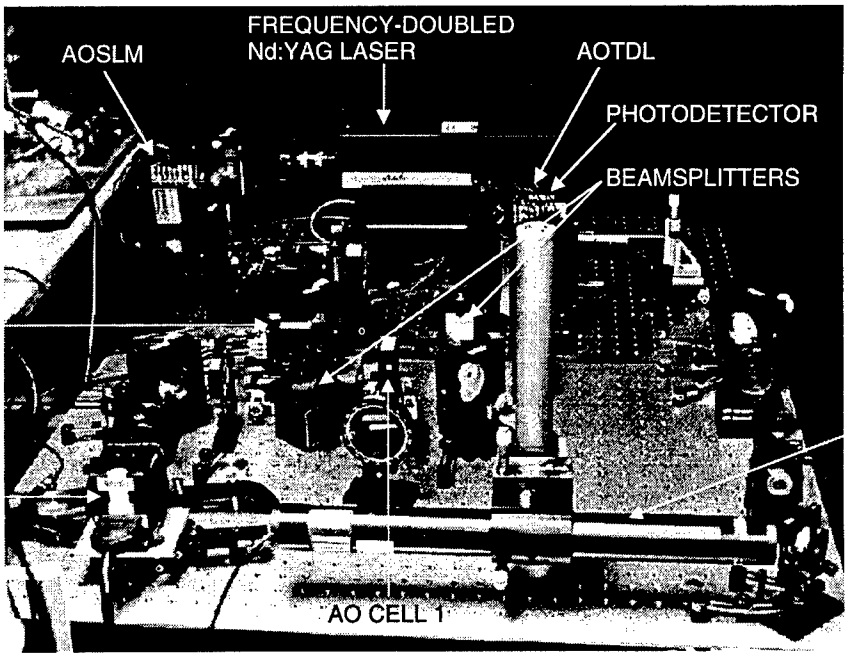

TR-95-0326-A003

Figure 4-4. MADOP AO Subsystems at the C-Band Radar Test Facility

After preliminary testing with laboratory signals, the jammer signals were turned on and testing began with the C-band radar testbed. The two jammers employed were the C-band jammer at 94.1° and the converted S-band jammer at 95.26°. For ***Figures 4-14 through 4-19***, the tap was set via computer control according to Equation 4-1. ***Figures 4-14 and 4-15*** show the results for a tone jammer and a tone signal with a –7-dB S/J ratio in the main channel. The adapted signal shows an S/J improvement of approximately 32 dB, but does have an intermodulation product term that arises due to processor nonlinearities. ***Figures 4-16 and 4-17*** show the same test but with a noise jammer and a tone signal (–9-dB S/J ratio in the main channel). The spectral weighting of the noise waveform occurs in the C-band radar testbed receiver, which has an 8-MHz bandwidth. The S/J improvement for this case was approximately 13 dB. A similar test with an 11-dB S/J ratio in the main channel is shown in ***Figures 4-18 and 4-19***. In this case, the S/J improvement was approximately 10 dB.

Following testing with various noise and tone power ratios, multipath cancellation was attempted. In order to prepare for this testing, the AOTDL system was characterized for two and three taps. ***Figures 4-20 through 4-25*** show the results of this testing. ***Figures 4-20, 4-22, and 4-24*** show the spectrum for each of the AOTDL tap weight inputs, and ***Figures 4-21, 4-23 and 4-25*** show the frequency response of the AOTDL for each set of taps. ***Figures 4-21 through 4-23*** show that the spacing of the taps changes the notch frequencies and spacing between notches in the frequency response plots. This is because the transfer function (Fourier transform of the impulse response) for an FIR tapped delay line with two taps is a sinusoid whose magnitude appears to have notches (zeros) at twice the period of the sinusoid. ***Figures 4-24 and 4-25*** show the frequencies input to the AOSLM and the frequency response for the more complex three-tap filter. One of the key challenges of future hardware testing is the phase alignment of each of these taps to allow correct estimation of the jammer signal.

At this point, multipath testing was performed with laboratory signals. ***Figures 4-26 through 4-28*** show the results for the cancellation of a pulsed jammer that has experienced both a direct-path and multipath transmission to the receiver, with a time separation of 100 ns. The cancellation ratio was approximately 15 dB, but no S/J improvement was measured since this test was done without a simulated target signal. ***Figure 4-28*** shows the oscilloscope plot of the main channel, the estimate, and the cancelled signal. We see that, by aligning the overlap of the pulses correctly in the estimate (formed by tapping the auxiliary), the envelope and phase of the jammer signal can be estimated, and effective cancellation can be achieved.

4.3 C-BAND RADAR TESTING: ON-SITE SUPPORT PERIOD THREE

As mentioned in Section 3, during the third period of on-site support, additional enhancements were made to the integrated MADOP system. System improvements to the electronic

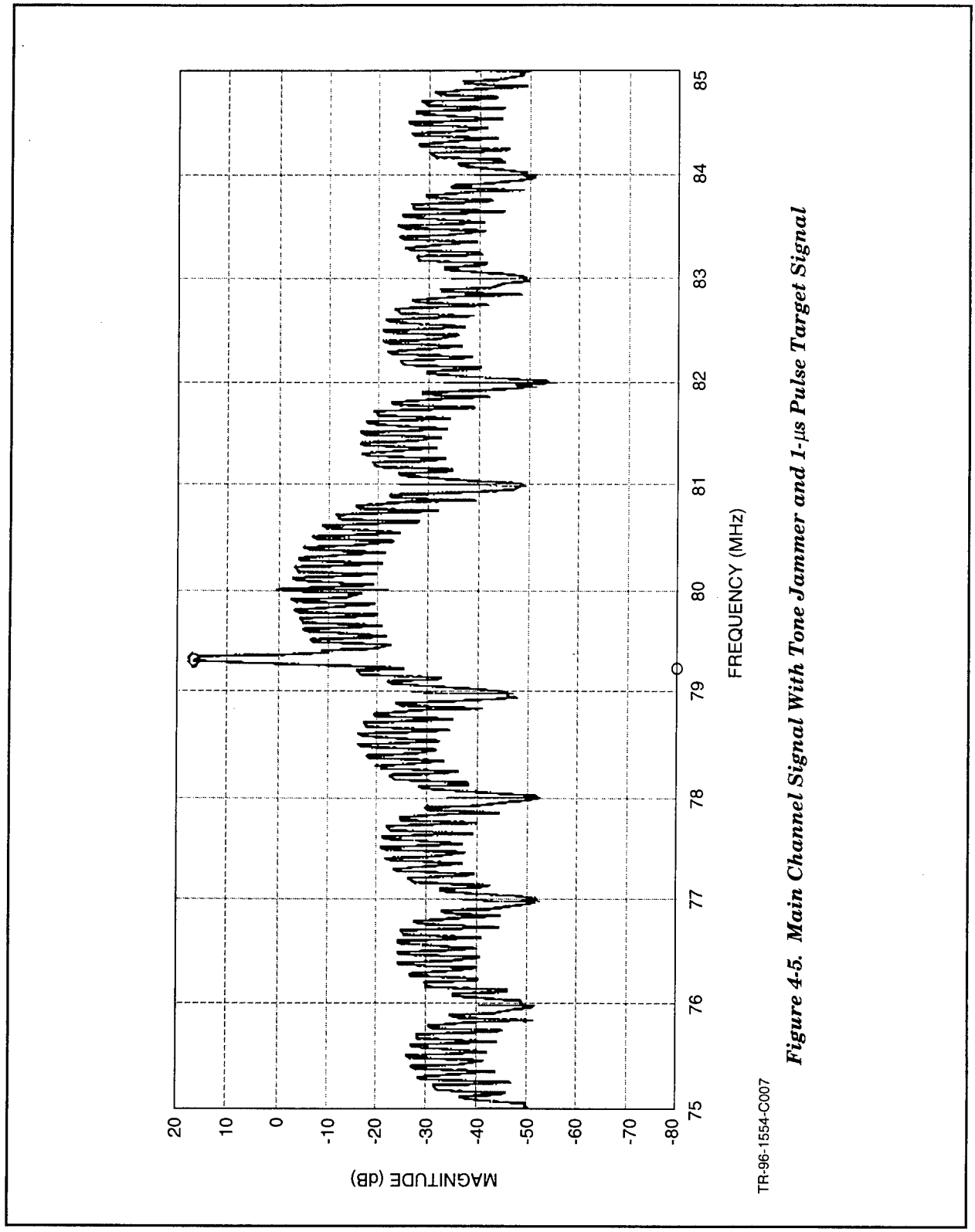

Figure 4-5. Main Channel Signal With Tone Jammer and 1-μs Pulse Target Signal

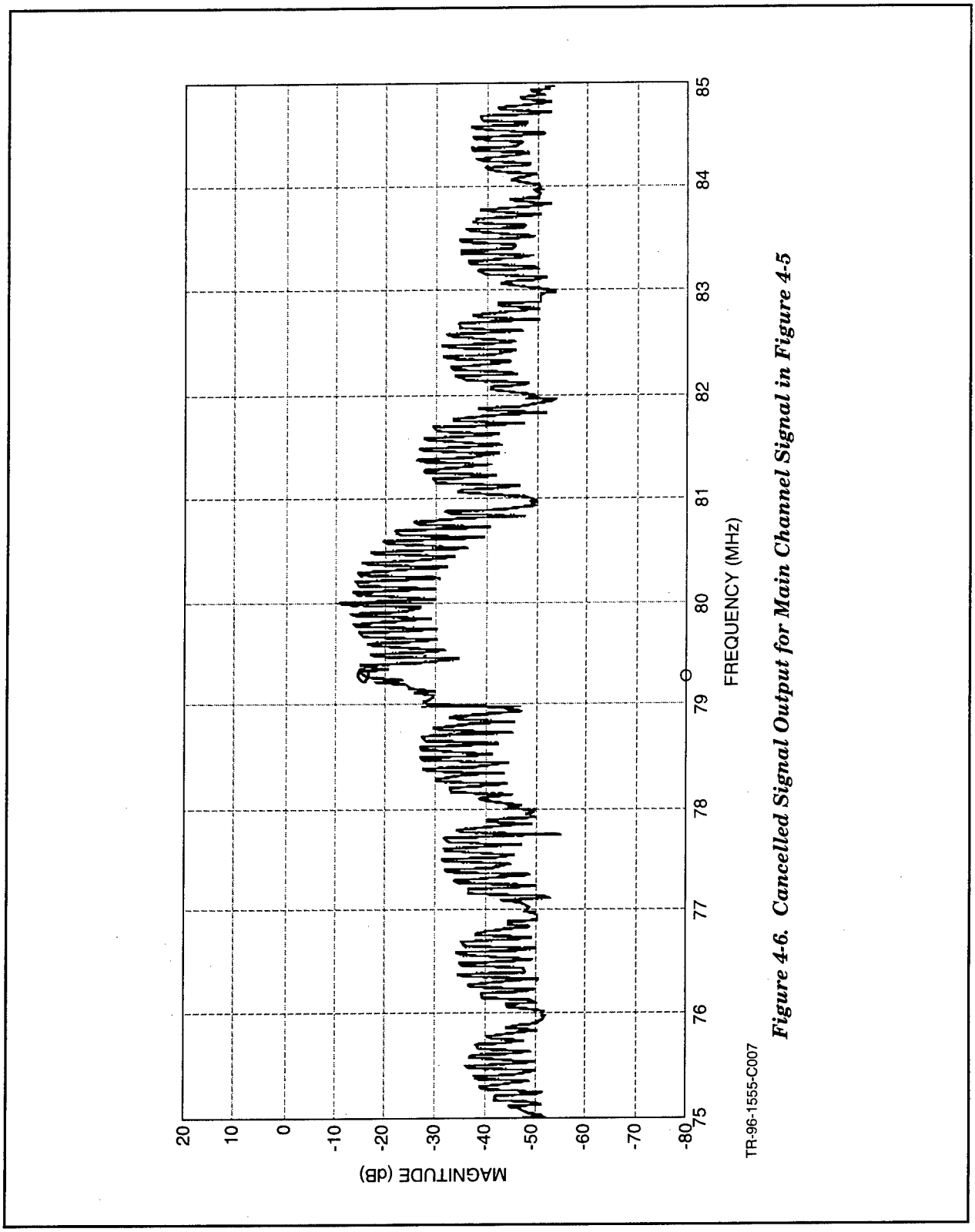

Figure 4-6. Cancelled Signal Output for Main Channel Signal in Figure 4-5

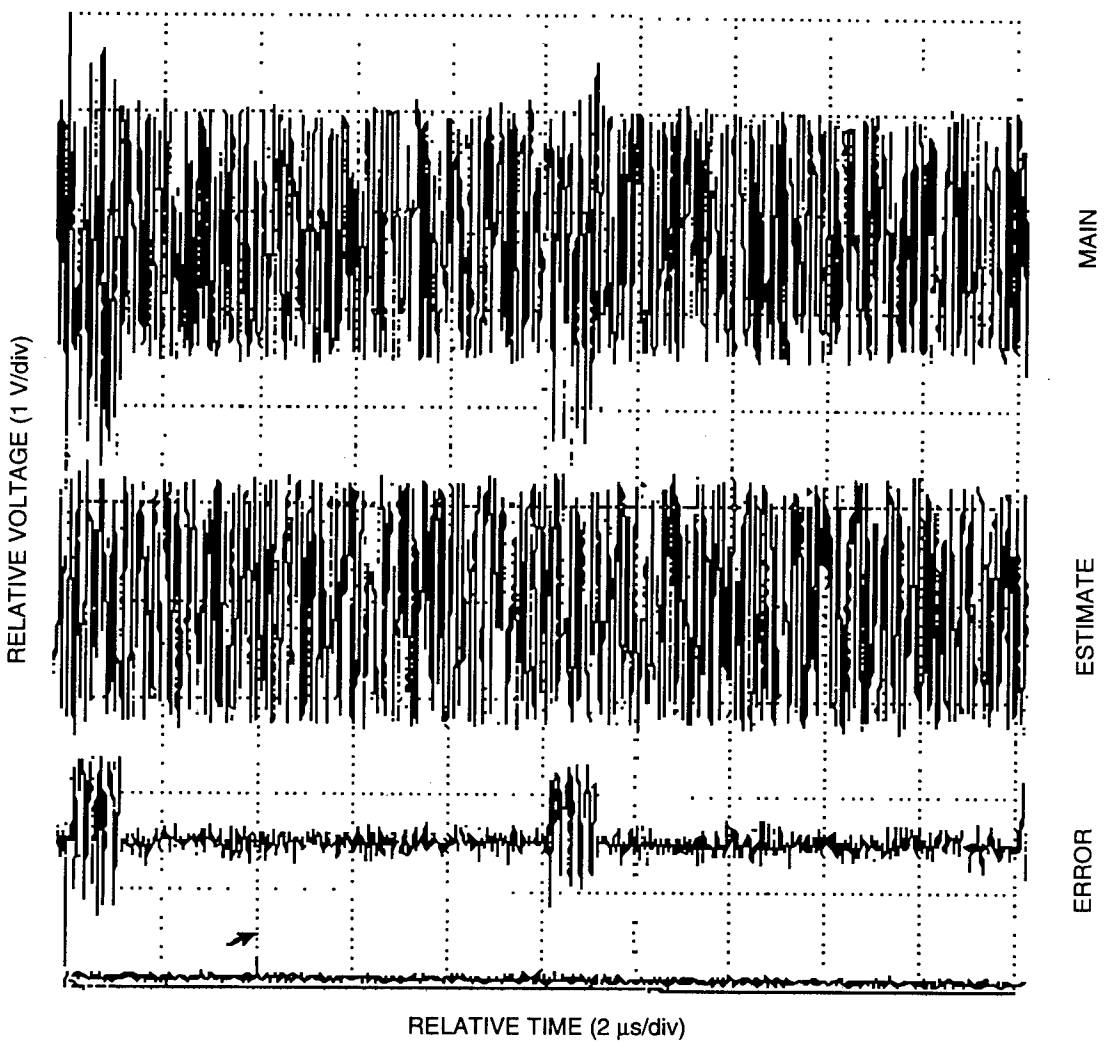

Figure 4-7. Oscilloscope Traces for Main Channel Signal in Figure 4-5

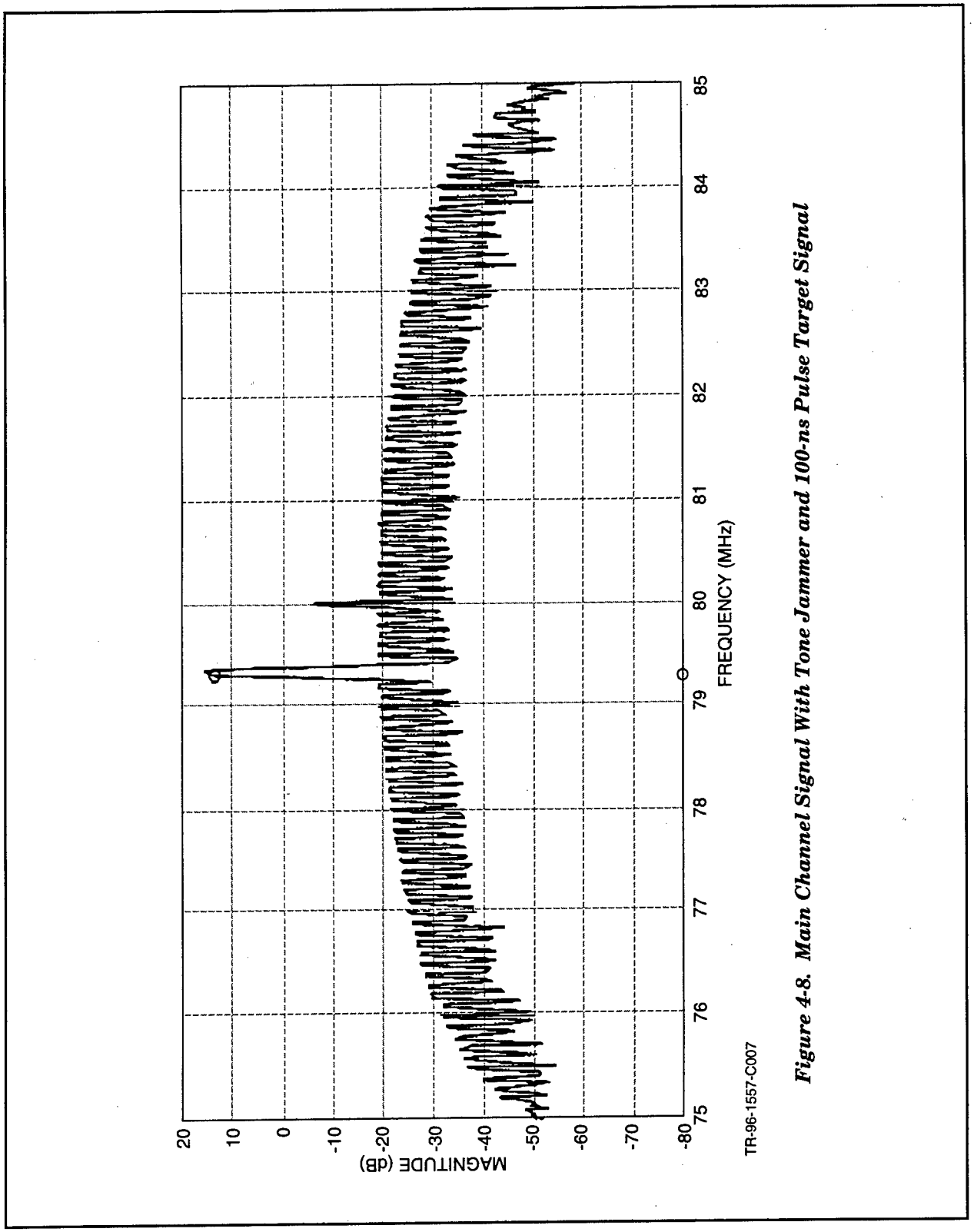

Figure 4-8. Main Channel Signal With Tone Jammer and 100-ns Pulse Target Signal

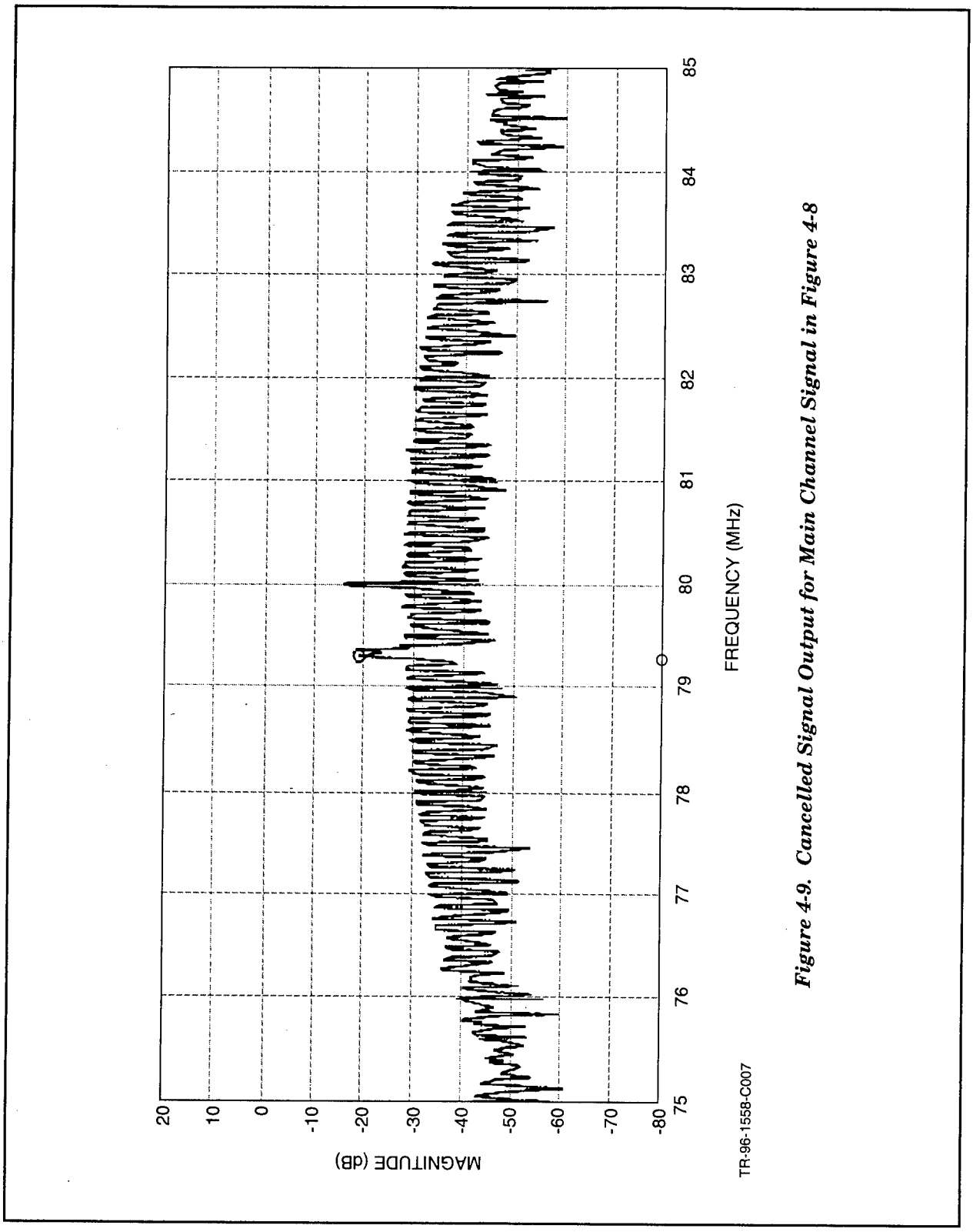

Figure 4-9. Cancelled Signal Output for Main Channel Signal in Figure 4-8

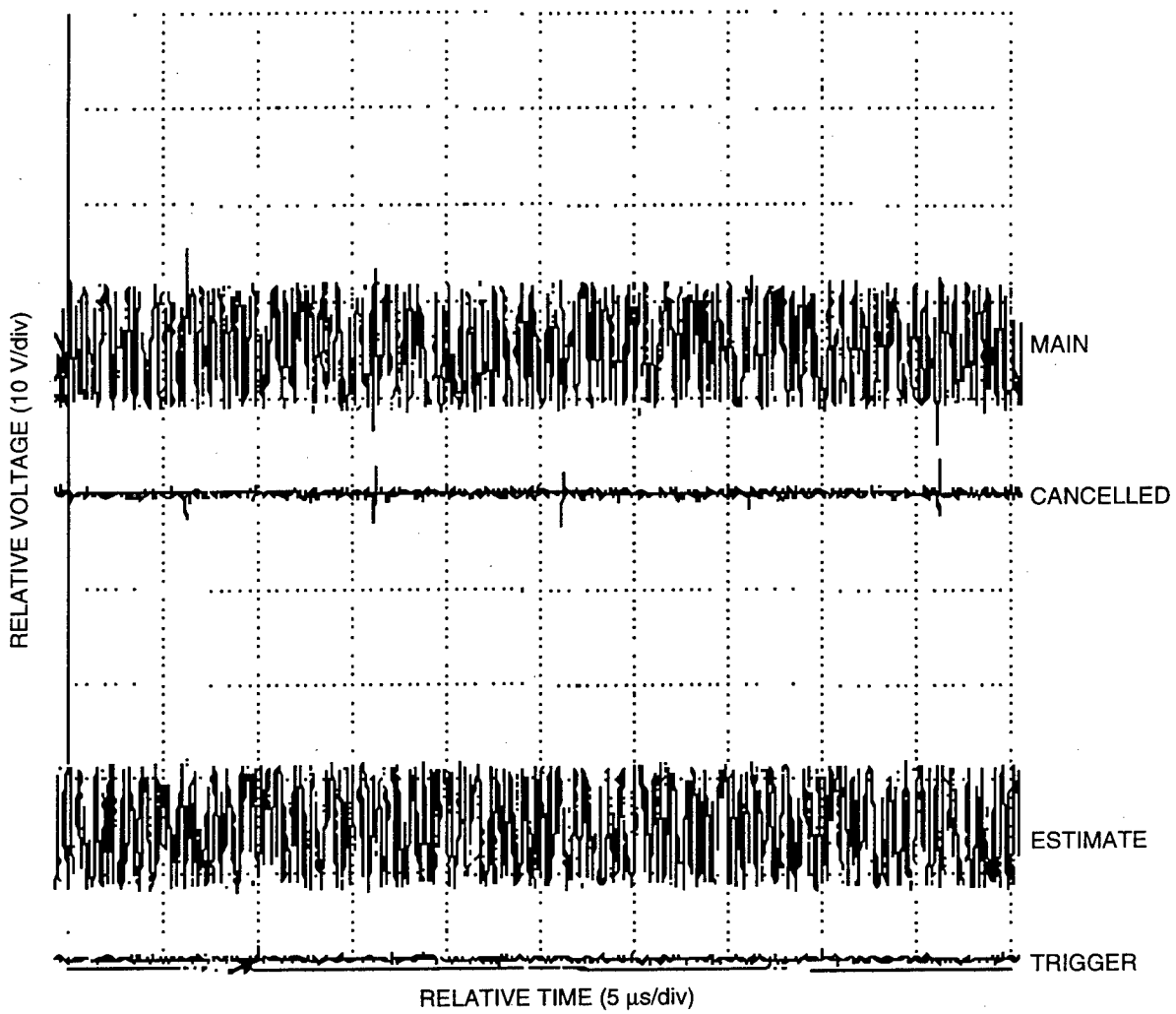

Figure 4-10. Oscilloscope Traces for Main Channel Signal in Figure 4-8

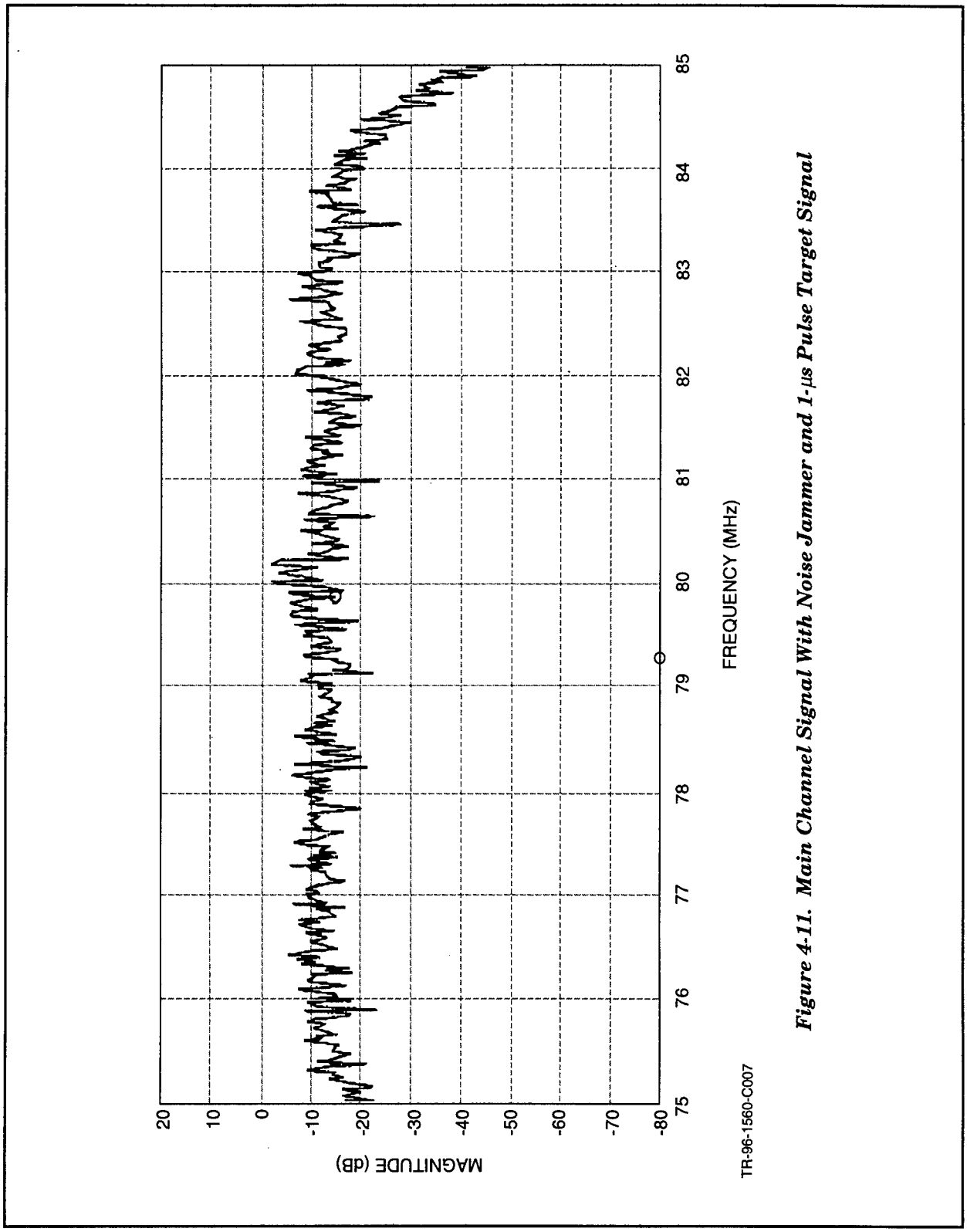

Figure 4-11. Main Channel Signal With Noise Jammer and 1-μs Pulse Target Signal

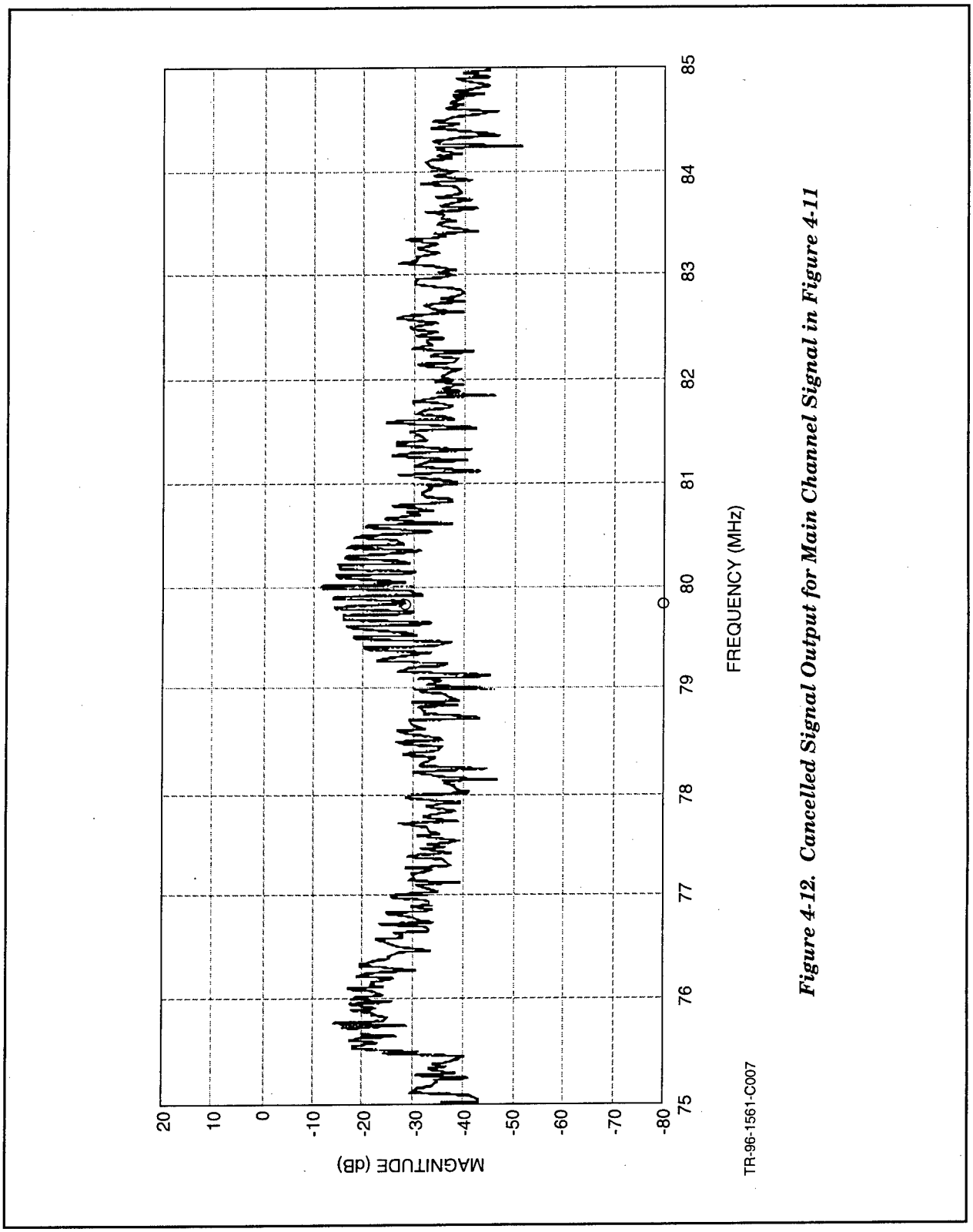

Figure 4-12. Cancelled Signal Output for Main Channel Signal in Figure 4-11

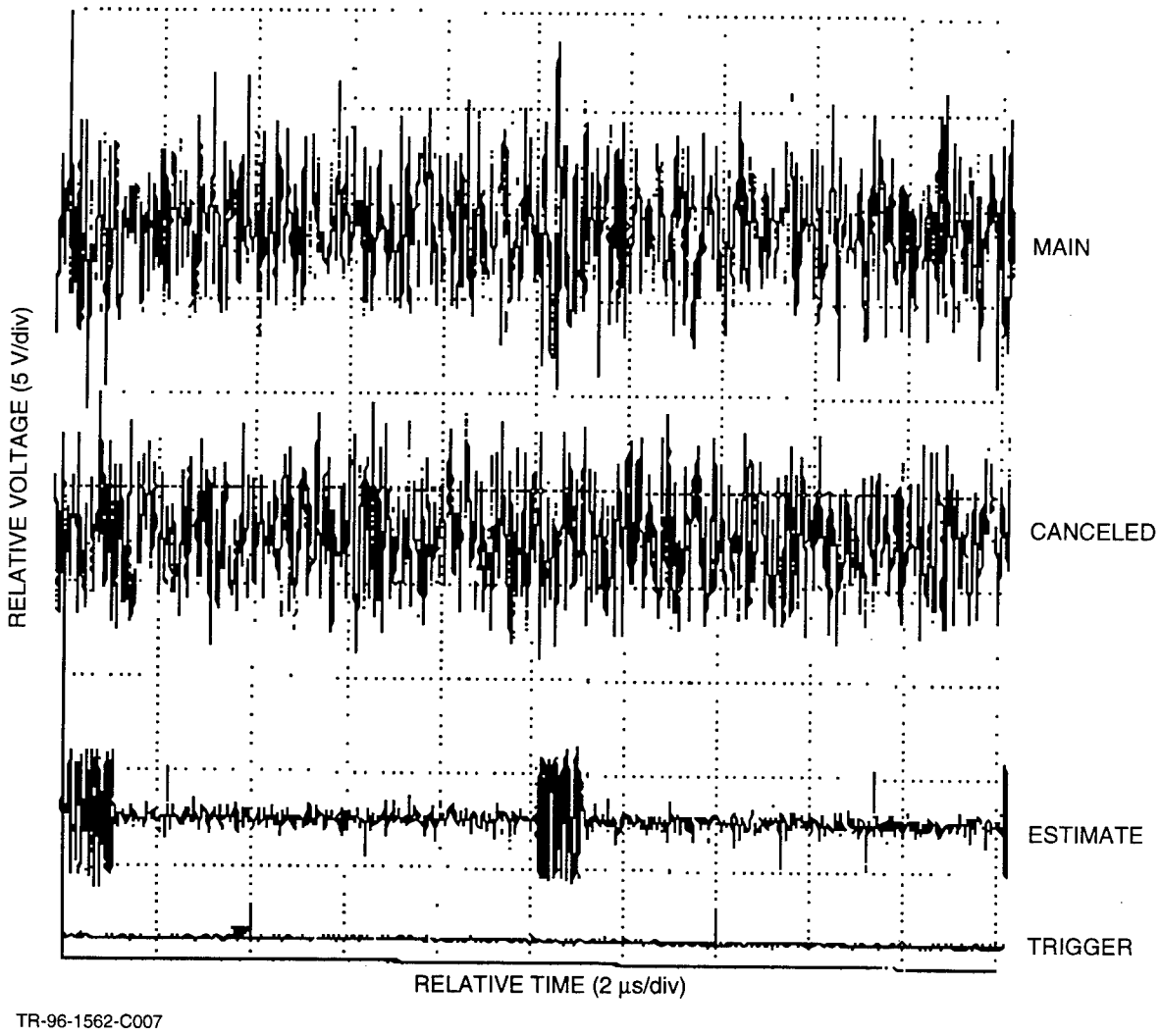

Figure 4-13. Oscilloscope Traces for Main Channel Signal in Figure 4-11

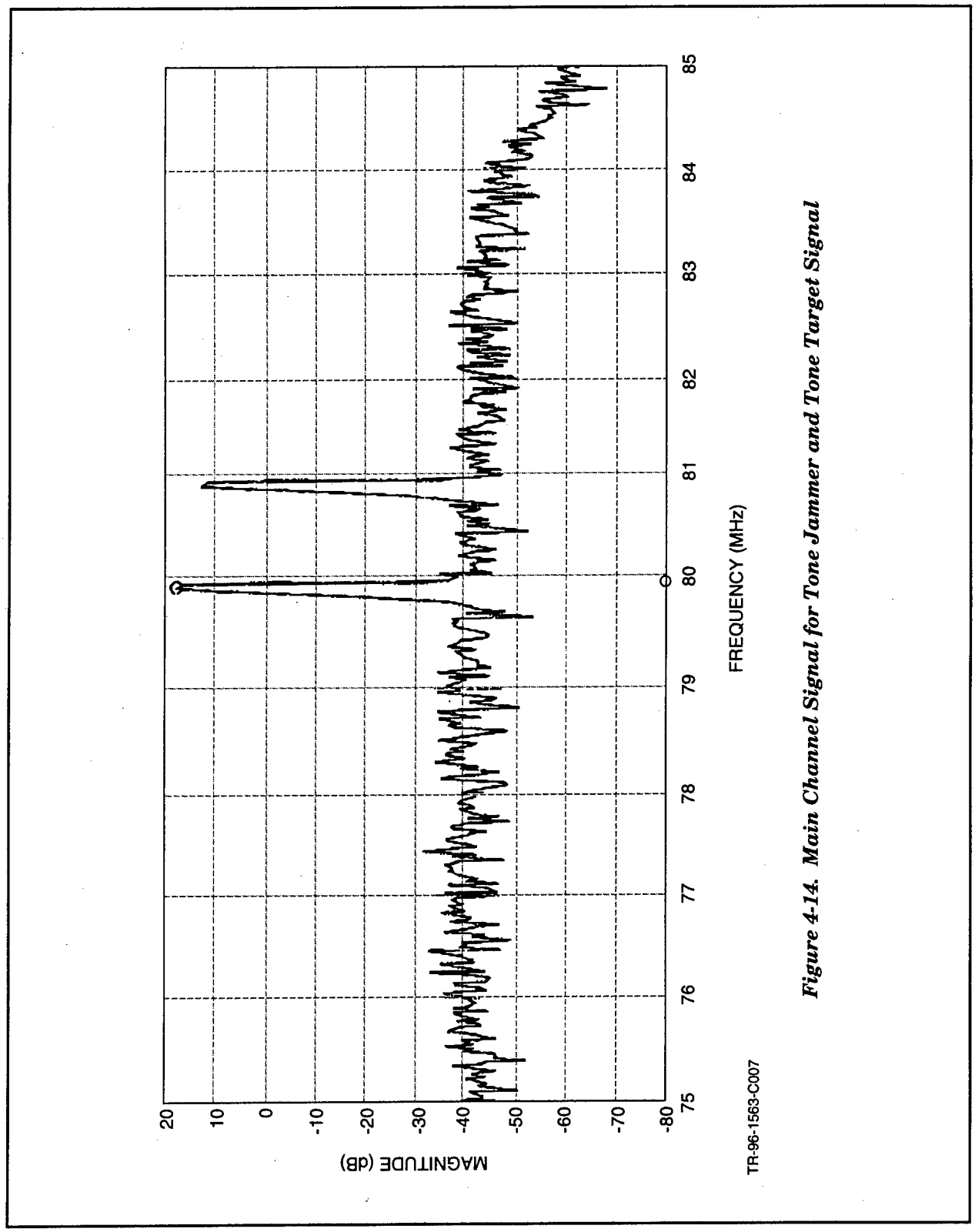

Figure 4-14. Main Channel Signal for Tone Jammer and Tone Target Signal

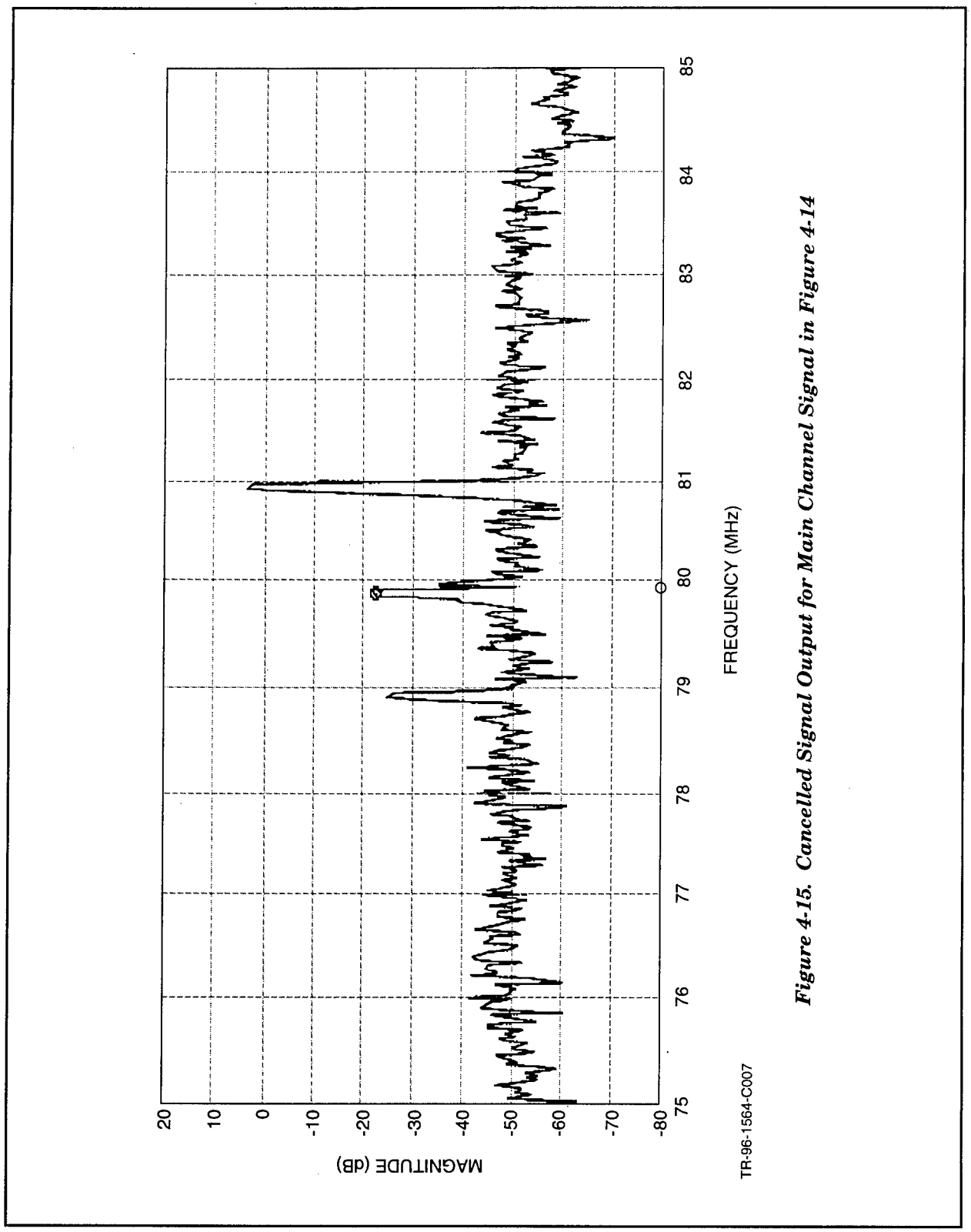

Figure 4-15. Cancelled Signal Output for Main Channel Signal in Figure 4-14

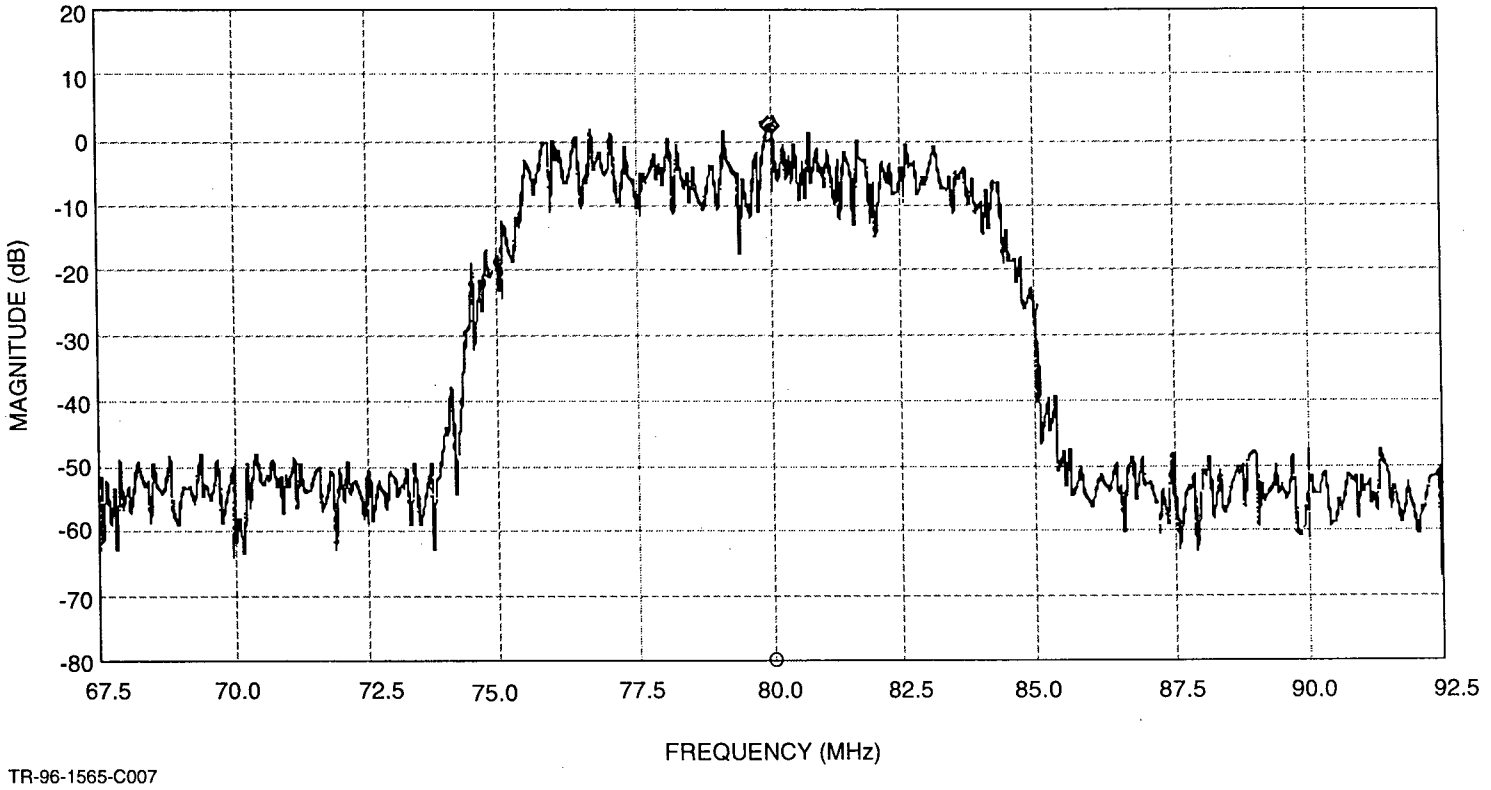

Figure 4-16. Main Channel Signal With Noise Jammer and Tone Target Signal

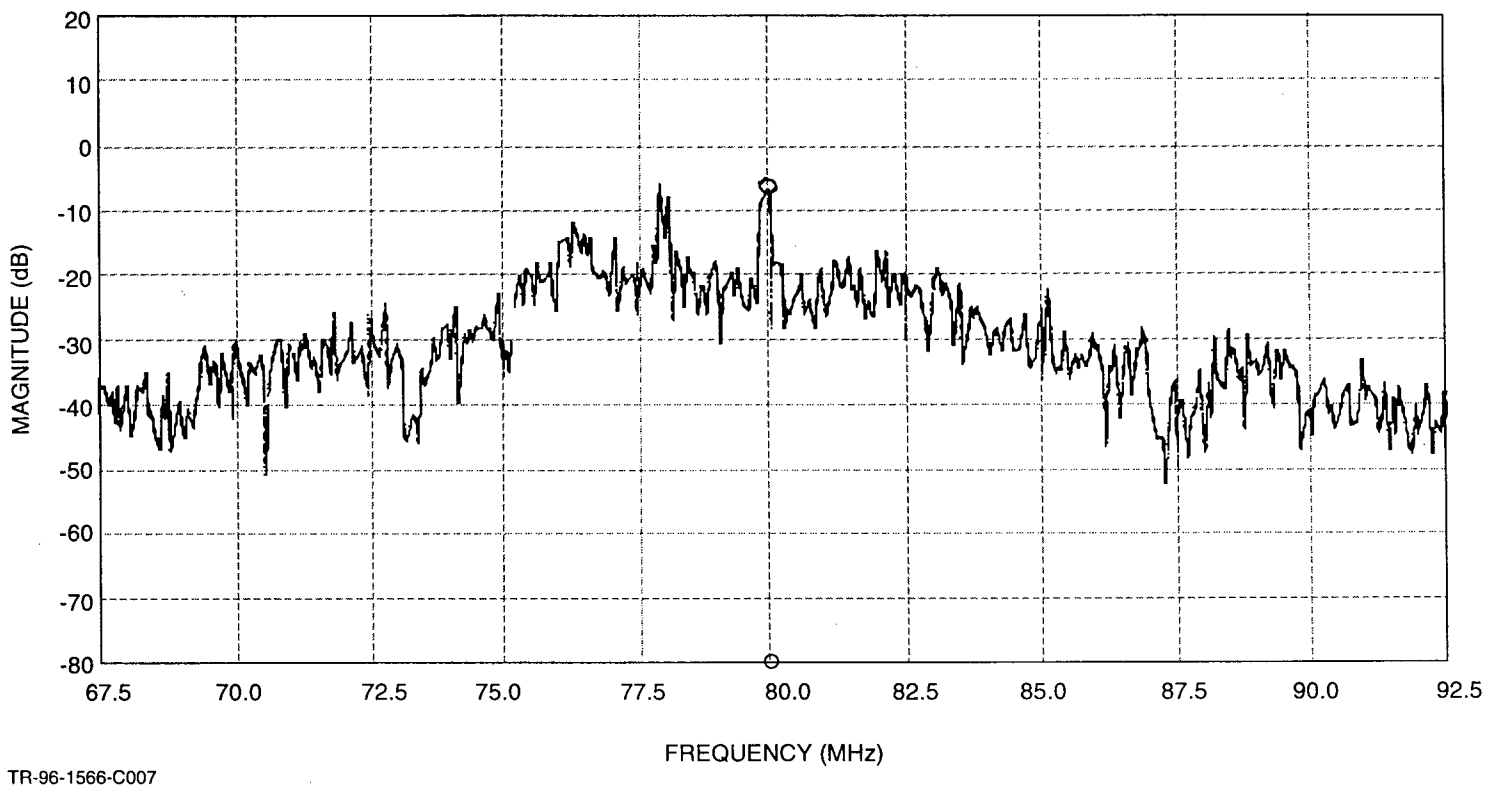

Figure 4-17. Cancelled Signal Output for Main Channel Signal in Figure 4-16

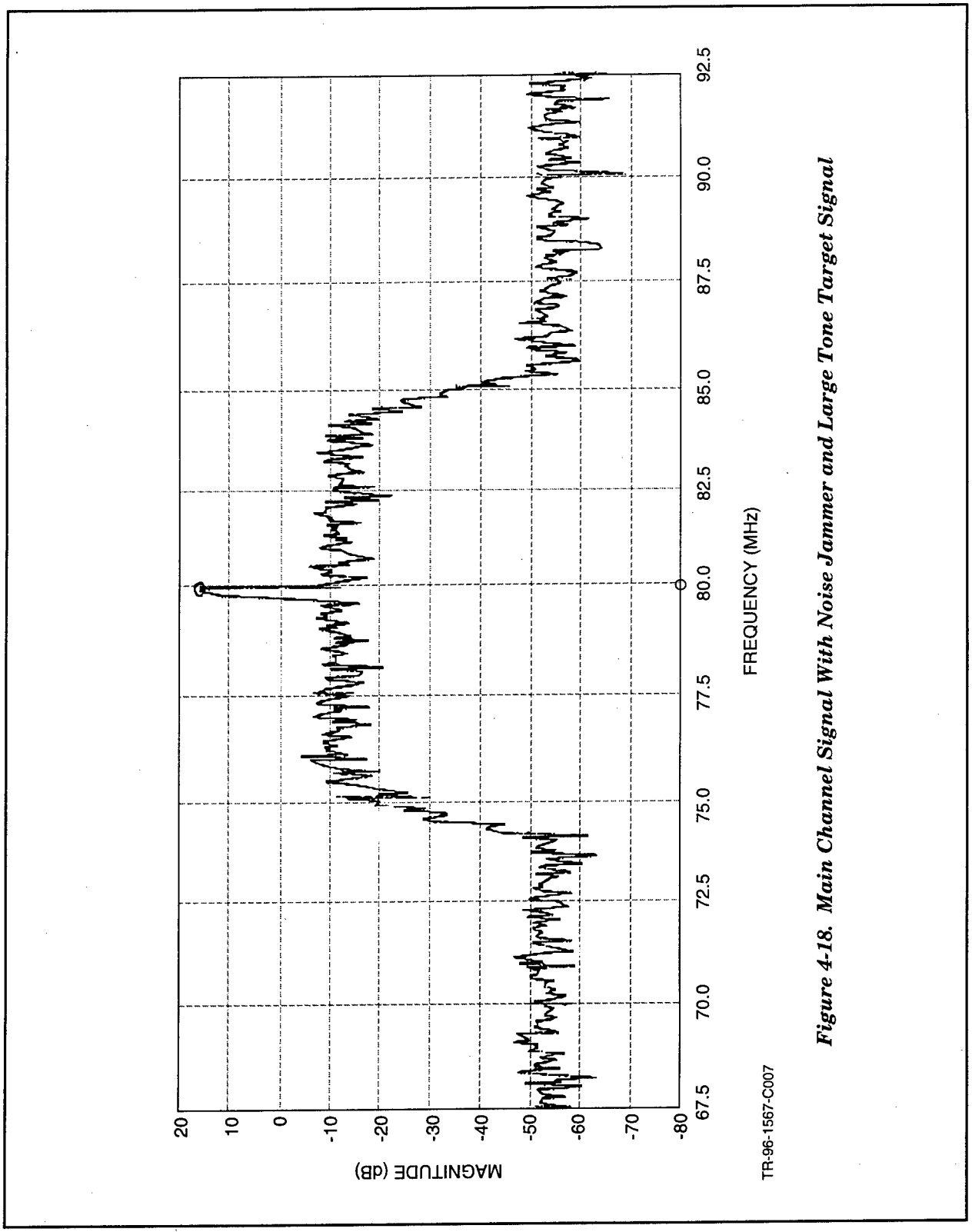

Figure 4-18. Main Channel Signal With Noise Jammer and Large Tone Target Signal

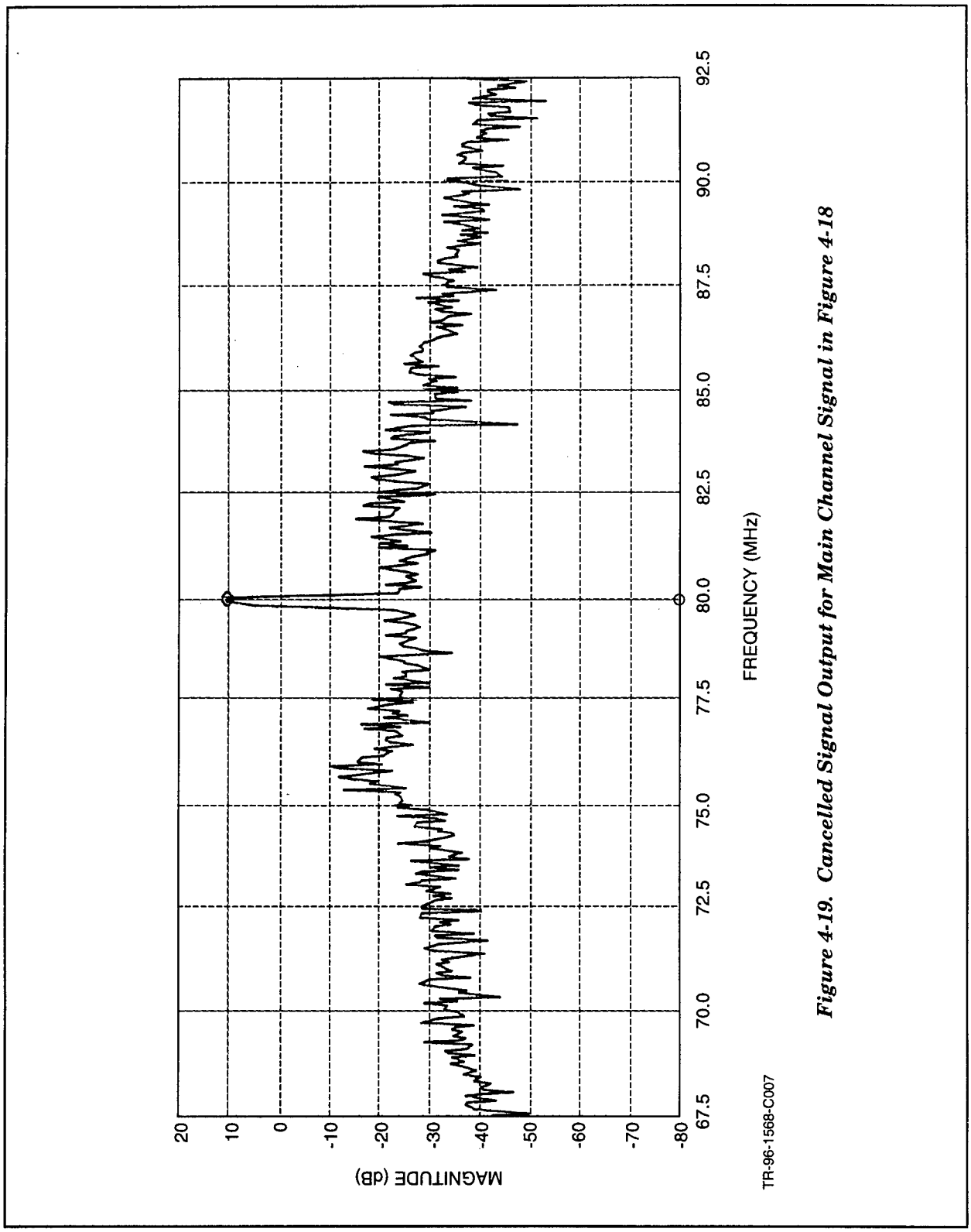

Figure 4-19. Cancelled Signal Output for Main Channel Signal in Figure 4-18

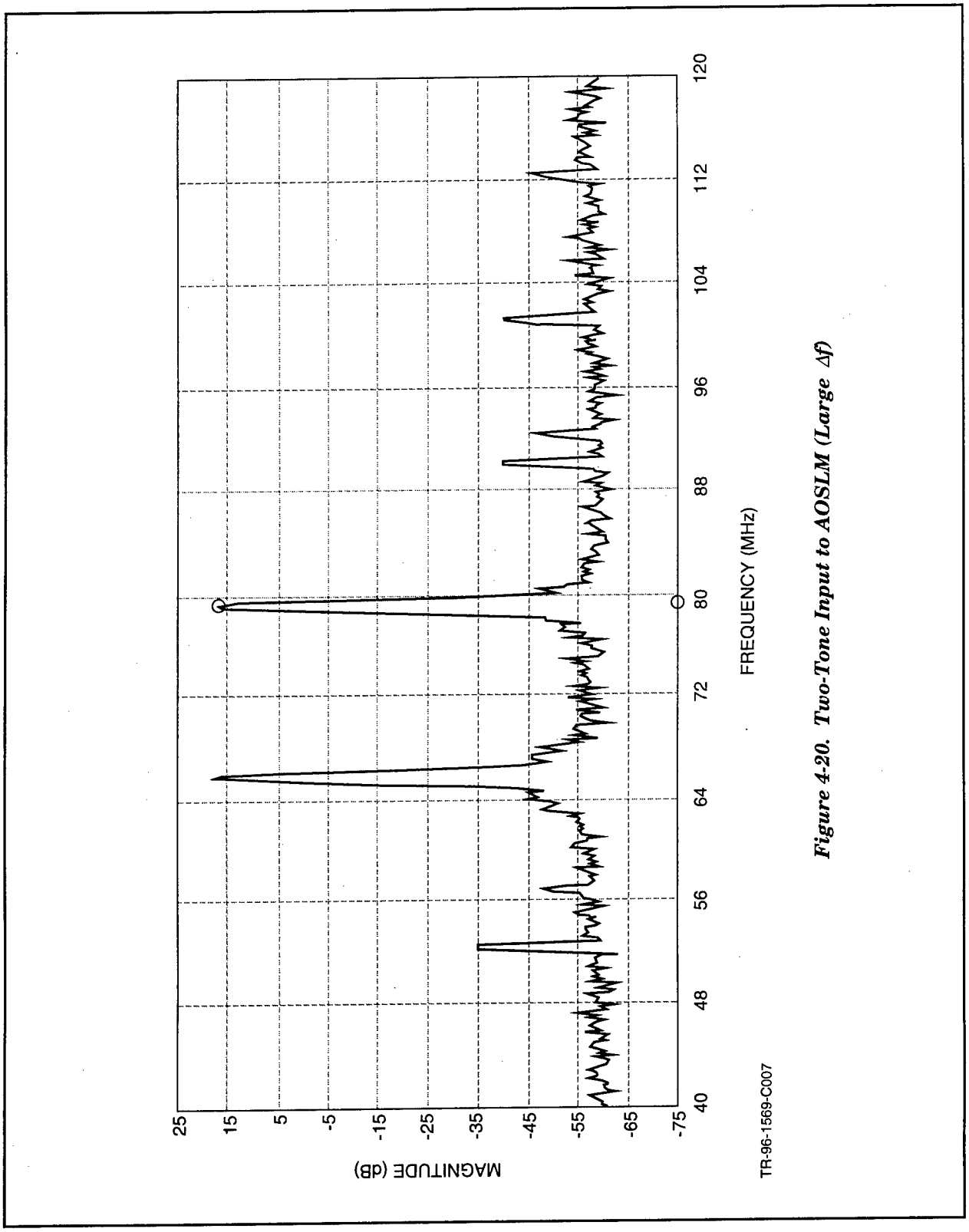

Figure 4-20. Two-Tone Input to AOSLM (Large Δf)

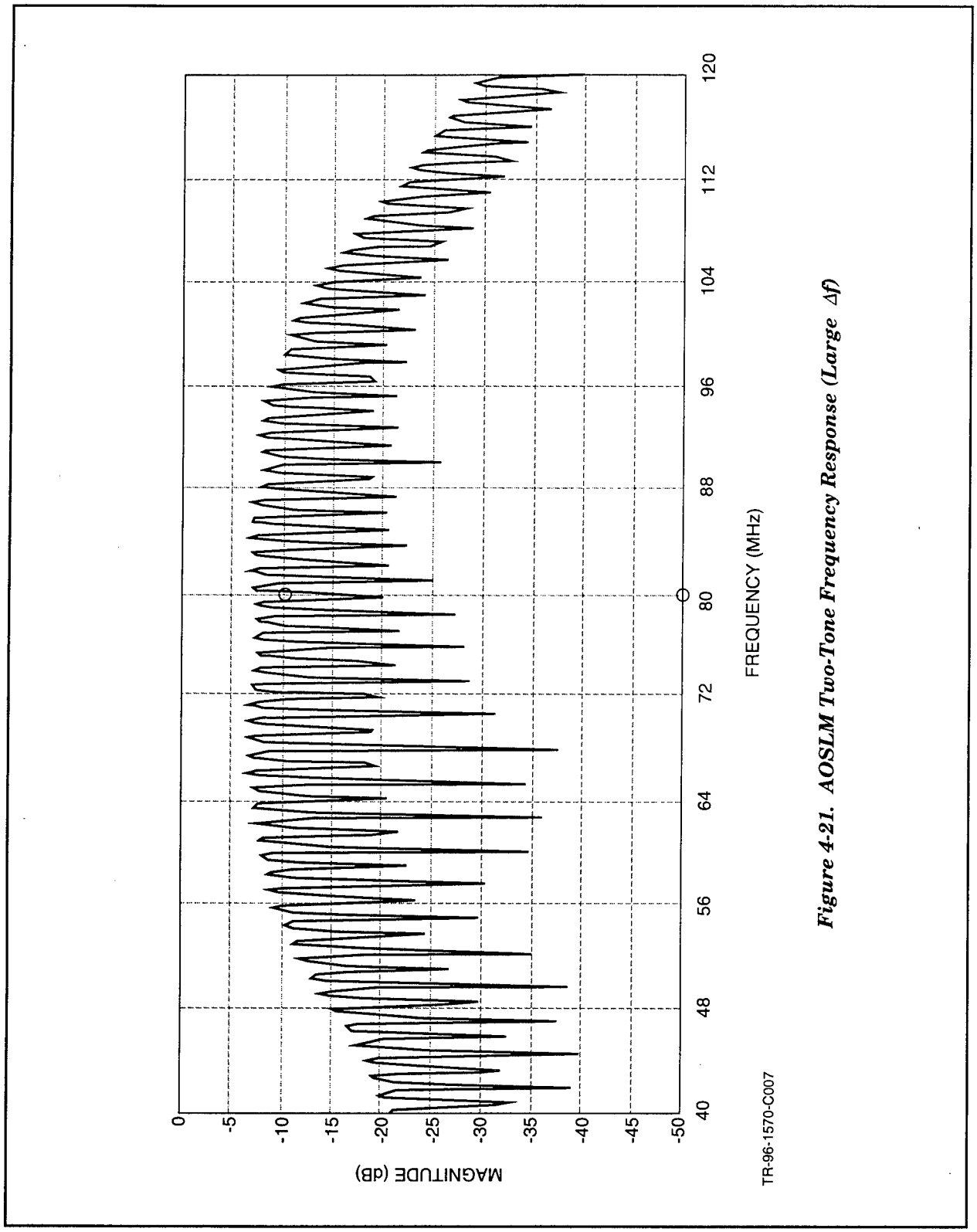

Figure 4-21. AOSLM Two-Tone Frequency Response (Large Δf)

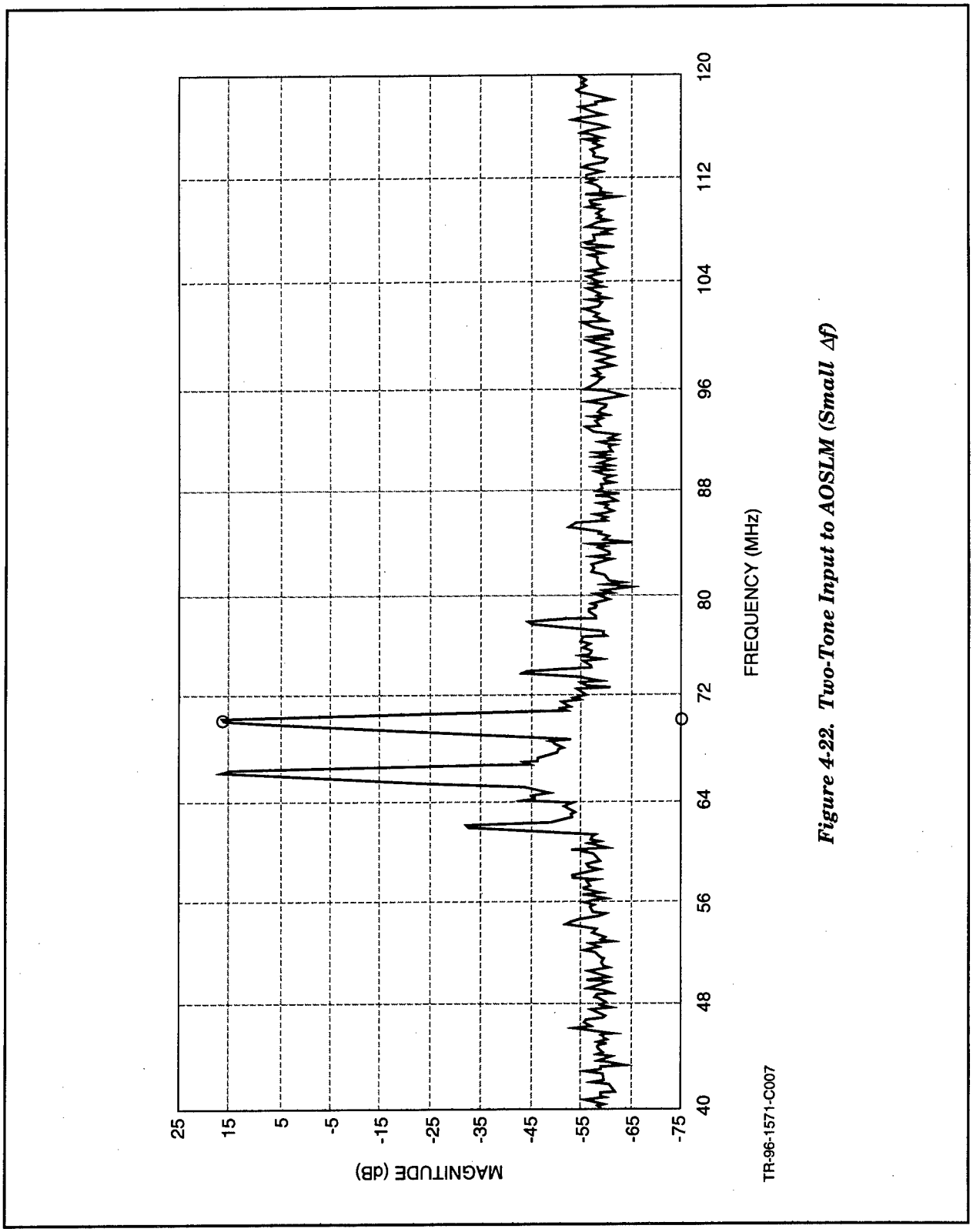

Figure 4-22. Two-Tone Input to AOSLM (Small Δf)

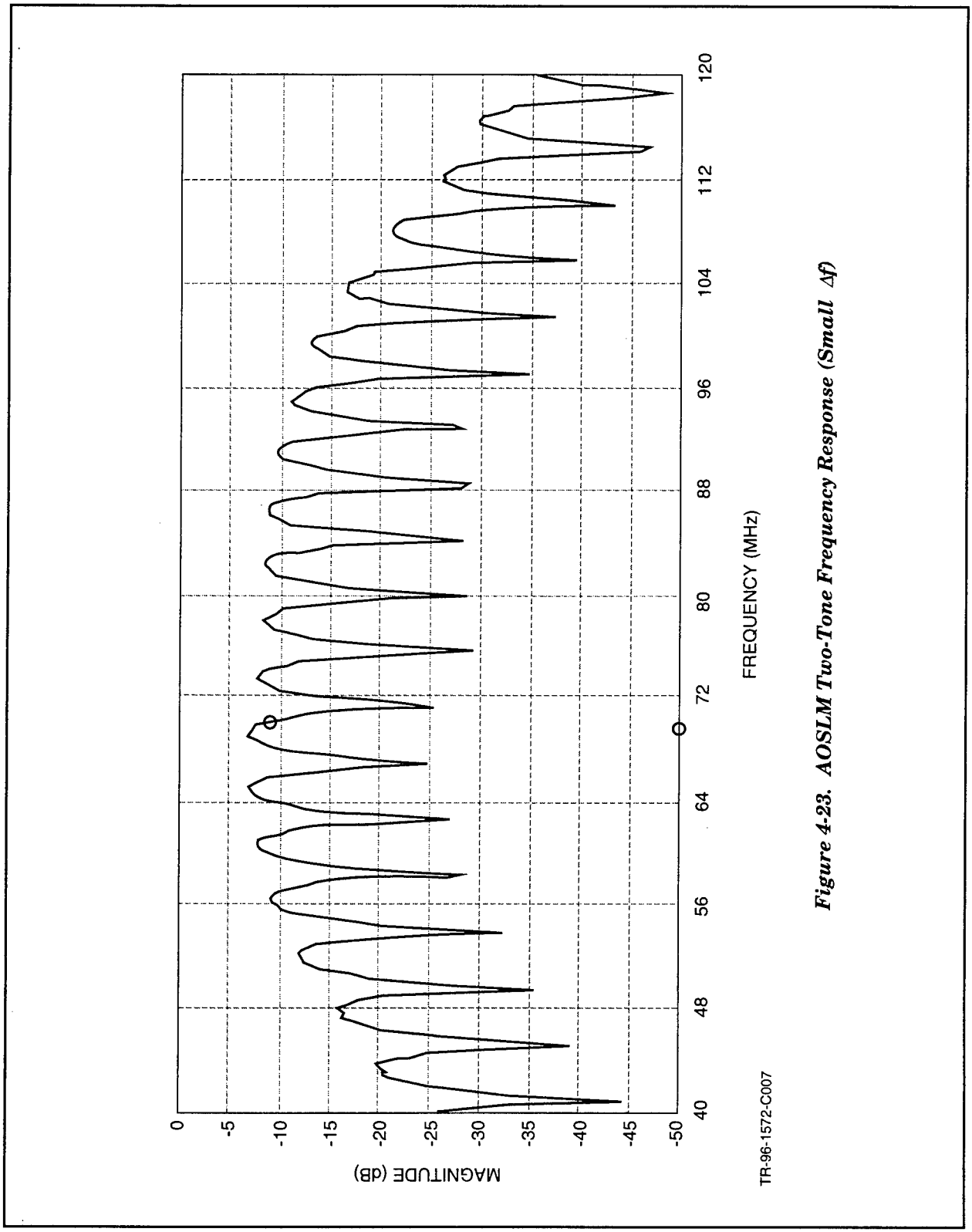

Figure 4-23. AOSLM Two-Tone Frequency Response (Small Δf)

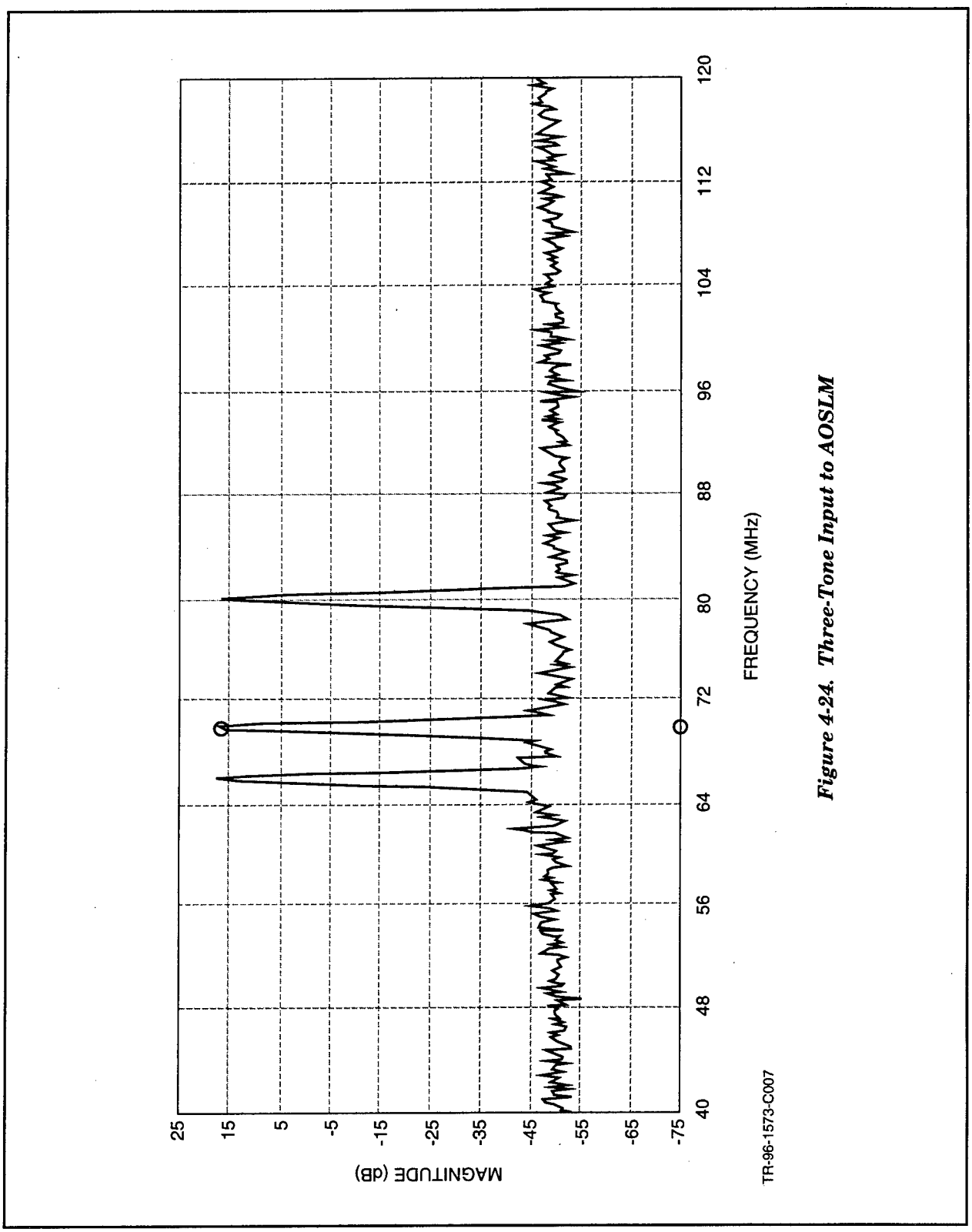

Figure 4-24. Three-Tone Input to AOSLM

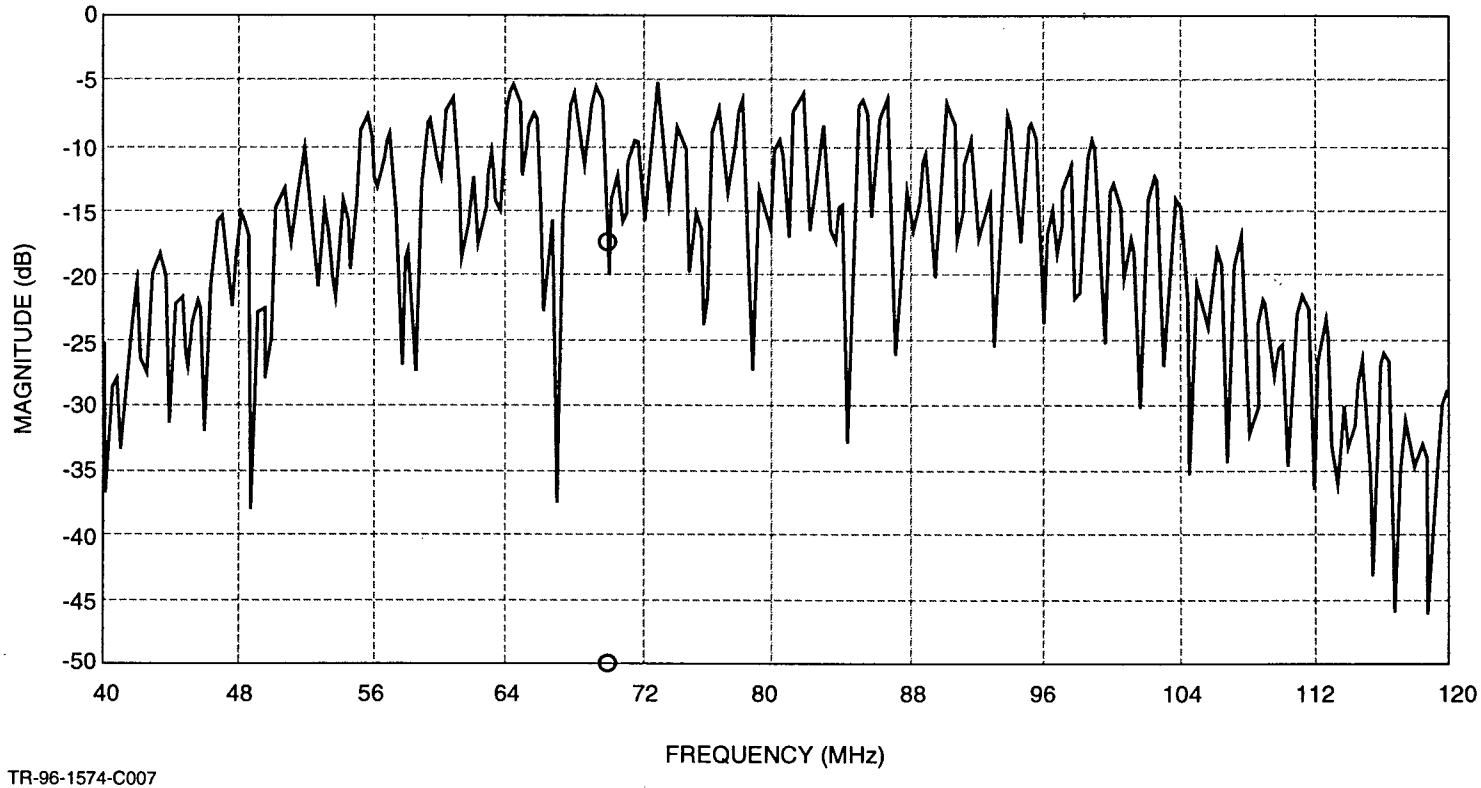

Figure 4-25. AOSLM Three-Tone Frequency Response

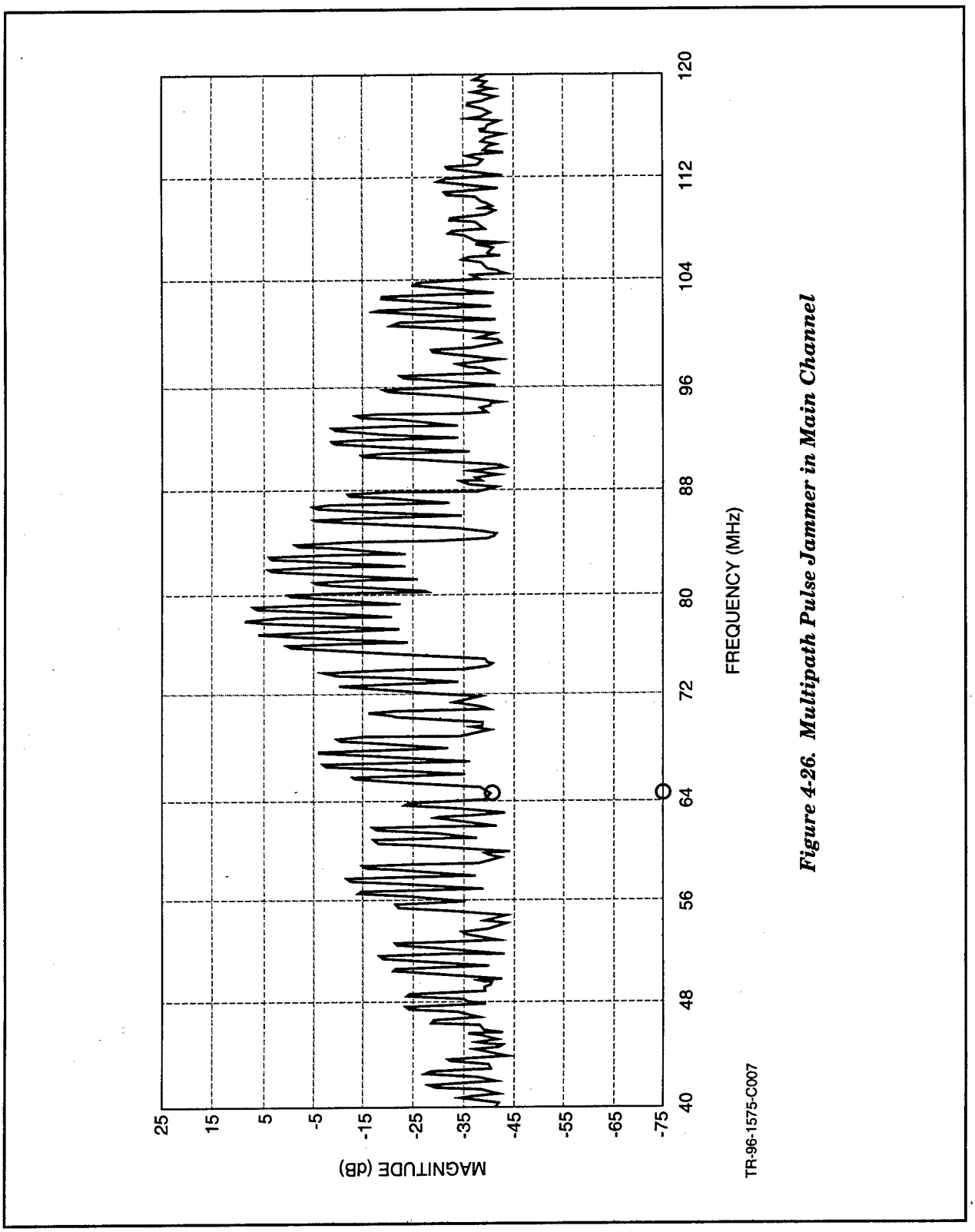

Figure 4-26. Multipath Pulse Jammer in Main Channel

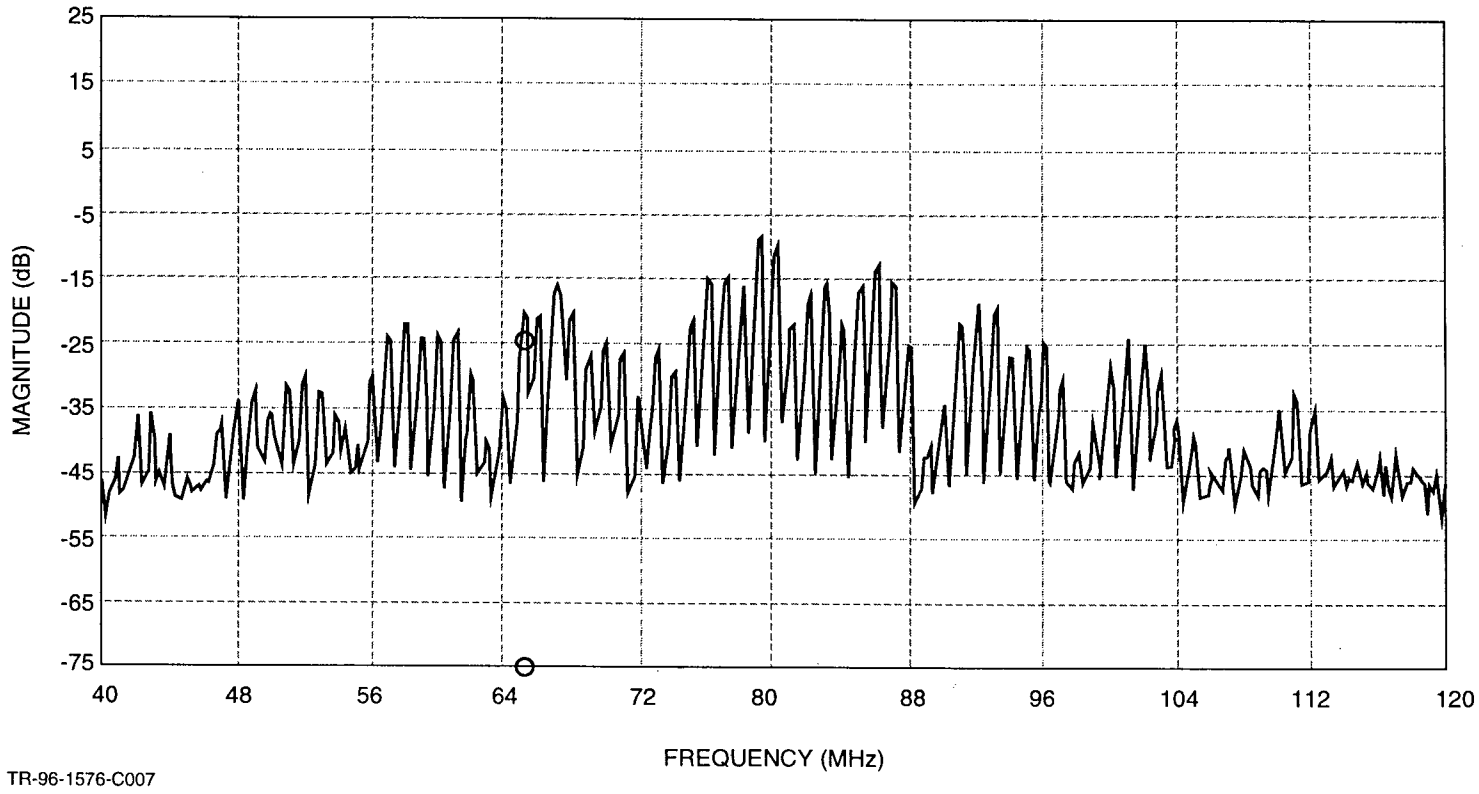

Figure 4-27. Cancelled Multipath Pulse Jammer for Main Channel Signal in Figure 4-26

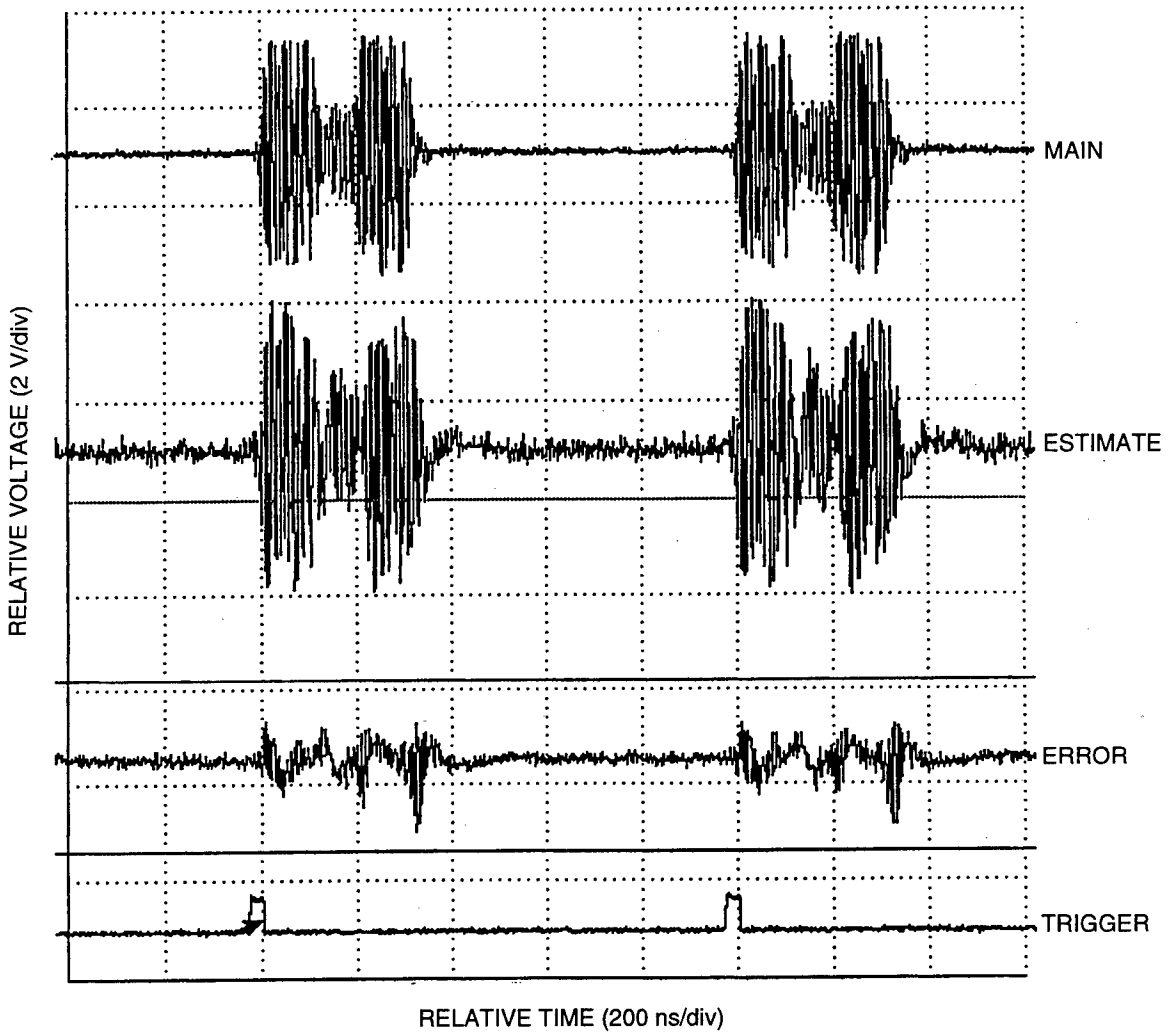

TR-96-1577-C007

Figure 4-28. Oscilloscope Traces for Main Channel Signal in Figure 4-26

canceller were also discussed in Subsection 3.2. Moreover, the almost-common path in-line time-integrating correlator was operated within the MADOP system for the first time and performed well. This correlator is shown in ***Figure 4-29***. The MADOP system was tested using realistic signal and jammer waveform types both in the laboratory and with the C-band radar. The HP4195A Spectrum/Network Analyzer was used to analyze system performance. In the lab tests, system cancellation was measured for CW, pulsed-tone, and noise waveforms. For these tests, pulsed-tone waveforms were created at baseband by the LeCroy AFG 9100 and placed on an 80-MHz carrier using the IntraAction Model DE. The improved integrated MADOP system was tested using the C-band radar with CW, pulsed-tone, and noise jammer waveforms in combination with CW and pulsed-tone signal waveforms. The results of all these tests were thoroughly documented. In addition, laboratory tests were performed to characterize the performance of the system in cancelling jammer signals comprised of either pulsed-tone or noise sources with a strong multipath element in the jammer signal. Additional tests were performed using the C-band radar to characterize system cancellation performance in the presence of multipath noise jammer waveforms in combination with a CW signal.

First, the pulsed-tone jammer cancellation performance of the MADOP system was determined in the laboratory using a variety of pulsewidths in the absence of a signal waveform. ***Figure 4-30*** provides the results for a pulsewidth of 500 ns and PRI of 5.0 ms. The dashed plot indicates the pulsed-tone waveform spectrum at the input to the reference channel, while the solid plot represents the cancelled pulse spectrum. The degree of cancellation for this jammer waveform is approximately 25 dB.

Next, the noise jammer cancellation performance of the MADOP system was determined through additional laboratory experiments. ***Figure 4-31*** reveals the cancellation performance of the system for this waveform type. In these tests, the Noise-Com noise source was used to provide the test waveform. The dashed plot indicates the noise waveform spectrum at the input to the reference channel, while the solid plot represents the spectrum of the cancelled waveform. The degree of cancellation for this waveform type is approximately 20 dB. This is not as good as the cancellation obtained with CW or pulsed-tone waveforms; however, the performance is not unexpected for this waveform type.

Next, the multipath cancellation performance of the MADOP system was determined through laboratory experiments using both pulsed-tone and noise waveforms in the absence of a signal waveform. Referring to ***Figure 3-30***, the MADOP system block diagram, multipath waveforms were constructed by dividing the main channel into two paths with each path containing a different BAW delay line. The BAW devices that were used had delays of 6.0 and 6.1 μs, resulting in a differential multipath delay of 100 ns. For the pulsed-tone waveforms, system cancellation performance for pulsewidths of 100 and 50 ns was tested. In each case, the multipath delay was 100 ns. ***Figure 4-32*** provides the system multipath cancellation performance using the 100-ns pulsewidth waveform. The

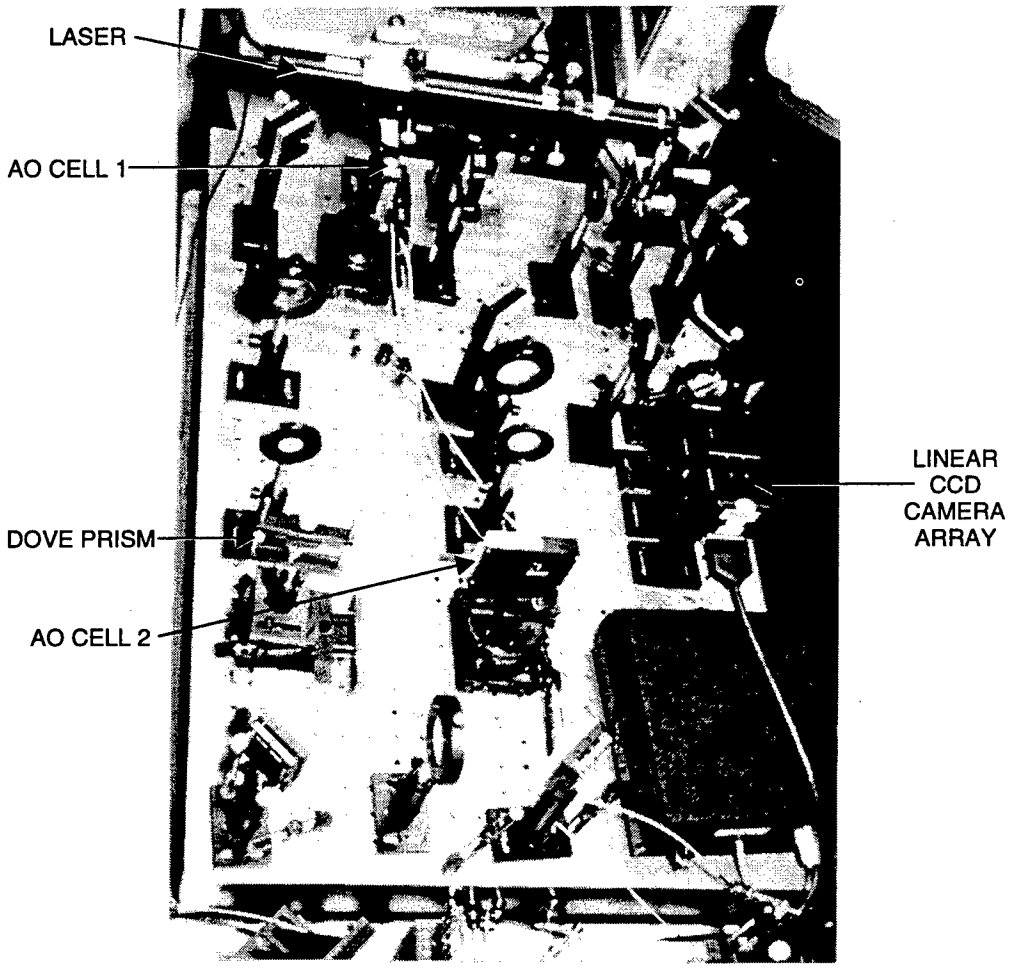

Figure 4-29. Almost-Common Path In-Line Time-Integrating Correlator at the C-Band Radar Laboratory

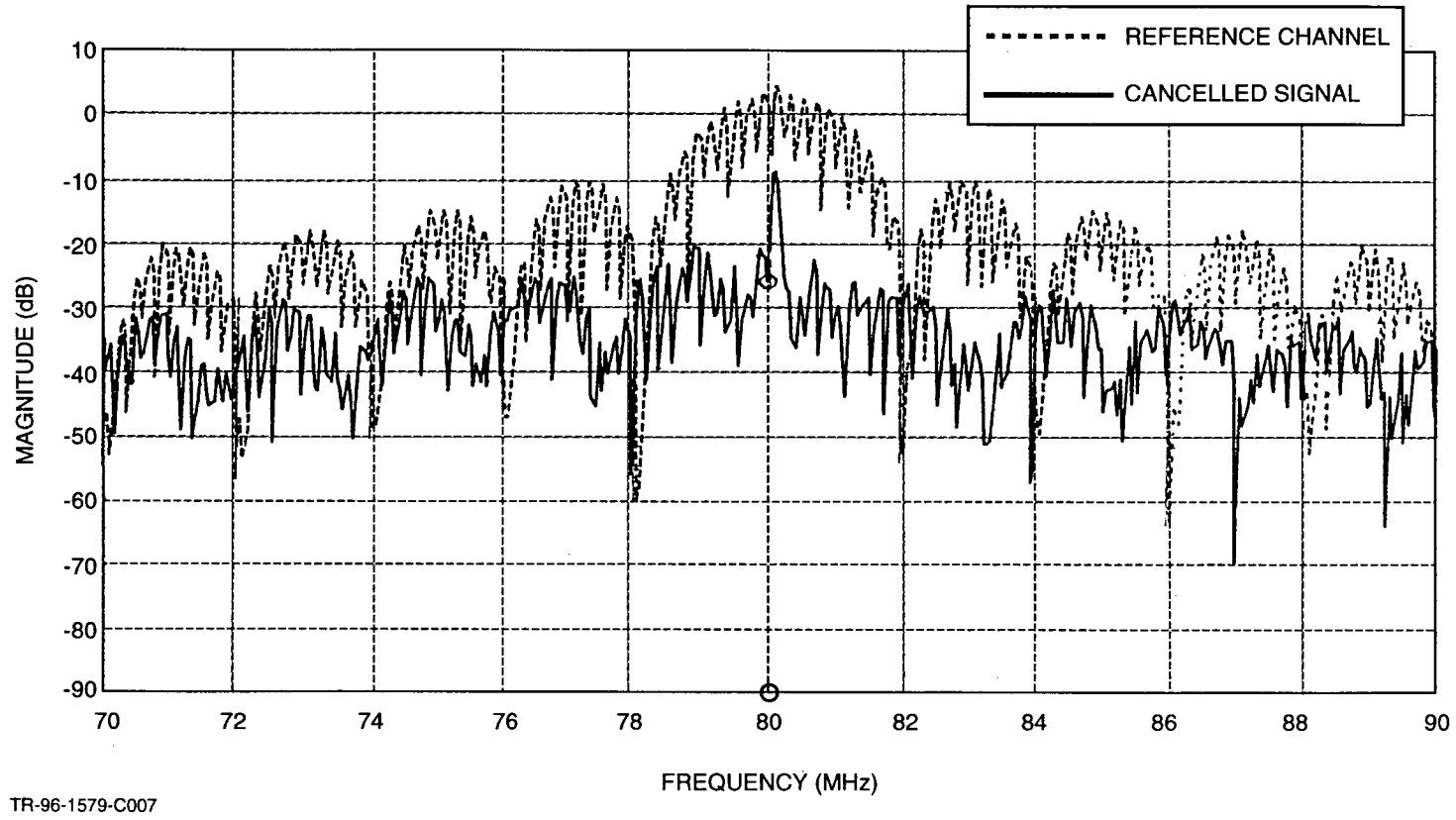

Figure 4-30. Laboratory Cancellation of a 500-ns Pulse With a 5-μs PRI

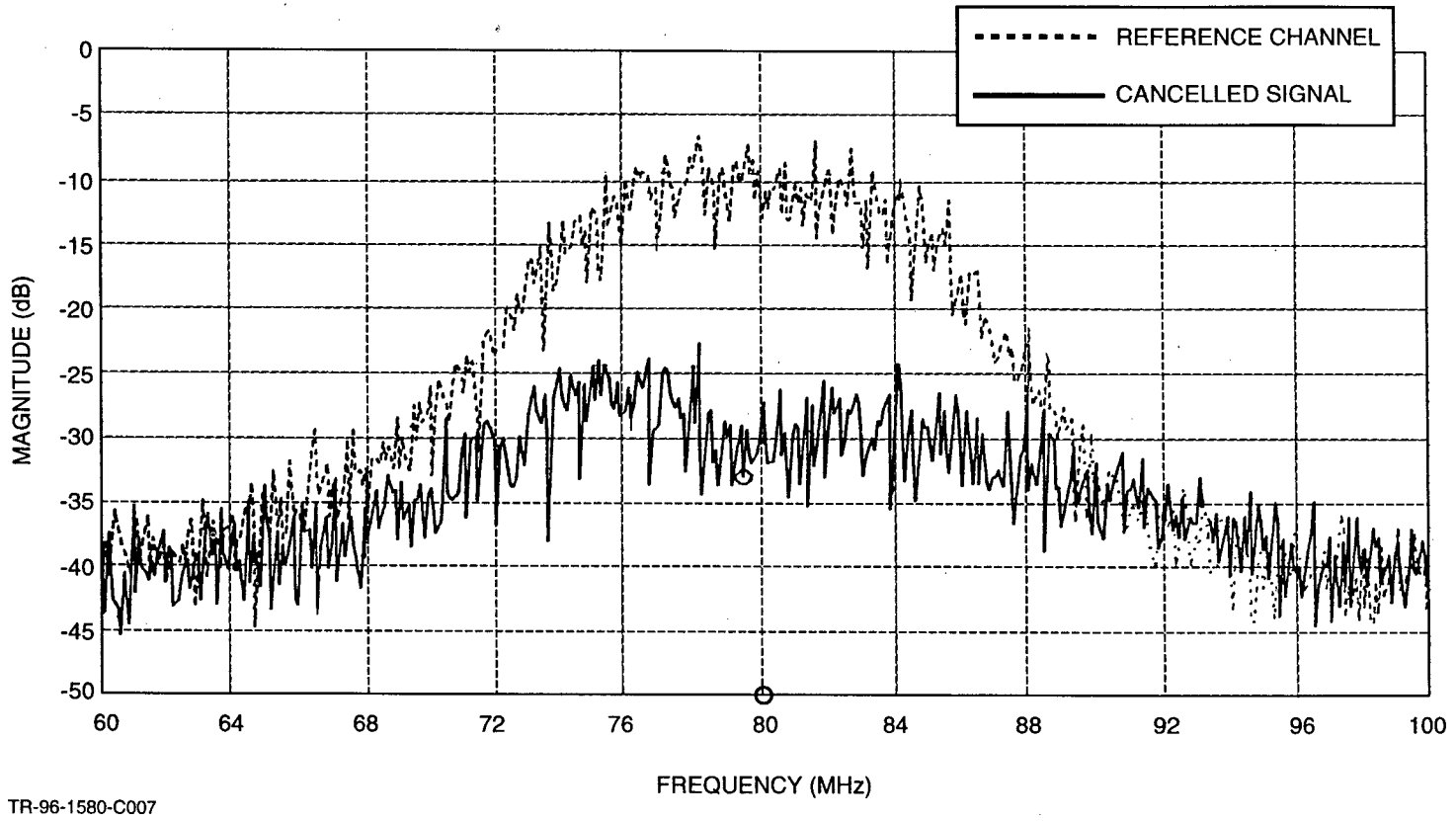

Figure 4-31. Laboratory Cancellation of Wideband Noise

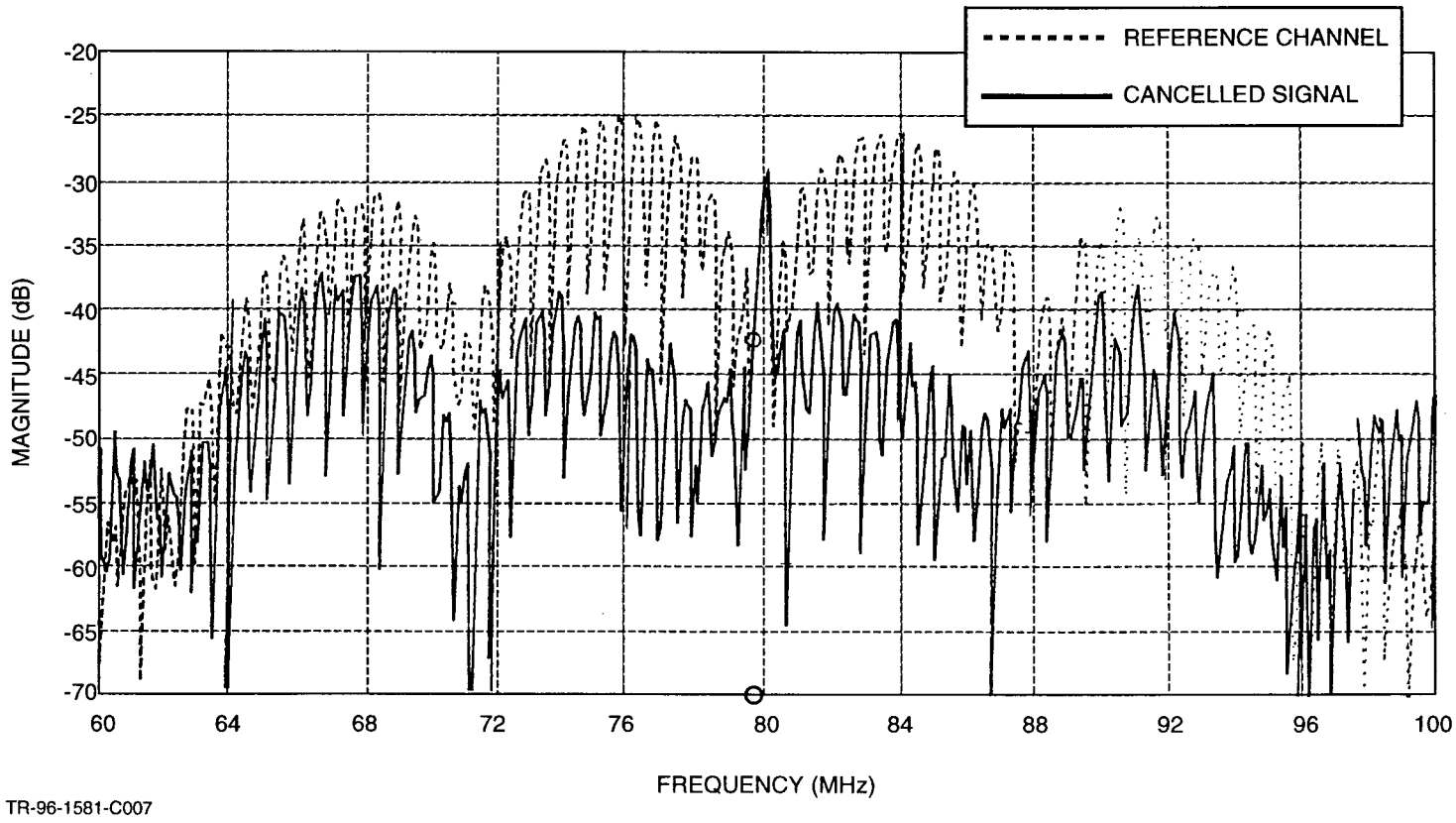

Figure 4-32. Laboratory Multipath Cancellation for a 100-ns Pulse With a 1-μs PRI

dashed plot indicates the spectrum of the multipath waveform at the input to the reference channel, while the solid curve represents the cancelled waveform spectrum. The degree of cancellation is estimated to be approximately 15 dB overall. For noise waveforms, system cancellation performance is presented in ***Figure 4-33***, in which the multipath delay is again 100 ns. The dashed plot indicates the multipath waveform spectrum at the input to the reference channel, while the solid curve represents the cancelled waveform spectrum. The degree of cancellation is estimated to be approximately 15 dB overall.

The next series of tests involved the C-band radar as the source of the signal and jammer waveforms to the MADOP system, and both of these waveforms originated at the jammer sources that are deployed at the airfield. That is, the jammer sources transmitted both signal and jammer waveforms to the C-band radar for the cancellation of the jammer by the MADOP system. In the first tests of this series, both signal and jammer waveforms were CW tones and were separated by a frequency of 25 kHz. The performance of the MADOP system was tested over a range of S/J to the auxiliary channel. ***Figure 4-34*** provides the system cancellation performance using an S/J of –3.0 dB in the auxiliary channel. Again, the dashed plot represents the spectrum of the waveform at the input to the reference channel, while the solid curve represents the cancelled waveform spectrum. The signal tone is to the left of the jammer tone. The S/J improvement is over 30 dB. Next, the system cancellation performance was tested for an auxiliary channel S/J ratio of –13 dB, and the results are shown in ***Figure 4-35***. The dashed plot indicates the waveform spectrum at the input to the reference channel, while the solid curve represents the spectrum of the cancelled waveform. Again, the signal tone is to the left of the jammer tone. The S/J improvement is again over 30 dB.

In the next tests involving the C-band radar system, a pulsed-tone waveform was transmitted to the C-band radar for use as the signal of interest and in place of the CW tone used previously. The pulsewidth used for the signal was 500 ms, and its duty cycle was 50%. The jammer waveform remained a CW tone, and the frequency separation between these waveforms remained at 25 kHz. The performance of the MADOP system was evaluated over a range of auxiliary channel S/J ratios from –10 to –30 dB. ***Figure 4-36*** provides the system cancellation performance using an S/J of –10 dB in the auxiliary channel. The dashed plot indicates the waveform spectrum at the input to the reference channel, while the solid curve represents the cancelled waveform spectrum. The signal spectrum is to the left of the jammer tone, and the S/J improvement is approximately 12 dB. This modest degree of cancellation should not be too surprising given the high relative level of the signal in the auxiliary channel. A high relative signal level in the auxiliary channel results in substantial cancellation of the signal by the MADOP system. Next, the system cancellation performance was tested for an auxiliary channel S/J ratio of –20 dB and the results are shown in ***Figure 4-37***. Again, the dashed plot indicates the waveform spectrum at the input to the reference channel, while the solid curve represents the cancelled waveform spectrum. The signal spectrum is to the left of the jammer

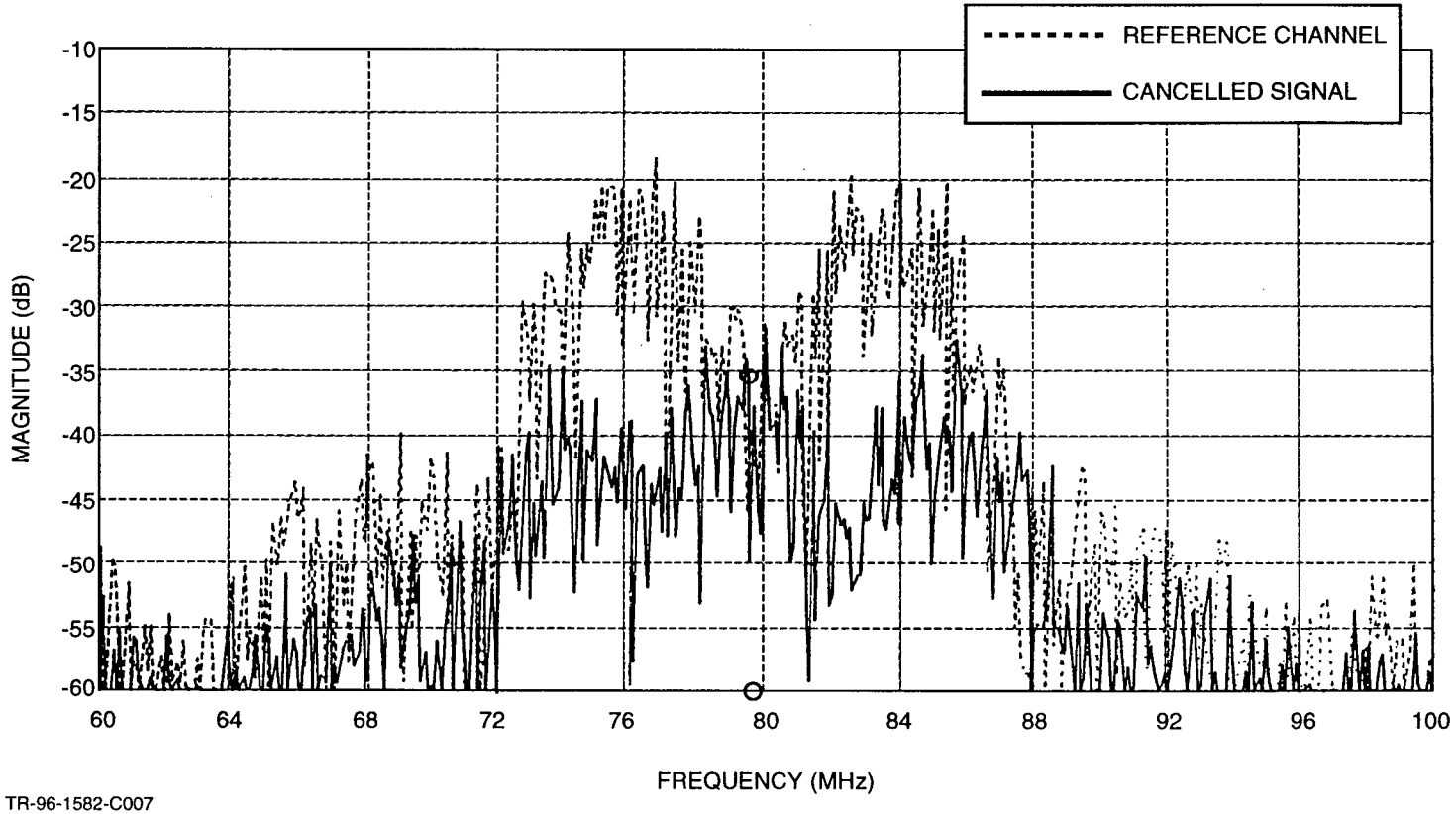

Figure 4-33. Laboratory Multipath Cancellation for a Noise Waveform

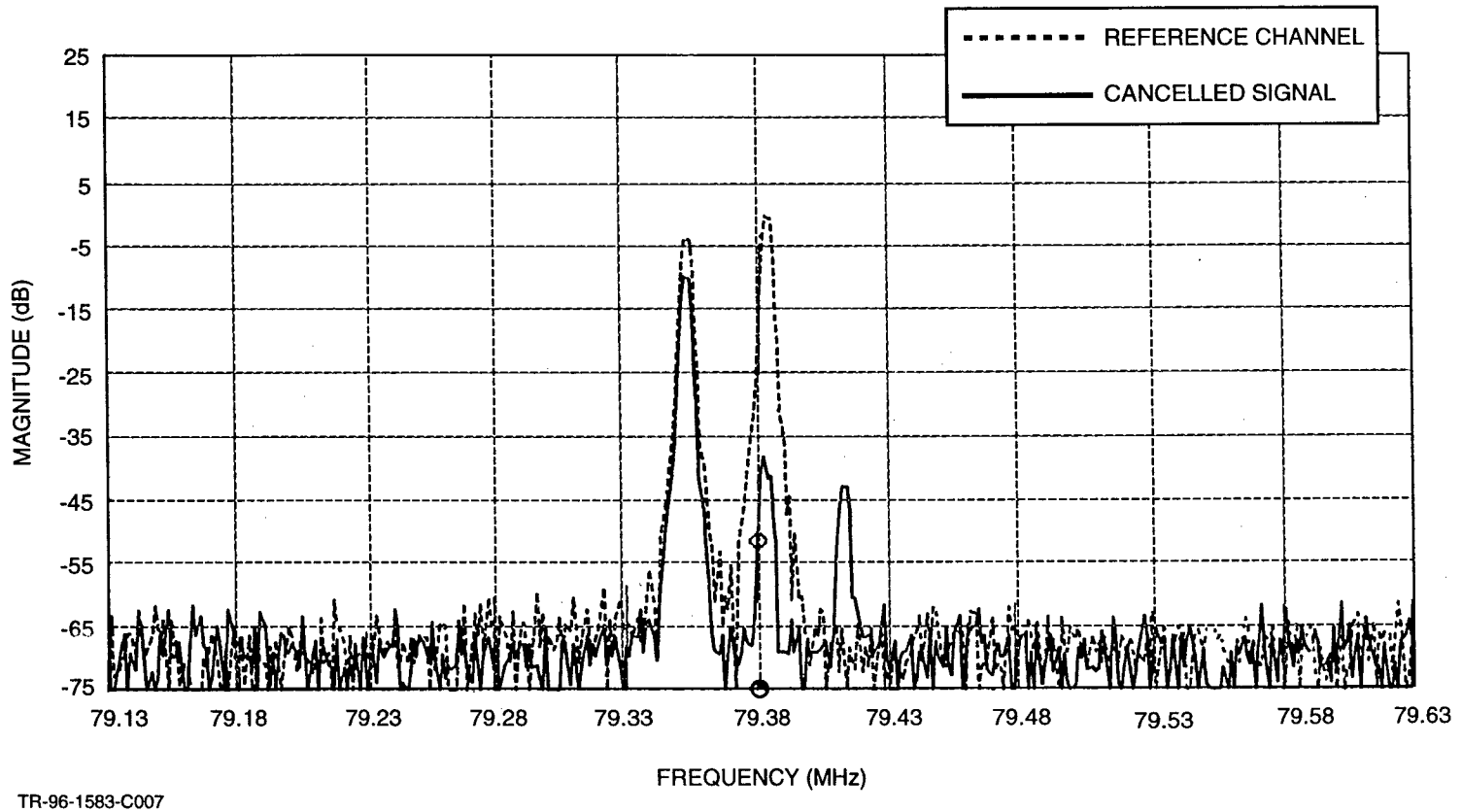

Figure 4-34. C-Band Jammer Cancellation (S/J Improvement = 31 dB, Input S/J = -3 dB)

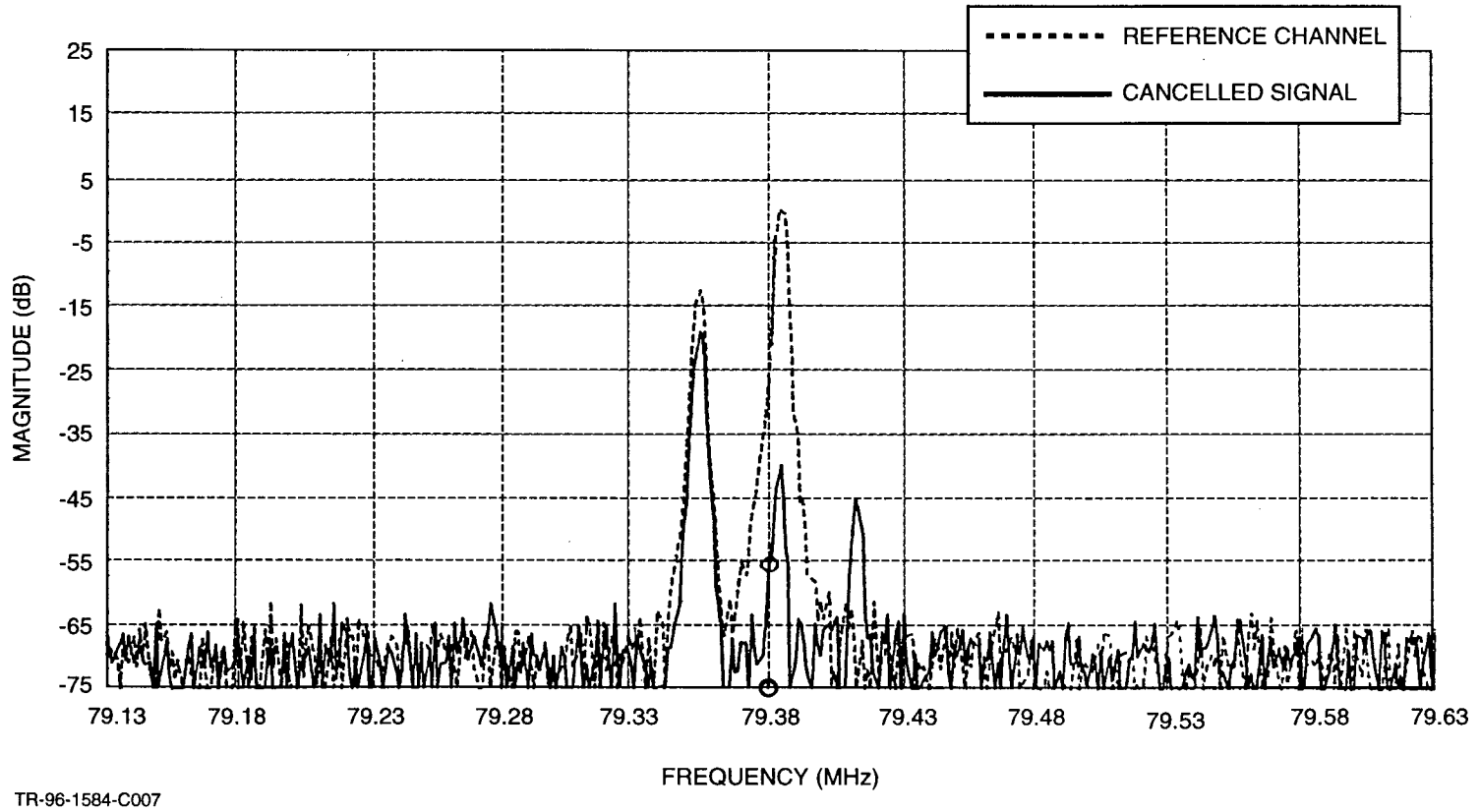

Figure 4-35. C-Band Jammer Cancellation (S/J Improvement = 34 dB, Input S/J = -13 dB)

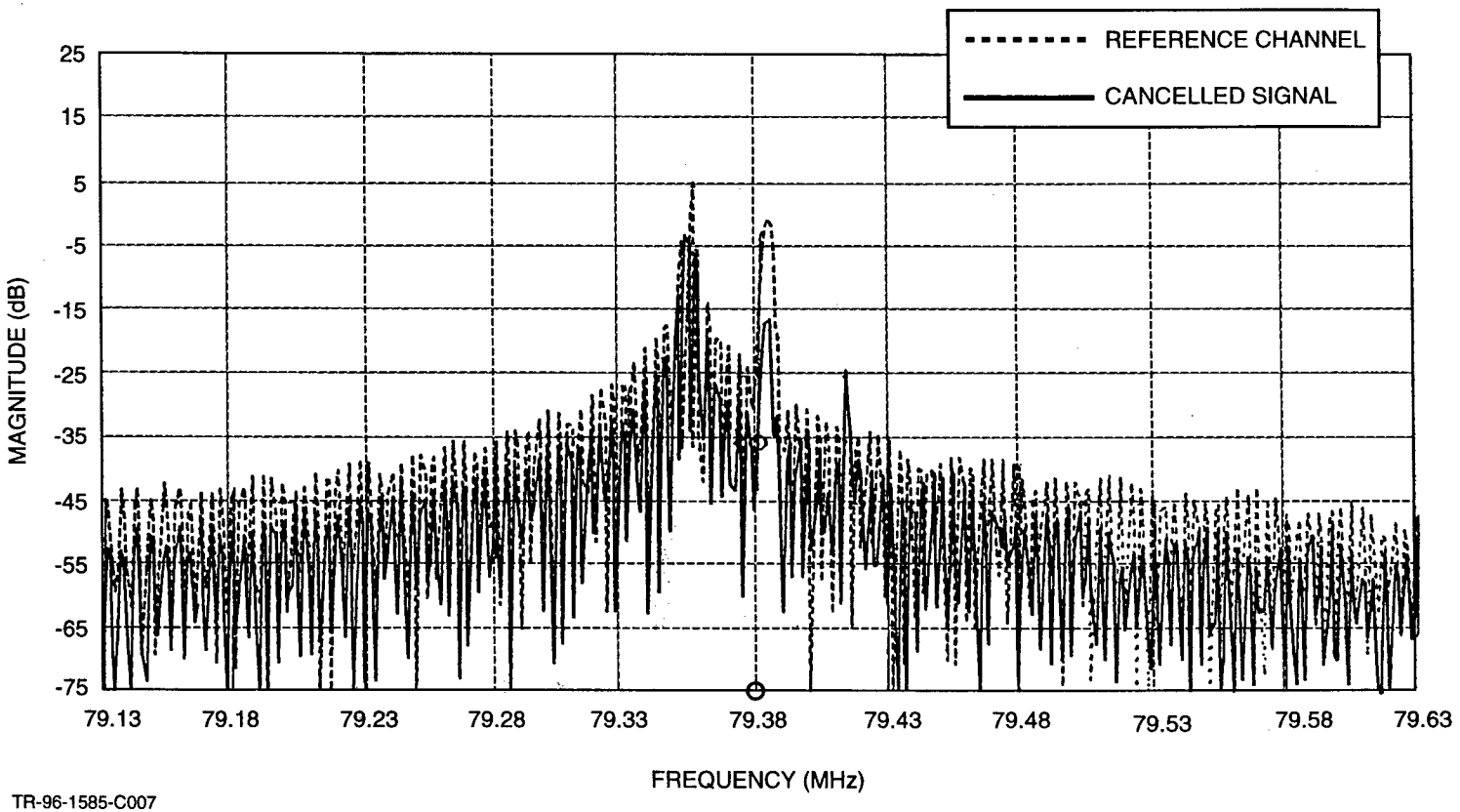

Figure 4-36. C-Band Jammer Cancellation With a Pulsed Signal (S/J Improvement = 15 dB, Input S/J = -15 dB)

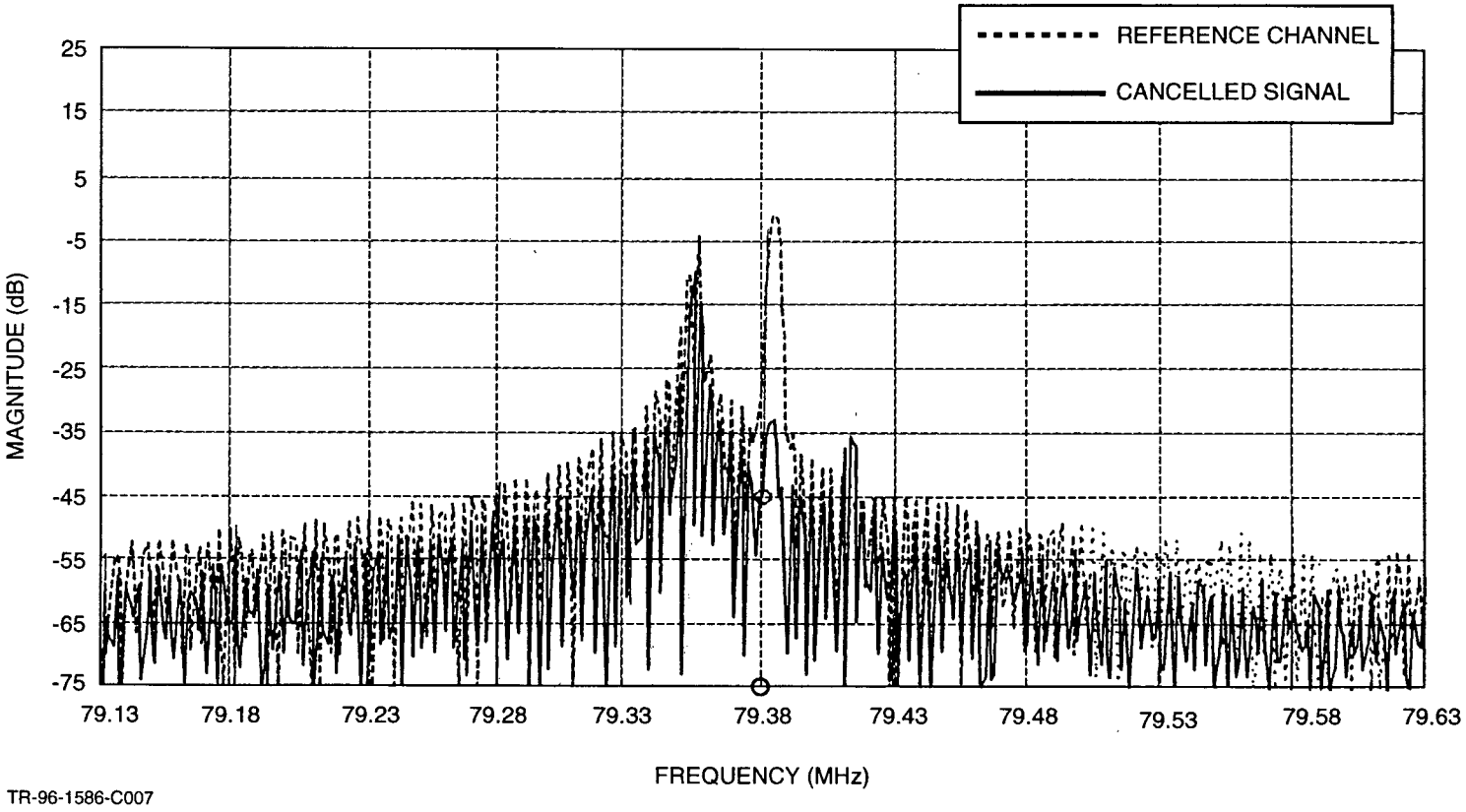

Figure 4-37. C-Band Jammer Cancellation With a Pulsed Signal (S/J Improvement = 30 dB, Input S/J = -20 dB)

tone, and the S/J improvement is nearly 30 dB. Finally, the system cancellation performance was tested for an auxiliary channel S/J ratio of –30 dB, and the results are shown in ***Figure 4-38***. The dashed plot indicates the waveform spectrum at the input to the reference channel, while the solid curve represents the spectrum of the cancelled waveform. The signal spectrum is to the left of the jammer tone, and the S/J improvement is approximately 35 dB.

Next, the role of the signal and the jammer were reversed by adjusting the levels of the waveforms to the auxiliary channel by carefully pointing the C-band array. That is, the pulsed-tone waveform became the jammer, and the CW waveform became the signal for this test. The parameters of the pulsed-tone waveform remained the same with a 500-ms pulsewidth and a 50% duty cycle and the frequency separation between these waveforms was kept at 25 kHz. The performance of the MADOP system was evaluated for an S/J ratio to the auxiliary channel of –25 dB. ***Figure 4-39*** presents the system cancellation performance in this configuration. The dashed plot indicates the spectrum of the waveform at the input to the reference channel, while the solid curve represents the cancelled waveform spectrum. The signal tone is to the right of the jammer spectrum, and the S/J improvement is approximately 40 dB.

Subsequently, a noise waveform was transmitted to the C-band radar for cancellation by the MADOP system. The signal used in these tests was a CW tone. The performance of the MADOP system was evaluated for an S/J ratio to the auxiliary channel of approximately –15 dB. ***Figure 4-40*** provides the system cancellation performance for these waveform types. The dashed plot indicates the waveform spectrum at the input to the reference channel, while the solid curve represents the cancelled waveform spectrum. The signal tone is in the center of the jammer spectrum frequency band, and the S/J improvement is approximately 15 dB for this signal and jammer.

Lastly, a noise waveform was transmitted to the C-band radar and used as a jammer signal to demonstrate multipath cancellation performance. The noise waveform, generated in jammer 1, was transmitted by both jammers one and three. The length of cable used to route this waveform from jammer one to jammer three provided the multipath delay. The waveform on the main channel was measured and recorded, and the results are provided in ***Figure 4-41***. The rippled texture of this plot is the result of multipath cancellation over the range of frequencies examined. The waveform on the auxiliary channel was also measured and recorded, and the results are provided in ***Figure 4-42***. The degree of multipath interference was intentionally reduced in this channel by carefully pointing the C-band array. The degree of multipath interference cancellation is presented in ***Figure 4-43***. The dashed plot indicates the spectrum of the jammer at the input to the reference channel as it was affected by multipath, while the solid curve represents the spectrum of the cancelled waveform. The signal is indicated by the marker in this plot, and its amplitude was measured separately to be –22 dBm to the auxiliary channel. Therefore, the S/J improvement is approximately 12 dB. These results are for an auxiliary channel S/J of approximately 30 dB.

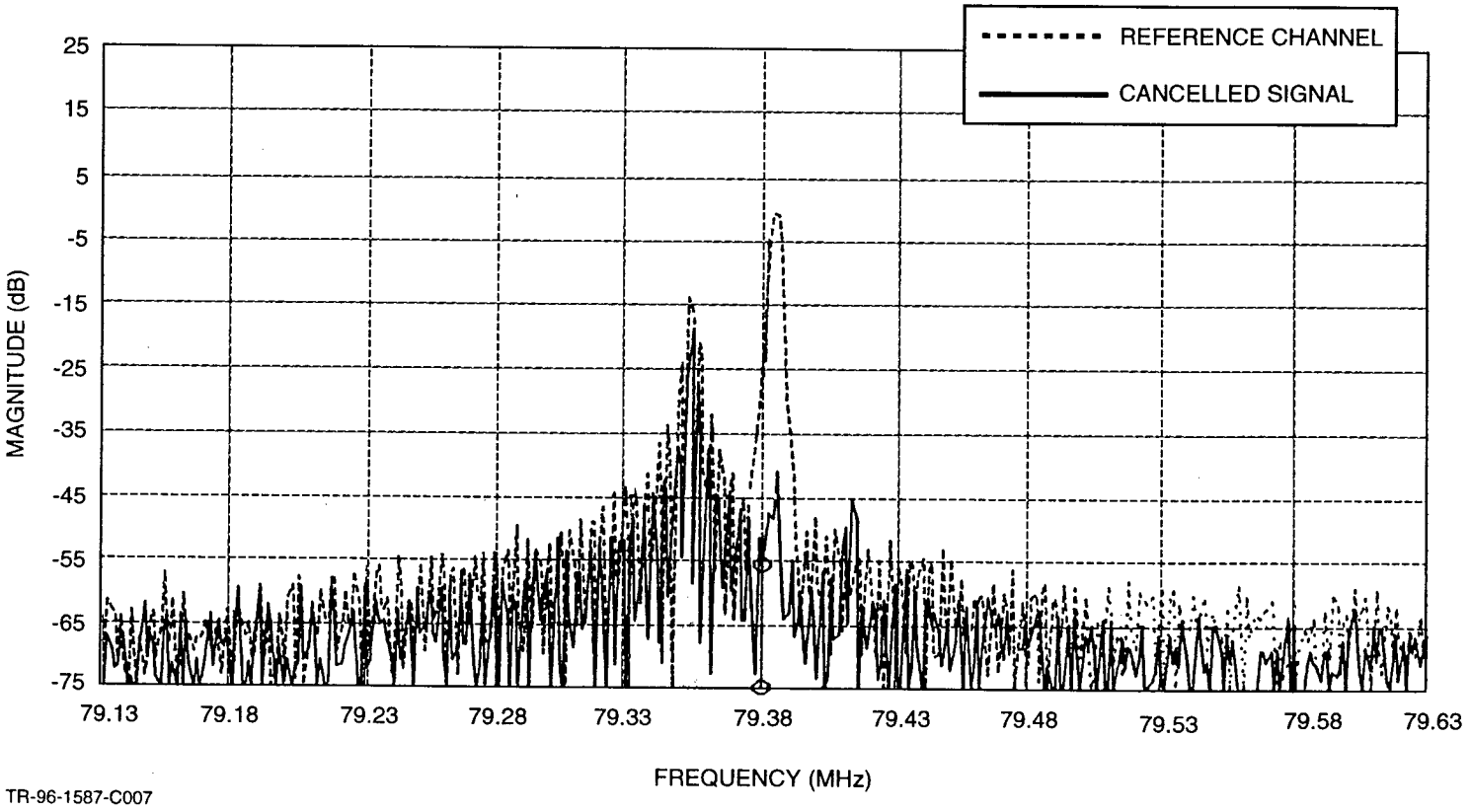

Figure 4-38. C-Band Jammer Cancellation With a Pulsed Signal (S/J Improvement = 35 dB, Input S/J = -30 dB)

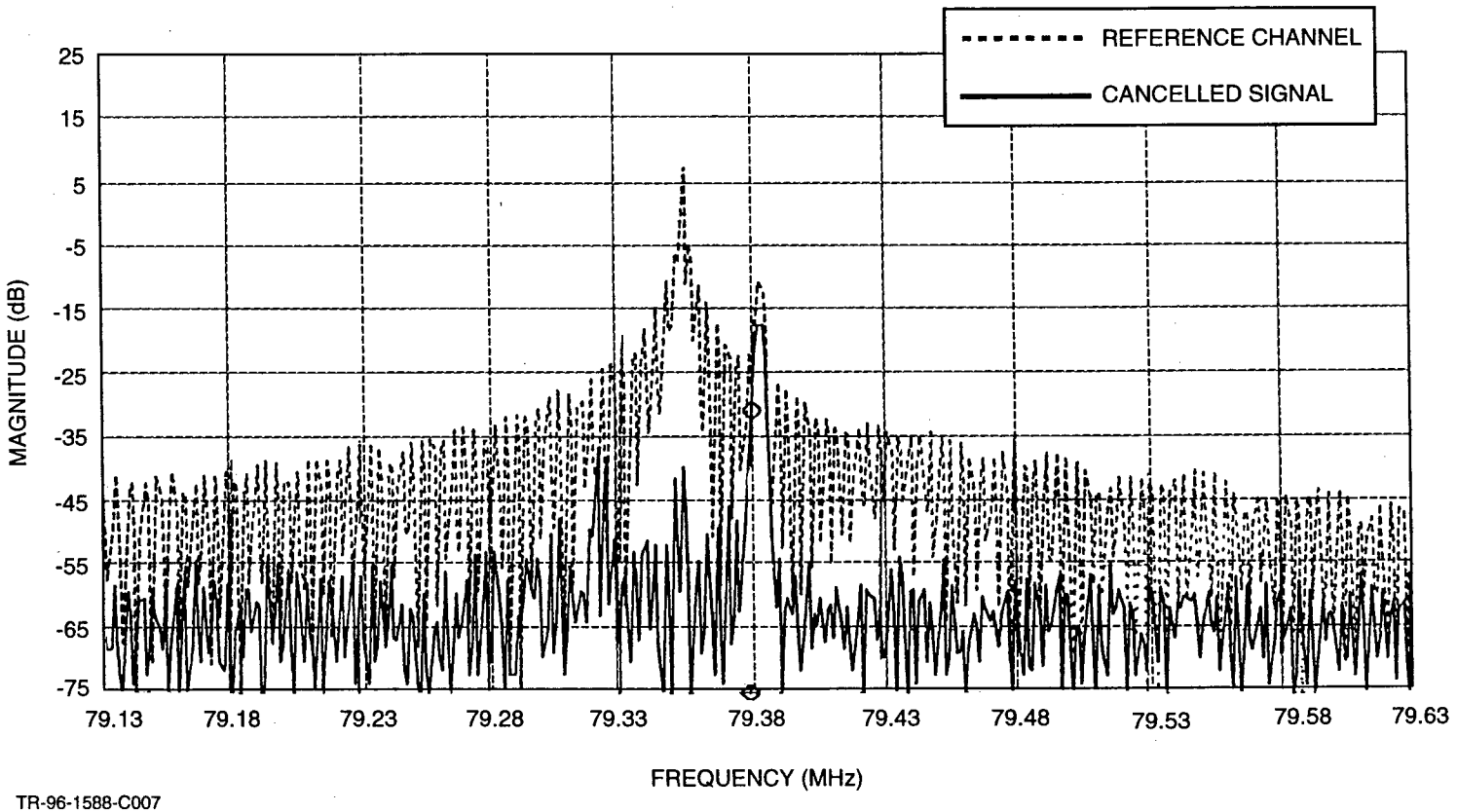

Figure 4-39. C-Band Jammer Cancellation With a Pulsed Signal (S/J Improvement = 40 dB, Input S/J = -25 dB)

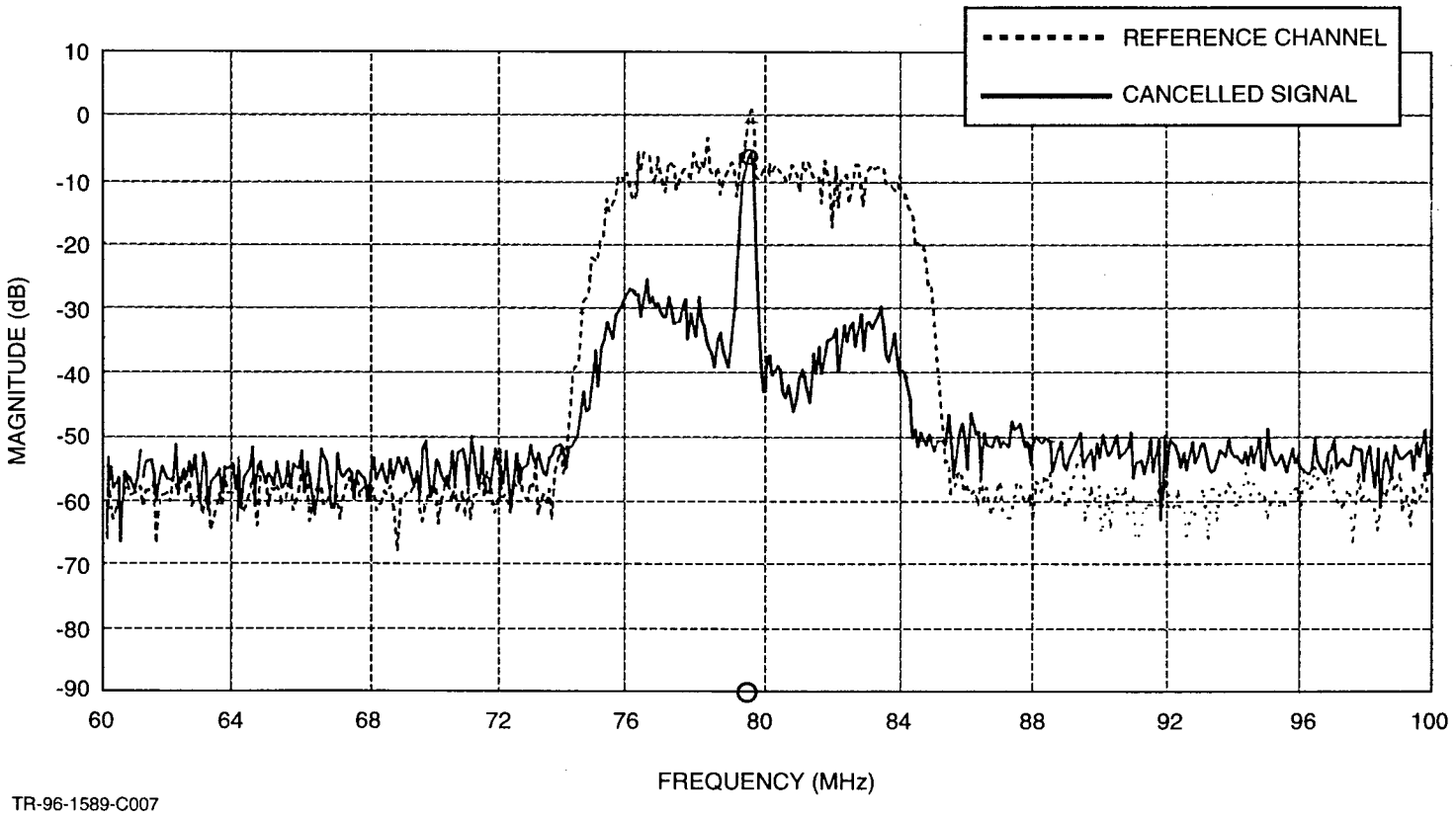

Figure 4-40. C-Band Jammer Cancellation With a Noise Jammer (S/J Improvement = 15 dB, Input S/J = -15 dB)

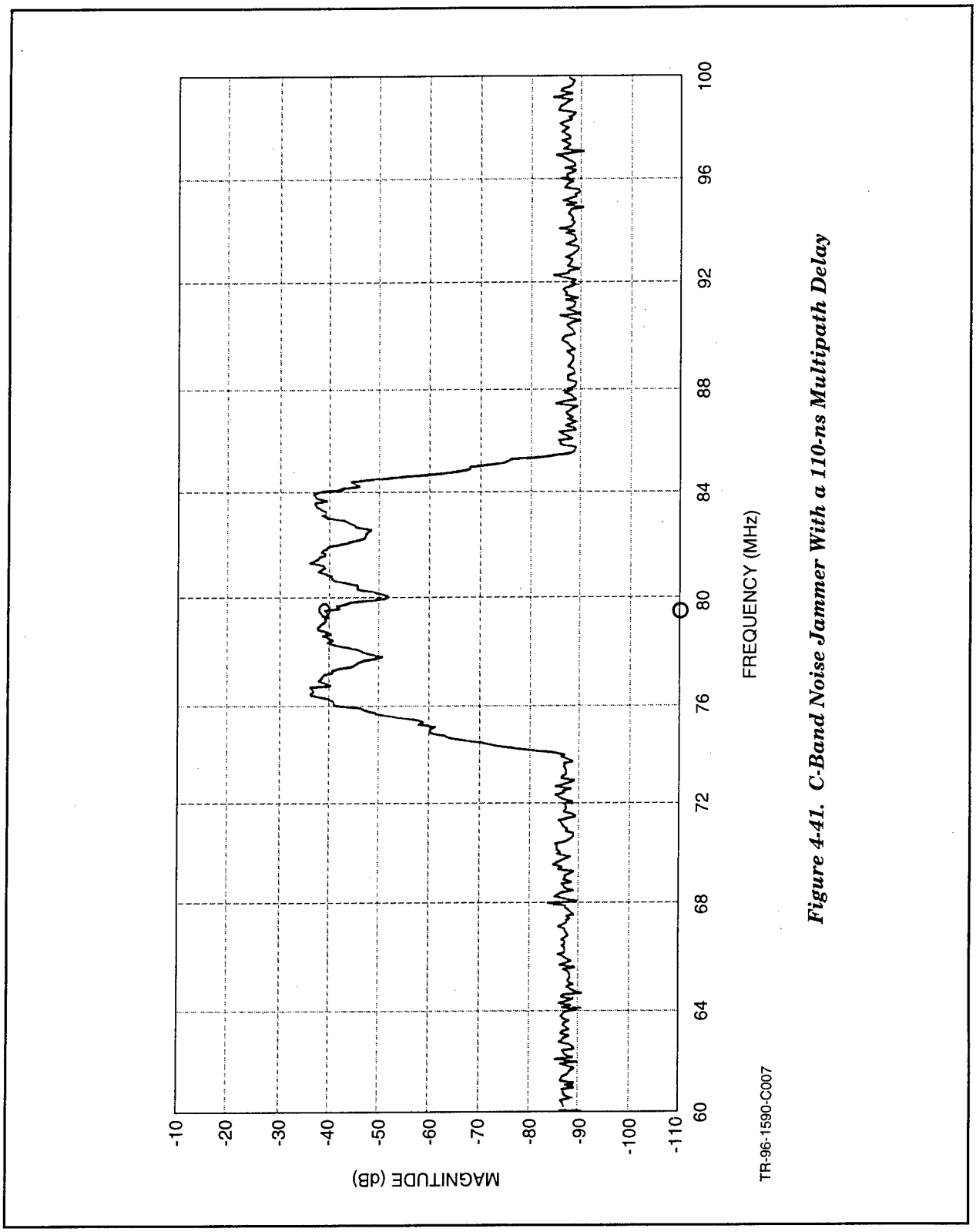

Figure 4-41. C-Band Noise Jammer With a 110-ns Multipath Delay

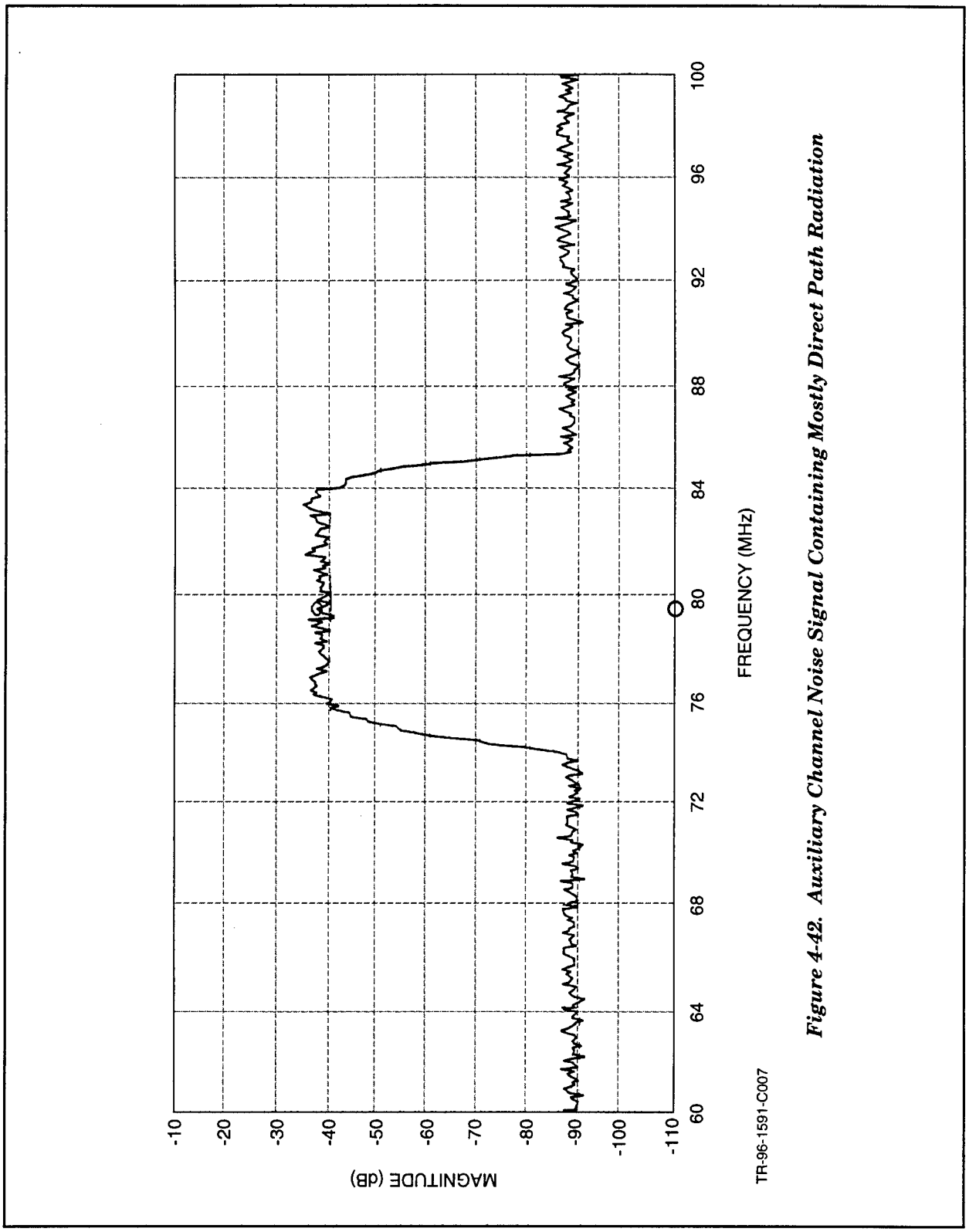

Figure 4-42. Auxiliary Channel Noise Signal Containing Mostly Direct Path Radiation

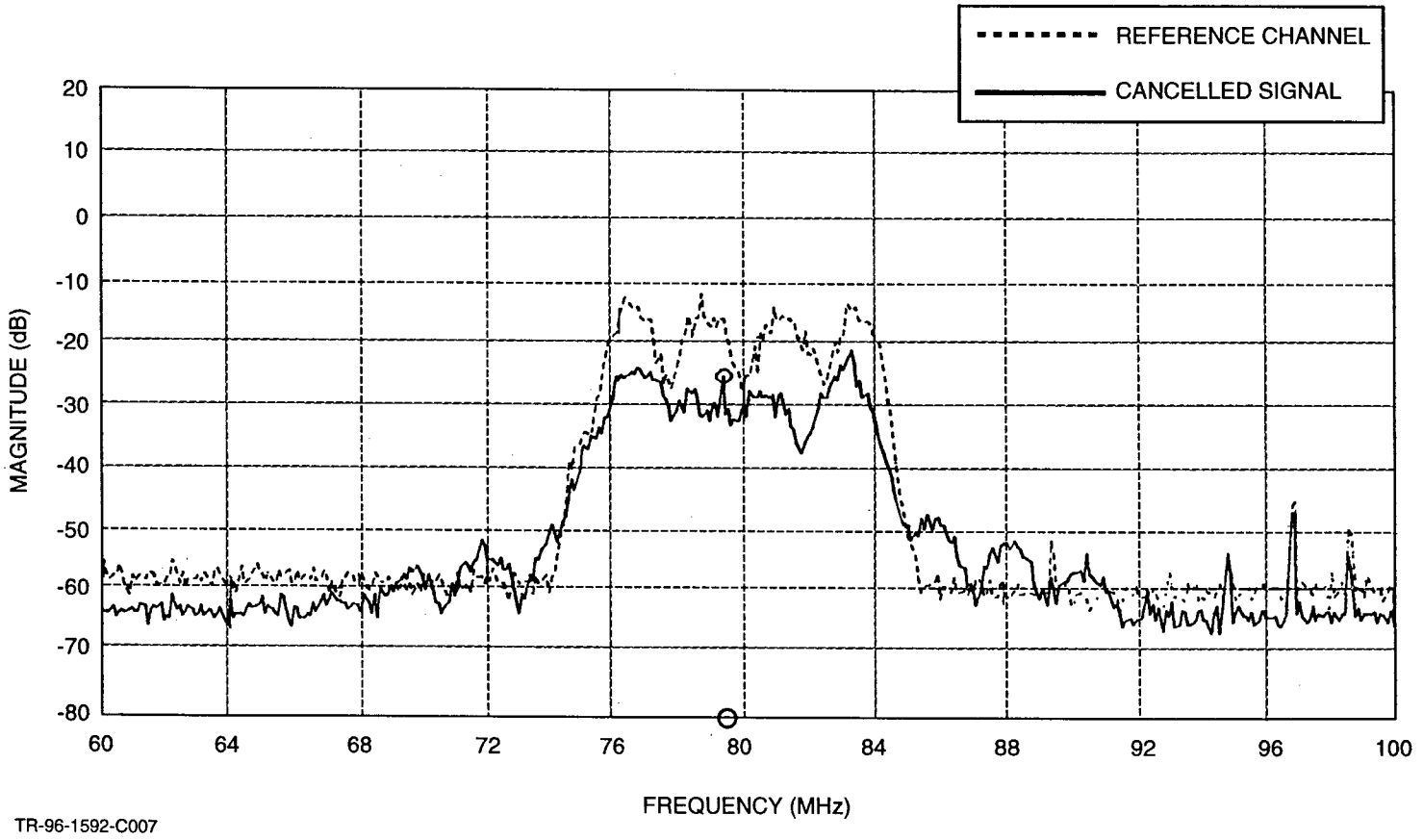

Figure 4-43. C-Band Multipath Jammer Cancellation (S/J Improvement = 12 dB, Input S/J = 30 dB)

5. CONCLUSIONS AND RECOMMENDATIONS

All of the key objectives for this 1-year ESE program were successfully achieved, culminating in the improved demonstration of the MADOP within the C-band radar testbed. The prospects for further improvement are strong because of the significant progress made during this effort.

Results to date have demonstrated approximately 15- to 20-dB cancellation of wideband jamming interference and 25- to 35-dB cancellation of narrowband jamming. This performance was demonstrated in both the laboratory and integrated with the C-band radar testbed during the first and third periods of on-site support.

It is recommended that follow-on activities be partitioned into three primary technical areas corresponding to each of the following subsections. To extend the performance capability of the MADOP and continue to demonstrate this processor within the C-band radar testbed or other RL testbed, the three major tasks to be accomplished include concept evaluation in realistic jammer scenarios, MADOP hardware improvements, and further testing of the MADOP in a phased-array radar, as detailed in Subsections 5.1, 5.2, and 5.3, respectively.

5.1 ENHANCED OPTICAL DEVICES, ARCHITECTURES, AND ALGORITHMS

The current MADOP system uses AO cells in the AO correlator and AOTDL subsystems to provide discrete tap frequencies. It is recommended that future programs address the use of alternative optical devices and architectures to perform the frequency tap estimation performed by the AOTDL and the correlation performed in the AO correlator. Alternative optical devices for performing these functions include: laser diode arrays such as Vertical Cavity Surface Emitting Laser (VCSEL) diodes, deformable mirror devices (DMDs), piezoelectric transducer devices, tunable laser diodes, and laser diodes with high-speed modulation capabilities. Architectures employing discrete laser diodes with large modulation bandwidths will also be investigated to increase performance of in-line optical architectures requiring a high-speed modulatable laser diode.

Advantages of using these types of devices in optical systems include:

1. Increased mechanical stability – smaller, lighter weight components;
2. Potential to easily scale and increase number of filter channels;
3. Potential for increased bandwidth;
4. Advancement of laser diode technology;
5. Solid-state technology reliability; and

6. Potential for new optical processor architectures.

The use of alternative optical devices of this nature is well matched to the overall RL missions in photonics technology advancement.

In addition to these optical architecture enhancements, this effort will address continued development of the electronic canceller and enhancements to algorithms that currently perform multipath cancellation. A first step in this development process is to ruggedize the current electronic canceller system. This will entail enclosing all of the components necessary to perform cancellation, such as power supplies, vector multiplier, phase comparator, circuit protoboard, etc. Thus, the electronic canceller will become a stand-alone unit ancillary to the MADOP. Development would then proceed to package this unit into a programmable microprocessor to perform the electronic signal cancellation.

Another activity to be performed under this effort is the analysis of multipath algorithms for achieving greater adaptivity within the PC controller. This will exploit understanding gained during recent successful testing of the MADOP with the RL C-band radar. During this testing, significant levels of multipath noise jamming were cancelled to reveal a CW tone target signal. These test results show significant promise for the utility of the MADOP processor for this challenging USAF problem.

5.2 MADOP ELECTRONIC INTERFACE ENHANCEMENTS

The system control, data gathering, and data analysis capabilities of the current MADOP system can be greatly enhanced. New data collecting and analysis approaches will streamline the characterization and testing of the overall MADOP system. Due to current limitations, analysis of results and implementation of new processing algorithms can be difficult to implement within the current architecture, resulting in slow overall MADOP processor performance characterization. As an example, the HP4195A spectrum/network analyzer is often used to make electronic measurements of optical processor cancellation performance. This instrument records data in the form of hard copy (paper) plots which are difficult to integrate into a report and further analyze. Enhanced system control approaches will allow new electronic processing algorithms to be developed and quickly integrated into the system.

Under this recommended ESE program, Dynetics will concentrate on integrating various measurement equipment and electronic signal processors into the MADOP system to form a cohesive and comprehensive measurement and analysis system. This effort will include the development of a modular object oriented software environment that facilitates integration of new algorithms. This effort will make use of the existing equipment and software as much as possible and will result in a user friendly environment for performing tests and analysis of the MADOP system.

Figure 5-1 is an outline of the system integration concepts. All the instrumentation and cameras will be controlled by a single PC under a Windows 95® environment. The existing P5-90 Pentium® processor PC with an upgrade to 32-MB random access memory (RAM) and a Windows 95® operating system is the logical development platform.

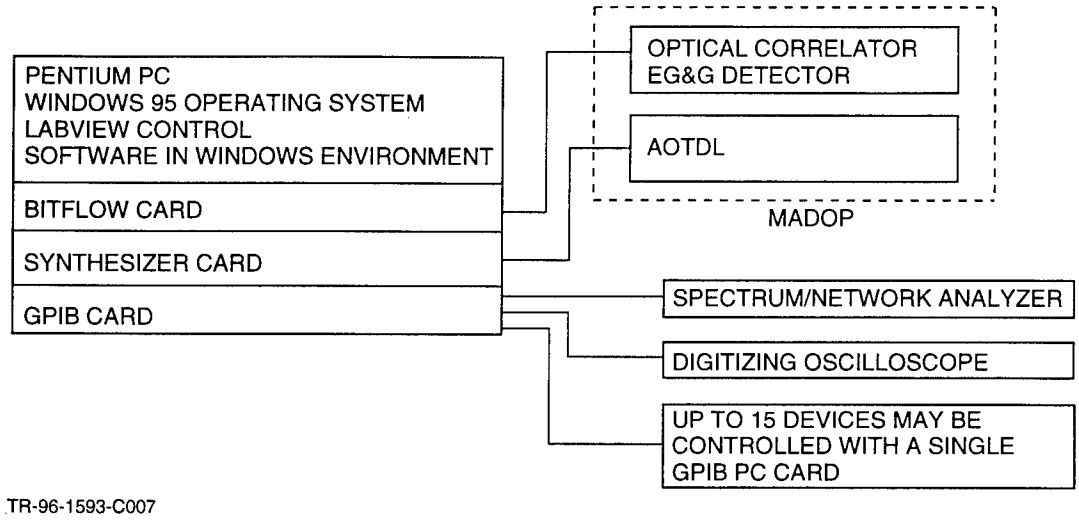

Figure 5-1. Integrated Control/Processing/Measurement System Depiction

Software development will be performed using LABVIEW® and/or LABWINDOWS®. LABWINDOWS software will allow existing C and C++ programs to be utilized in a LABVIEW environment, which is an ideal language for software development and an optimized language for instrumentation system control. This will make it possible to use current MADOP algorithms written in C in the LABVIEW environment. Additionally, the current BitFlow Raptor® detector driver card has many display routines written in the C language. The combination of LABVIEW / LABWINDOWS should allow great flexibility and easy insertion of existing processing code in the integrated system. Additionally, software developed on the PC using LABVIEW/LABWINDOWS/C++ is portable to/from Sun UNIX and Macintosh platforms making multiplatform software development possible. For those instruments with a GPIB bus controller, software will be written in LABVIEW for control and data storage since it provides many of the needed interface drivers for GPIB instruments. Processing of

large amounts of detector data may necessitate a dedicated system for camera control with the use of a GPIB interface to transfer data for electronic storage.

Much of the software and processing algorithms can be developed separately from the optical processors. Software development will require availability of the PC with appropriate LABVIEW/LABWINDOWS software, BitFlow camera card, and GPIB card. This would allow theoretical processors to be further developed separately from the control system. Final system integration will test the control algorithms, software, and optical processor.

5.3 CONCEPT EVALUATION IN COMPLEX JAMMER SCENARIOS

It is recommended that this activity be pursued to continue to evaluate the MADOP algorithm performance in realistic jamming environments using computer simulation. This will further detail the analysis of the MADOP algorithm as described in Section 2 of this report. Parameters that drive these simulations should be based on the measured and achievable MADOP performance and on the specific parameters of the radar selected for MADOP insertion.

Results of this concept evaluation should drive further improvements to the MADOP and its electronic interfaces, including: 1) the possible use of multiple MADOP systems in an IIR filter configuration, as described in Section 2 of this report; 2) the development of digital interface algorithms to more effectively select the filter tap weighting functions; 3) requirements for weight update time as a function of jammer environment; and 4) the possible benefits and limitations of using discrete tap weighting schemes using VCSEL arrays.

APPENDIX A

ON-SITE SUPPORT PERIOD ONE TEST MATRICES

DATE	TIME	PLOT NUMBE	DESCRIPTION OF TEST	COMMENTS
18-Jul		18001	Correlator Frequency Response	
18-Jul		18002		
18-Jul		18003		
18-Jul		18004		
18-Jul		18005		
18-Jul		18006		
18-Jul		18007		
18-Jul		18008		
18-Jul		18009		
18-Jul		18010		
18-Jul		18011		
18-Jul		18012		
18-Jul		18013		
18-Jul		18014		
18-Jul		18015		
18-Jul		18016		
18-Jul		18017		
18-Jul		18018		
18-Jul		18019		
18-Jul		18020		
18-Jul		18021		
18-Jul		18022		
18-Jul		18023		
18-Jul		18024		
18-Jul		18025		
18-Jul		18026		
18-Jul		18027		
18-Jul		18028		
18-Jul		18029		
18-Jul		18030		
18-Jul		18031		
18-Jul		18032		
18-Jul		18033		
18-Jul		18034		
18-Jul		18035		
18-Jul		18036		
18-Jul		18037		
18-Jul		18038		
18-Jul		18039		
18-Jul		18040		

DATE	TIME	PLOT NUMBER	DESCRIPTION OF TEST	COMMENTS
19-Jul	8:30 AM	19001	AO Correlator Output, 72 MHz	During on-site support day 3, further alignment and initial characterization of the
19-Jul		19002	AO Correlator Output, 74 MHz	2 AO processors was accomplished.
19-Jul		19003	AO Correlator Output, 75 MHz	
19-Jul		19004	AO Correlator Output, 76 MHz	The AO correlator plots were regenerated because of some errors made in transferring
19-Jul		19005	AO Correlator Output, 78 MHz	the data to excel and plotting during 7/18.
19-Jul		19006	AO Correlator Output, 80 MHz	The power into each path was 14 dBm, generated by the HP83623A synthesizer.
19-Jul		19007	AO Correlator Output, 82 MHz	The stored file names on the computer are: JUL19_01.XLS through JUL19_17.XLS.
19-Jul		19008	AO Correlator Output, 84 MHz	
19-Jul		19009	AO Correlator Output, 85 MHz	
19-Jul		19010	AO Correlator Output, 86 MHz	
19-Jul		19011	AO Correlator Output, 88 MHz	
19-Jul		19012	AO Correlator Output, 90 MHz	
19-Jul		19013	AO Correlator Output, 92 MHz	
19-Jul		19014	AO Correlator Output, 94 MHz	
19-Jul		19015	AO Correlator Output, 96 MHz	
19-Jul		19016	AO Correlator Output, 98 MHz	
19-Jul		19017	AO Correlator Output, 100 MHz	
19-Jul	10:45 AM	19018	AO Correlator Output, 66 MHz	The AO correlator plots were regenerated in order to obtain a better frequency response
19-Jul		19019	AO Correlator Output, 68 MHz	at frequencies at the low end of the band. Kyle was not happy with the performance and
19-Jul		19020	AO Correlator Output, 70 MHz	chose not to print them, although they are stored.
19-Jul		19021	AO Correlator Output, 72 MHz	The power into each path was 14 dBm, generated by the HP83623A synthesizer.
19-Jul		19022	AO Correlator Output, 74 MHz	The stored file names on the computer are: JUL19_18.XLS through JUL19_41.XLS.
19-Jul		19023	AO Correlator Output, 75 MHz	
19-Jul		19024	AO Correlator Output, 76 MHz	
19-Jul		19025	AO Correlator Output, 78 MHz	
19-Jul		19026	AO Correlator Output, 80 MHz	
19-Jul		19027	AO Correlator Output, 82 MHz	
19-Jul		19028	AO Correlator Output, 84 MHz	
19-Jul		19029	AO Correlator Output, 85 MHz	
19-Jul		19030	AO Correlator Output, 86 MHz	
19-Jul		19031	AO Correlator Output, 88 MHz	
19-Jul		19032	AO Correlator Output, 90 MHz	
19-Jul		19033	AO Correlator Output, 92 MHz	
19-Jul		19034	AO Correlator Output, 94 MHz	
19-Jul		19035	AO Correlator Output, 96 MHz	
19-Jul		19036	AO Correlator Output, 98 MHz	
19-Jul		19037	AO Correlator Output, 100 MHz	
19-Jul		19038	AO Correlator Output, 102 MHz	
19-Jul		19039	AO Correlator Output, 104 MHz	
19-Jul		19040	AO Correlator Output, 106 MHz	
19-Jul		19041	AO Correlator Output, 108 MHz	
19-Jul	2:30 PM	19042	tap=64 MHz, tap power = 131 mW	AOTDL frequency response, RF Input Power was +20 dBm
19-Jul		19043	tap=66 MHz, tap power = 156 mW	
19-Jul		19044	tap=68 MHz, tap power = 178 mW	
19-Jul		19045	tap=70 MHz, tap power = 200 mW	These plots are without the knife edge in place, and only slightly optimized. They
19-Jul		19046	tap=72 MHz, tap power = 226 mW	represent a starting point and future plots will show an improvement. The tap power
19-Jul		19047	tap=74 MHz, tap power = 270 mW	measurements made right after the AO TDL cell for various tap frequencies is shown next
19-Jul		19048	tap=76 MHz, tap power = 344 mW	to the frequency label. These measurements were made slightly earlier than the
19-Jul		19049	tap=78 MHz, tap power = 427 mW	frequency response plots. The power shown is with a polarizer inserted to cut down on
19-Jul		19050	tap=80 MHz, tap power = 497 mW	the optical power and avoid saturation of the Newport 835 power meter. The true power
19-Jul		19051	tap=82 MHz, tap power = 521 mW	is approximately 10 times higher than the values shown.
19-Jul		19052	tap=84 MHz, tap power = 492 mW	
19-Jul		19053	tap=86 MHz, tap power = 405 mW	
19-Jul		19054	tap=88 MHz, tap power = 282 mW	
19-Jul		19055	tap=90 MHz, tap power = 159 mW	
19-Jul		19056	tap=92 MHz, tap power = 82 mW	
19-Jul		19057	tap=94 MHz, tap power = 41.8 mW	
19-Jul		19058	tap=96 MHz, tap power = 26.2 mW	
19-Jul		19059	tap=98 MHz, tap power = 19.3 mW	
19-Jul		19060	tap=100 MHz, tap power = 13.7 mW	

DATE	TIME	PLOT NUMBER	DESCRIPTION OF TEST	COMMENTS
20-Jul				During on-site support day 4, further alignment and initial characterization of the
				2 AO processors was accomplished. The two subsystems were also interfaced to the IF
				electronics and the single-loop electronic canceller with results that appeared to be
				comparable to the results during the last on-site C-band testing. Tomorrow we will
				more thoroughly test the integrated system.
20-Jul	8:15 AM	20001	AO Correlator Output, 62 MHz	
20-Jul		20002	AO Correlator Output, 64 MHz	
20-Jul		20003	AO Correlator Output, 66 MHz	
20-Jul		20004	AO Correlator Output, 68 MHz	
20-Jul		20005	AO Correlator Output, 70 MHz	
20-Jul		20006	AO Correlator Output, 72 MHz	
20-Jul		20007	AO Correlator Output, 74 MHz	
20-Jul		20008	AO Correlator Output, 75 MHz	
20-Jul		20009	AO Correlator Output, 76 MHz	These AO Correlator plots represent the final iteration of alignment. The 3-dB frequency
20-Jul		20010	AO Correlator Output, 78 MHz	response went from approximately 66 MHz to 106 MHz.
20-Jul		20011	AO Correlator Output, 80 MHz	The power into each path was 14 dBm, generated by the HP83623A synthesizer.
20-Jul		20012	AO Correlator Output, 82 MHz	The stored file names on the computer are: JUL20_01.XLS through JUL20_31.XLS.
20-Jul		20013	AO Correlator Output, 84 MHz	
20-Jul		20014	AO Correlator Output, 85 MHz	Background subtraction was performed once at 82 MHz prior to any data collection.
20-Jul		20015	AO Correlator Output, 86 MHz	
20-Jul		20016	AO Correlator Output, 88 MHz	Excel files each contain 4 columns of 512 points representing 1) camera pixel values,
20-Jul		20017	AO Correlator Output, 90 MHz	2 and 3) the two background subtraction values, and 4) background subtracted data.
20-Jul		20018	AO Correlator Output, 92 MHz	Column 4 was plotted.
20-Jul		20019	AO Correlator Output, 94 MHz	
20-Jul		20020	AO Correlator Output, 96 MHz	
20-Jul		20021	AO Correlator Output, 98 MHz	
20-Jul		20022	AO Correlator Output, 100 MHz	
20-Jul		20023	AO Correlator Output, 102 MHz	
20-Jul		20024	AO Correlator Output, 104 MHz	
20-Jul		20025	AO Correlator Output, 106 MHz	
20-Jul		20026	AO Correlator Output, 108 MHz	
20-Jul		20027	AO Correlator Output, 110 MHz	
20-Jul		20028	AO Correlator Output, 112 MHz	
20-Jul		20029	AO Correlator Output, 114 MHz	
20-Jul		20030	AO Correlator Output, 116 MHz	
20-Jul	9:40 AM	20031	AO Correlator Output, 118 MHz	
20-Jul	9:45 AM	20032	tap=60 MHz, tap power = 1720 mW	
20-Jul		20033	tap=62 MHz, tap power = 2150 mW	
20-Jul		20034	tap=64 MHz, tap power = 2520 mW	AOTDL frequency response, RF Input Power was +20 dBm
20-Jul		20035	tap=66 MHz, tap power = 2890 mW	
20-Jul		20036	tap=68 MHz, tap power = 3330 mW	
20-Jul		20037	tap=70 MHz, tap power = 3790 mW	These plots are without the knife edge in place. The knife edge didn't seem to improve
20-Jul		20038	tap=72 MHz, tap power = 4240 mW	performance for the configuration. The optical tap power measurements (between the two
20-Jul		20039	tap=74 MHz, tap power = 4700 mW	lenses prior to the detector) are shown next to the frequency label.
20-Jul		20040	tap=76 MHz, tap power = 5070 mW	These measurements were made slightly earlier than the frequency response plots.
20-Jul		20041	tap=78 MHz, tap power = 5100 mW	
20-Jul		20042	tap=80 MHz, tap power = 4560 mW	The power was measured with the Newport 835 power meter with a polarizer before the
20-Jul		20043	tap=82 MHz, tap power = 3600 mW	AO SLM. The polarizer was set to achieve a 10X attenuation, and the power shown to the
20-Jul		20044	tap=84 MHz, tap power = 2490 mW	left is 10X times the actual power meter reading. Power is 213 mW with AO SLM power
20-Jul		20045	tap=86 MHz, tap power = 1520 mW	off, and 0.75 mW (not multiplied by 10X) with the light completely blocked.
20-Jul	11:00 AM	20046	tap=88 MHz, tap power = 846 mW	Each plot also contains a number of measurements of the network analyzer time delay
20-Jul		20047	tap=90 MHz, tap power = 529 mW	estimates. This will aid in tap frequency selection and time delay verification when
20-Jul		20048	tap=92 MHz, tap power = 424 mW	testing with signals begins.
20-Jul		20049	tap=94 MHz, tap power = 383 mW	
20-Jul		20050	tap=96 MHz, tap power = 337 mW	
20-Jul		20051	tap=98 MHz, tap power = 296 mW	
20-Jul		20052	tap=100 MHz, tap power = 283 mW	
20-Jul	2:30 PM	20053	Undesired tap feedthrough frequency r	Taken with network analyzer driving AO SLM at 0 dBm, nothing into AO TDL.
				Not clear why plots coming out in smaller scale.
20-Jul	3:00 PM			
				The AO TDL subsystem was interfaced to the desired RF front end and the single-loop
				electronic canceller, as shown in Figure 4-22, p. 4-16, of 2/95 Final Report. With this
				configuration, the electronic canceller worked as it had during the last C-band testing,
				and we were able to get satisfactory looking cancellation of pulses by manually selecting
				a tap frequency to align the pulses at the subtractor.
				Plots will be generated for this cancellation performance during the "pre-testing" phase
				tomorrow.
20-Jul	4:15 PM			
				When pulsed signals were put into the AO correlator, correlations occurred but the zero
				delay position of the correlation was off of the CCD array. Therefore the CCD array was
				moved to a better position in the beam to achieve a zero delay condition on the array.
20-Jul	4:45 PM	20054	AO Correlator Output, 58 MHz	
20-Jul		20055	AO Correlator Output, 60 MHz	
20-Jul		20056	AO Correlator Output, 62 MHz	These AO correlator frequency response plots were generated and saved in the files
20-Jul		20057	AO Correlator Output, 64 MHz	JUL20_32.XLS through JUL20_62.XLS. The results were comparable to the first set
20-Jul		20058	AO Correlator Output, 66 MHz	of tests for this day, but were not printed out in order to save time. The primary
20-Jul		20059	AO Correlator Output, 68 MHz	difference was a lower amplitude of correlation due to looking at a different location of the
20-Jul		20060	AO Correlator Output, 70 MHz	AO cells, further away from the transducer.
20-Jul		20061	AO Correlator Output, 72 MHz	
20-Jul		20062	AO Correlator Output, 74 MHz	
20-Jul		20063	AO Correlator Output, 75 MHz	
20-Jul		20064	AO Correlator Output, 76 MHz	

20-Jul		20065	AO Correlator Output, 78 MHz	
20-Jul		20066	AO Correlator Output, 80 MHz	
20-Jul		20067	AO Correlator Output, 82 MHz	
20-Jul		20068	AO Correlator Output, 84 MHz	
20-Jul		20069	AO Correlator Output, 85 MHz	
20-Jul		20070	AO Correlator Output, 86 MHz	
20-Jul		20071	AO Correlator Output, 88 MHz	
20-Jul		20072	AO Correlator Output, 90 MHz	
20-Jul		20073	AO Correlator Output, 92 MHz	
20-Jul		20074	AO Correlator Output, 94 MHz	
20-Jul		20075	AO Correlator Output, 96 MHz	
20-Jul		20076	AO Correlator Output, 98 MHz	
20-Jul		20077	AO Correlator Output, 100 MHz	
20-Jul		20078	AO Correlator Output, 102 MHz	
20-Jul		20079	AO Correlator Output, 104 MHz	
20-Jul		20080	AO Correlator Output, 106 MHz	
20-Jul		20081	AO Correlator Output, 108 MHz	
20-Jul		20082	AO Correlator Output, 110 MHz	
20-Jul		20083	AO Correlator Output, 112 MHz	
20-Jul		20084	AO Correlator Output, 114 MHz	

DATE	TIME	PLOT NUMBER	DESCRIPTION OF TEST	COMMENTS
21-Jul	8:30 AM			We discussed the GT310 frequency synthesizer card with Capt. Andy Andrews via telecon
				(210-536-4456, DSN 240-4456 dial 94 instead of 99). As configured, the software
				was driving the HP83623A and not the GT310 card. We had to go into Borland C++ in
				windows and reset the source to GT310, and then recompile. After this was accomplished,
				the tones were generated out of each card. The 0 cable provided a better response than
				the 1, 2, and 3 cables. A 100-MHz LPF was placed after the synthesizer to reject
				harmonics.
21-Jul	9:30 AM	21001	Computer GT310 frequency = 60 MHz	
21-Jul		21002	Computer GT310 frequency = 65 MHz	
21-Jul		21003	Computer GT310 frequency = 70 MHz	These plots are of the frequency output from the GT310 cards. These tones will drive the
21-Jul		21004	Computer GT310 frequency = 75 MHz	AO SLM. The frequency was changed by changing the "F Offset" in the camera windows
21-Jul		21005	Computer GT310 frequency = 80 MHz	while keeping "F Rate" at 0 MHz/pel.
21-Jul		21006	Computer GT310 frequency = 85 MHz	
21-Jul		21007	Computer GT310 frequency = 90 MHz	
21-Jul		21008	Computer GT310 frequency = 95 MHz	
21-Jul		21009	Computer GT310 frequency = 100 MHz	
21-Jul		21010	Prelim Pre-test - Main Channel	
21-Jul		21011	Prelim Pre-test - Cancelled Signal #1	See Merv's notes and the "Parameters 7/21" file for additional details on these tests.
21-Jul		21012	Prelim Pre-test - Cancelled Signal #2	Performance seemed to be comparable for the computer and HP generated taps.
21-Jul		21013	Prelim Pre-test - Cancelled Signal #3	
21-Jul		21014	Prelim Pre-test - O-scope output	
21-Jul		21015	Pre-test #1 Main Channel Signal	Measured as input to AO correlator
21-Jul		21016	Pre-test #1 Main Channel Signal	Measured as main into electronic canceller
21-Jul		21017	Pre-test #1 Error Signal #1	
21-Jul		21018	Pre-test #1 Error Signal #2	
21-Jul		21019	Pre-test #1 Estimate	Measured as estimate at electronic canceller
21-Jul		21020	Pre-test #1 Aux Signal	Measured at input to AO correlator
21-Jul		21021	Pre-test #1 O-scope output	
21-Jul		21022	Pre-test #X Main Channel Signal	Measured as input to AO correlator
21-Jul		21023	Pre-test #X Main Channel Signal	Measured as main into electronic canceller
21-Jul		21024	Pre-test #X Error Signal #1	
21-Jul		21025	Pre-test #X Error Signal #2	
21-Jul		21026	Pre-test #X Estimate	Measured as estimate at electronic canceller
21-Jul		21027	Pre-test #X Aux Signal	Measured at input to AO correlator
21-Jul		21028	Pre-test #X O-scope output	
21-Jul		21029	Pre-test #2 Main Channel Signal	Measured as input to AO correlator
21-Jul		21030	Pre-test #2 Main Channel Signal	Measured as main into electronic canceller
21-Jul		21031	Pre-test #2 Error Signal #1	
21-Jul		21032	Pre-test #2 Error Signal #2	
21-Jul		21033	Pre-test #2 Estimate	Measured as estimate at electronic canceller
21-Jul		21034	Pre-test #2 Aux Signal	Measured at input to AO correlator
21-Jul		21035	Pre-test #2 O-scope output	
21-Jul		21036	Pre-test #3 Main Channel Signal	Measured as input to AO correlator
21-Jul		21037	Pre-test #3 Main Channel Signal	Measured as main into electronic canceller
21-Jul		21038	Pre-test #3 Error Signal #1	
21-Jul		21039	Pre-test #3 Error Signal #2	
21-Jul		21040	Pre-test #3 Estimate	Measured as estimate at electronic canceller
21-Jul		21041	Pre-test #3 Aux Signal	Measured at input to AO correlator
21-Jul		21042	Pre-test #3 O-scope output	
21-Jul		21043	Pre-test #4 Main Channel Signal	Measured as input to AO correlator

21-Jul		21044	Pre-test #4 Main Channel Signal	Measured as main into electronic canceller
21-Jul		21045	Pre-test #4 Error Signal #1	
21-Jul		21046	Pre-test #4 Error Signal #2	
21-Jul		21047	Pre-test #4 Estimate	Measured as estimate at electronic canceller
21-Jul		21048	Pre-test #4 Aux Signal	Measured at input to AO correlator
21-Jul		21049	Pre-test #4 O-scope output	
21-Jul		21050	Pre-test #5 Main Channel Signal	Measured as input to AO correlator
21-Jul		21051	Pre-test #5 Main Channel Signal	Measured as main into electronic canceller
21-Jul		21052	Pre-test #5 Error Signal #1	
21-Jul		21053	Pre-test #5 Error Signal #2	
21-Jul		21054	Pre-test #5 Estimate	Measured as estimate at electronic canceller
21-Jul		21055	Pre-test #5 Aux Signal	Measured at input to AO correlator
21-Jul		21056	Pre-test #5 O-scope output	

See Figure 7/21-1 for the definition of the parameters																
Plot Number	**P1**	**P2**	**P3**	**P4**	**P5**	**P6**	**P7**	**P8**	**P9**	**P10**	**P11**	α1	α2	α3	α4	α5
21010	16.9	-	13.3	5.2	-	25.1	18.8	19.3	19	19.5	25.1	0	8	-	-	21.5
21011																
21012																
21013																
21014																
21015	15	15	11.5	11.5	11.6	11.6	17.7	20.1	17.7	20.2	25.1	0	8	20	8	21.5
21016																
21017																
21018																
21019																
21020																
21021																
21022														55		
21023																
21024																
21025																
21026																
21027																
21028																
21029														30	8	
21030																
21031																
21032																
21033																
21034																
21035																
21036														20	18	
21037																
21038																
21039																

21040																
21041																
21042																
21043														30	18	
21044																
21045																
21046																
21047																
21048																
21049																
21050	15	6.1	11.5	11.5	2.7	2.7	17.7	17.7	17.7	17.9	25.1	0	8	20	8	21.5
21051																
21052																
21053																
21054																
21055																
21056																

DATE	PLOT NUMBER	DESCRIPTION OF TEST	COMMENTS
24-Jul			We met at 9:00 to review progress to date and plans for further testing this week.
			Demos are planned for Thursday afternoon, and we plan to have all the formal testing
			completed by Wednesday afternoon.
			At about 11:00, our tone generator card in the pc began putting out a very poor quality
			tone. Therefore, for all the measurements below, the HP 83623A was employed without
			computer control.
24-Jul	24001	Pre-test #6 Main Channel Signal	Measured as input to AO correlator
24-Jul	24002	Pre-test #6 Main Channel Signal	Measured as main into electronic canceller
24-Jul	24003	Pre-test #6 Error Signal #1	***This test is same as 7/21 pre-test #5 with a 200-ns pulse width***
24-Jul	24004	Pre-test #6 Error Signal #2	
24-Jul	24005	Pre-test #6 Estimate	Measured as estimate at electronic canceller
24-Jul	24006	Pre-test #6 Aux Signal	Measured at input to AO correlator
24-Jul	24007	Pre-test #6 O-scope output	
24-Jul	24008	Pulse Cancellation, O-scope output	200-ns pulse cancellation, tap at 66.7 MHz
24-Jul	24009	Pulse Cancellation, Main Channel Signal	Measured at electronic canceller
24-Jul	24010	Pulse Cancellation, Error Signal	Note that there was 20 dB attn. on one channel, system worked well with or without this.
24-Jul	24011	Noise Spectrum #1	80/10 MHz BPF after Noise Com noise generator, 10 dB attn., AR 1W1000 amplifier.
24-Jul	24012	Noise Spectrum #2	Power for these measurements was 23.5 dBm
24-Jul	24013	Pre-test #7 Main Channel Signal	Measured as input to AO correlator
24-Jul	24014	Pre-test #7 Main Channel Signal	Measured as main into electronic canceller
24-Jul	24015	Pre-test #7 Error Signal #1	***This test is a noise jammer with a tone signal, 20 dB J/S in the aux,***
24-Jul	24016	Pre-test #7 Error Signal #2	***0 dB J/S in the main***
24-Jul	24017	Pre-test #7 Estimate	Measured as estimate at electronic canceller
24-Jul	24018	Pre-test #7 Aux Signal	Measured at input to AO correlator
24-Jul	24019	Pre-test #7 O-scope output	
24-Jul	24020	Pre-test #8 Main Channel Signal	Measured as input to AO correlator
24-Jul	24021	Pre-test #8 Main Channel Signal	Measured as main into electronic canceller
24-Jul	24022	Pre-test #8 Error Signal #1	***This test is a noise jammer with pulsed signal, 20 dB J/S in the aux,***
24-Jul	24023	Pre-test #8 Error Signal #2	***0 dB J/S in the main, PW = 1 μs, PRI = 10 μs***
24-Jul	24024	Pre-test #8 Estimate	Measured as estimate at electronic canceller
24-Jul	24025	Pre-test #8 Aux Signal	Measured at input to AO correlator
24-Jul	24026	Pre-test #8 O-scope output	
24-Jul	24027	Pre-test #8 O-scope output, main waveforms	
24-Jul	24028	Pre-test #9 Main Channel Signal	Measured as input to AO correlator
24-Jul	24029	Pre-test #9 Main Channel Signal	Measured as main into electronic canceller
24-Jul	24030	Pre-test #9 Error Signal #1	***This test is a noise jammer with pulsed signal, 20 dB J/S in the aux,***
24-Jul	24031	Pre-test #9 Error Signal #2	***0 dB J/S in the main, PW = 200 ns, PRI = 10 μs***
24-Jul	24032	Pre-test #9 Estimate	Measured as estimate at electronic canceller
24-Jul	24033	Pre-test #9 Aux Signal	Measured at input to AO correlator
24-Jul	24034	Pre-test #9 O-scope output	
24-Jul	24035	Pre-test #9 O-scope output	For twice the pulse amplitude/offset, 2-μs/div scale
24-Jul	24036	Pre-test #9 O-scope output	For twice the pulse amplitude/offset, 5-μs/div scale

See Figure 7/21-1 for the definition of the parameters																
Plot Number	**P1**	**P2**	**P3**	**P4**	**P5**	**P6**	**P7**	**P8**	**P9**	**P10**	**P11**	α1	α2	α3	α4	α5
24001	15.1	-1	11.6	11.6	-4	-4	17.6	17.4	17.6	17.5	24	0	8	20	8	-
24002																
24003																
24004																
24005																
24006																
24007																
24008	-	12.7	-	-	9.3	9.4	-4.1	14.5	-4.1	14.7	24	0	8	20	8	-
24009																
24010																
24011	N/A															
24012	N/A															
24013	13.1	13.1	9.7	9.6	9.7	9.7	15.5	18.3	15.5	18.3	24	0	8	20	8	
24014																
24015																
24016																
24017																
24018																
24019																
24020	14.6	4.7	11.2	11.1	1.2	1.2	17	17	16.9	17.2	24	0	8	20	8	-
24021																
24022																
24023																
24024																
24025																
24026																
24027																
24028	14.6	-1.8	11.2	11.1	-5.4	-5.2	16.9	16.7	16.9	16.9	24	0	8	20	8	-
24029																
24030																
24031																
24032																
24033																
24034																
24035																
24036																

DATE	PLOT NUMBER	DESCRIPTION OF TEST	COMMENTS
25-Jul			
25-Jul	25001	Pre-test #10 Main Channel Signal	Measured as input to AO correlator
25-Jul	25002	Pre-test #10 Error Signal #1	***This test replaces the jammer with the C-band radar aux signal for***
25-Jul	25003	Pre-test #10 Aux Signal	Measured at input to AO correlator
25-Jul	25004	Pre-test #10 O-scope output	***pre-test #5***
25-Jul	25005	Pre-test #11 Main Channel Signal	Measured as input to AO correlator
25-Jul	25006	Pre-test #11 Error Signal #1	***This test replaces the jammer with the C-band radar aux signal for***
25-Jul	25007	Pre-test #11 Aux Signal	Measured at input to AO correlator
25-Jul	25008	Pre-test #11 O-scope output	***pre-test #6***
25-Jul	25009	Tone Jammer used in Pre-Tests #10,11	For all these aux channel C-band pre-tests, this radar signal was for the T/R switch
25-Jul	25010	Noise Jammer used in Pre-Tests #12,13	being on.
25-Jul	25011	Pre-test #12 Main Channel Signal	Measured as input to AO correlator
25-Jul	25012	Pre-test #12 Error Signal #1	***This test replaces the jammer with the C-band radar aux signal for***
25-Jul	25013	Pre-test #12 Aux Signal	Measured at input to AO correlator
25-Jul	25014	Pre-test #12 O-scope output	***pre-test #8***
25-Jul	25015	Pre-test #13 Main Channel Signal	Measured as input to AO correlator
25-Jul	25016	Pre-test #13 Error Signal #1	***This test replaces the jammer with the C-band radar aux signal for***
25-Jul	25017	Pre-test #13 Aux Signal	Measured at input to AO correlator
25-Jul	25018	Pre-test #13 O-scope output	***pre-test #9***
25-Jul	25019	Pre-test #14 Main Channel Signal	Measured as input to AO correlator
25-Jul	25020	Pre-test #14 Error Signal #1	***This test repeats Pre-test #12 for computer control of HP83623A,***
25-Jul	25021	Pre-test #14 Error Signal #2	***with 40ms int. time, 60 MHz f0, .02MHz/pel***
25-Jul	25022	Pre-test #14 Aux Signal	Measured at input to AO correlator
25-Jul	25023	Pre-test #14 O-scope output #1	
25-Jul	25024	Pre-test #14 O-scope output #2	
25-Jul	25025	Pre-test #14 O-scope output #3	
25-Jul	25026	Pre-test #14 O-scope output #4	
25-Jul	25027	Pre-test #15 Main Channel Signal	Measured as input to AO correlator
25-Jul	25028	Pre-test #15 Error Signal #1	***This test repeats Pre-test #10 for computer control of HP83623A,***
25-Jul	25029	Pre-test #15 Error Signal #2	***with 40ms int. time, 60 MHz f0, .02MHz/pel***
25-Jul	25030	Pre-test #15 Aux Signal	Measured at input to AO correlator
25-Jul	25031	Pre-test #15 O-scope output #1	
25-Jul	25032	Pre-test #15 O-scope output #2	***Note: sometimes error signal looked just like main channel, which***
25-Jul	25033	Pre-test #15 O-scope output #3	***occurred when tap switching was happening. This case wasn't plotted,***
25-Jul	25034	Pre-test #15 O-scope output #4	***although the o-scope outputs reflect this occurrence.***
25-Jul	25035	Test #1A Main Channel Signal	Measured as input to AO correlator
25-Jul	25036	Test #1A Error Signal #1	***Tone jammer, tone target, +7 dB J/S in main***
25-Jul	25037	Test #1A Error Signal #2	***computer controlled tap with 5 ms int. time, 60 MHz f0, .02MHz/pel***
25-Jul	25038	Test #1A Aux Signal	Measured at input to AO correlator
25-Jul	25039	Test #1A O-scope output #1	
25-Jul	25040	Test #1A O-scope output #2	***Note: sometimes error signal looked just like main channel, which***
25-Jul	25041	Test #1A O-scope output #3	***occurred when tap switching was happening. This case wasn't plotted,***
25-Jul	25042	Test #1A O-scope output #4	***although the o-scope outputs reflect this occurrence.***

25-Jul	25043	Test #1B Main Channel Signal	Measured as input to AO correlator
25-Jul	25044	Test #1B Error Signal #1	***Tone jammer, tone target, +7 dB J/S in main***
25-Jul	25045	Test #1B Error Signal #2	***computer controlled tap with 5 ms int. time, 66.7 MHz f0, 0 MHz/pel***
25-Jul	25046	Test #1B Aux Signal	Measured at input to AO correlator
25-Jul	25047	Test #1B O-scope output #1	
25-Jul	25048	Test #1B O-scope output #2	
25-Jul	25049	Test #1B O-scope output #3	
25-Jul	25050	Test #1B O-scope output #4	

See Figures 7/21-1 and 7/24-1 for the definition of the parameters																	
Plot Number	**P1**	**P2**	**P3**	**P4**	**P5**	**P6**	**P7**	**P8**	**P9**	**P10**	**P11**	α1	α2	α3	α4		
25001	11.5	6.4	7.8	7.8	3.3	3.3	13.7	14.2			24	0	8	20	8		
25005		0.9															
25011	11.8	6.5															
25015		1.1															
25019	11	4.5															
25027	11.3	4.5															
	P1	**P2**	**P3**	**P4**	**P5**	**P6**	**P7**	α1	α2	α3	α4	α5	θ	**fj**	**ft**		
25035	11.5	12.5	20.4	20.9	20.3	21.2	24	0	8	-	0	20	96.49	80	81		

DATE	PLOT NUMBER	DESCRIPTION OF TEST	COMMENTS
26-Jul			The morning was taken up with getting the jammers up and operating because the main
			power was lost in last night's storm. A generator was found and hooked up, and at that ti
			the power company fixed the main power generator. Also in the morning, photographs
			were taken of the MADOP system and C-band radar. After lunch, testing resumed.
26-Jul	26001	Aux Channel Frequency Response	Measured from radar input to splitter before AO correlator and AO TDL
26-Jul	26002	Sum Channel Frequency Response	Measured from radar input to splitter before AO correlator and electronic canceller
			The delay measurement went up to 6.26 μm for some reason after plot (probably a
			network analyzer anomaly. Returned to aux channel and correct measurement obtained.
26-Jul	26003	Test #2A Main Channel Signal	Measured as input to AO correlator
26-Jul	26004	Test #2A Error Signal #1	***Tone jammer, tone target, 0 dB J/S in main***
26-Jul	26005	Test #2A Error Signal #2	***computer controlled tap with 20 ms int. time, 66.7 MHz f0, 0 MHz/pel***
26-Jul	26006	Test #2A Aux Signal	Measured at input to AO correlator
26-Jul	26007	Test #2A O-scope output #1	
26-Jul	26008	Test #2B Error Signal #1	***Tone jammer, tone target, 0 dB J/S in main***
26-Jul	26009	Test #2B Error Signal #2	***computer controlled tap with 20 ms int. time, 60 MHz f0, .02MHz/pel***
26-Jul	26010	Test #2B O-scope output #1	
26-Jul	26011	Test #2B O-scope output #2	
26-Jul	26012	Test #2B O-scope output #3	
26-Jul	26013	Test #2B O-scope output #4	
			At this point, we realized that we are using antenna channel 2, but the
			beam pattern was made using channel 1. This explains the 20 dB sidelobe
			level as opposed to the 30 dB sidelobe level.
26-Jul	26014	Test #2C Main Channel Signal	Measured as input to AO correlator
26-Jul	26015	Test #2C Error Signal #1	***Tone jammer, tone target, 0 dB J/S in main***
26-Jul	26016	Test #2C Error Signal #2	***computer controlled tap with 20 ms int. time, 66.7 MHz f0, 0 MHz/pel***
26-Jul	26017	Test #2C Aux Signal	Measured at input to AO correlator
26-Jul	26018	Test #2C O-scope output #1	
26-Jul	26019	Test #2D Error Signal #1	***Tone jammer, tone target, 0 dB J/S in main***
26-Jul	26020	Test #2D Error Signal #2	***computer controlled tap with 20 ms int. time, 60 MHz f0, .02MHz/pel***
26-Jul	26021	Test #2D O-scope output #1	
26-Jul	26022	Test #2D O-scope output #2	
26-Jul	26023	Test #2D O-scope output #3	
26-Jul	26024	Test #2D O-scope output #4	
26-Jul	26025	Test #3A Main Channel Signal	Measured as input to AO correlator
26-Jul	26026	Test #3A Error Signal #1	***Noise jammer, tone target, 19 dB J/S in main***
26-Jul	26027	Test #3A Error Signal #2	***computer controlled tap with 20 ms int. time, 66.7 MHz f0, 0 MHz/pel***
26-Jul	26028	Test #3A Aux Signal	Measured at input to AO correlator
26-Jul	26029	Test #3A O-scope output #1	
26-Jul	26030	Test #3B Error Signal #1	***Noise jammer, tone target, 19 dB J/S in main***
26-Jul	26031	Test #3B Error Signal #2	***computer controlled tap with 20 ms int. time, 60 MHz f0, .02MHz/pel***
26-Jul	26032	Test #3B O-scope output #1	
26-Jul	26033	Test #3B O-scope output #2	
26-Jul	26034	Test #3B O-scope output #3	

26-Jul	26035	Test #3B O-scope output #4	
26-Jul	26036	Test #4A Main Channel Signal	Measured as input to AO correlator
26-Jul	26037	Test #4A Error Signal #1	***Noise jammer, tone target, 9 dB J/S in main***
26-Jul	26038	Test #4A Error Signal #2	***computer controlled tap with 20 ms int. time, 66.7 MHz f0, 0 MHz/pel***
26-Jul	26039	Test #4A Aux Signal	Measured at input to AO correlator
26-Jul	26040	Test #4A O-scope output #1	
26-Jul	26041	Test #4B Error Signal #1	***Noise jammer, tone target, 9 dB J/S in main***
26-Jul	26042	Test #4B Error Signal #2	***computer controlled tap with 20 ms int. time, 60 MHz f0, .02MHz/pel***
26-Jul	26043	Test #4B O-scope output #1	
26-Jul	26044	Test #4B O-scope output #2	***This J/S was measured, the 19 and -1 dB J/S's were based on attenuator***
26-Jul	26045	Test #4B O-scope output #3	***settings. J/S measurements were: 9.5 dBm jammer in main and 0.7 dbm***
26-Jul	26046	Test #4B O-scope output #4	***target in main, 8.6 dBm jammer in aux and -31 dBm target in aux***
26-Jul	26047	Test #5A Main Channel Signal	Measured as input to AO correlator
26-Jul	26048	Test #5A Error Signal #1	***Noise jammer, tone target,-1 dB J/S in main***
26-Jul	26049	Test #5A Error Signal #2	***computer controlled tap with 20 ms int. time, 66.7 MHz f0, 0 MHz/pel***
26-Jul	26050	Test #5A Aux Signal	Measured at input to AO correlator
26-Jul	26051	Test #5A O-scope output #1	
26-Jul		Test #5B Error Signal #1	***Noise jammer, tone target, -1 dB J/S in main***
26-Jul		Test #5B Error Signal #2	***computer controlled tap with 20 ms int. time, 60 MHz f0, .02MHz/pel***
26-Jul		Test #5B O-scope output #1	
26-Jul		Test #5B O-scope output #2	***The correlator was giving erroneous results during background***
26-Jul		Test #5B O-scope output #3	***subtraction, etc., so the tap was stuck at 60 MHz. We therefore didn't***
26-Jul		Test #5B O-scope output #4	***run these tests.***
26-Jul	26052	Test #6A Main Channel Signal	Measured as input to AO correlator
26-Jul	26053	Test #6A Error Signal #1	***Tone jammer, tone target, 7 dB J/S in main***
26-Jul	26054	Test #6A Error Signal #2	***computer controlled tap with 20 ms int. time, 66.7 MHz f0, 0 MHz/pel***
26-Jul	26055	Test #6A Aux Signal	Measured at input to AO correlator
26-Jul	26056	Test #6A O-scope output #1	
26-Jul	26057	Test #6B Error Signal #1	***Tone jammer, tone target, 7 dB J/S in main***
26-Jul	26058	Test #6B Error Signal #2	***computer controlled tap with 20 ms int. time, 60 MHz f0, .02MHz/pel***
26-Jul	26059	Test #6B O-scope output #1	
26-Jul	26060	Test #6B O-scope output #2	
26-Jul	26061	Test #6B O-scope output #3	
26-Jul	26062	Test #6B O-scope output #4	
26-Jul	26063	Test #7A Main Channel Signal	Measured as input to AO correlator
26-Jul	26064	Test #7A Error Signal #1	***Tone jammer, tone target, -13 dB J/S in main***
26-Jul	26065	Test #7A Error Signal #2	***computer controlled tap with 20 ms int. time, 66.7 MHz f0, 0 MHz/pel***
26-Jul	26066	Test #7A Aux Signal	Measured at input to AO correlator
26-Jul	26067	Test #7A O-scope output #1	
26-Jul		Test #7B Error Signal #1	***Tone jammer, tone target, -13 dB J/S in main***
26-Jul		Test #7B Error Signal #2	***computer controlled tap with 20 ms int. time, 60 MHz f0, .02MHz/pel***
26-Jul		Test #7B O-scope output #1	
26-Jul		Test #7B O-scope output #2	***The correlator was giving erroneous results during background***
26-Jul		Test #7B O-scope output #3	***subtraction, etc., so the tap was stuck at 60 MHz. We therefore didn't***
26-Jul		Test #7B O-scope output #4	***run these tests.***

See Figure 7/24-1 for the definition of the parameters																		
Plot Number	**P1**	**P2**	**P3**	**P4**	**P5**	**P6**	**P7**	α1	α2	α3	α4	Θ	**f J**	**f t**	αA	αM		
26001								0	8	-	-	96.49	80	81	17	6		
26003	9.8	12.7	16	21.3	15.6	21.4	23.9	0	8	0	10		79.95	80.95	26	12		
26014	10.3	12.7	16	21.3	15.8	21.2		0	8	0	20	96.5			26	1		
26025	8.6	9.9	15.1	18.9	14.8	18.9				0	40		N/A	79.93	26	1		
26036	8.5	10.7	15.1	19.5	15	19.5		0	8	0	30				26	1		
26047	10.9	12.9	17.2	21.3	17.2	21.7		0	8	0	20				23	1		
26052	9.7	8.4	16	17.9	15.8	18.5				0	30		79.93	80.93	23	0		
26063	12	11.7	18.5	20.4	18.4	20.5				0	10				21	10.5		

DATE	PLOT NUMBER	DESCRIPTION OF TEST	COMMENTS
27-Jul			
27-Jul	27001	AO TDL frequency response	tap frequency = 67.7 MHz (was the same at 66.7 MHz also).
27-Jul	27002	AO TDL frequency response	measured through Aux channel path (from radar input connector)
27-Jul	27003	AO TDL frequency response	larger scale
27-Jul	27004	AO TDL frequency response	larger scale with 3 dB / div
27-Jul	27005	Test #5A Main Channel Signal	Measured as input to AO correlator
27-Jul	27006	Test #5A Error Signal #1	Noise jammer, tone target,-1 dB J/S in main
27-Jul	27007	Test #5A Error Signal #2	computer controlled tap with 20 ms int. time, 66.7 MHz f0, 0 MHz/pel
27-Jul	27008	Test #5A Aux Signal	Measured at input to AO correlator
27-Jul	27009	Test #5A O-scope output #1	***These tests were repeated with a 25 MHz span on spectrum analyzer.***
27-Jul	27010	Test #5B Error Signal #1	Noise jammer, tone target, -1 dB J/S in main
27-Jul	27011	Test #5B Error Signal #2	computer controlled tap with 20 ms int. time, 60 MHz f0, .02MHz/pel
27-Jul	27012	Test #5B O-scope output #1	
27-Jul	27013	Test #5B O-scope output #2	The correlator was giving better results this time.
27-Jul	27014	Test #5B O-scope output #3	
27-Jul	27015	Test #5B O-scope output #4	These tests were also run with an extra splitter to split the main channel AO correlator inp
27-Jul	27016	Test #4A Main Channel Signal	Measured as input to AO correlator
27-Jul	27017	Test #4A Error Signal #1	Noise jammer, tone target, 9 dB J/S in main
27-Jul	27018	Test #4A Error Signal #2	computer controlled tap with 20 ms int. time, 66.7 MHz f0, 0 MHz/pel
27-Jul	27019	Test #4A Aux Signal	Measured at input to AO correlator
27-Jul	27020	Test #4A O-scope output #1	***These tests were repeated with a 25 MHz span on spectrum analyzer.***
27-Jul	27021	Test #4B Error Signal #1	Noise jammer, tone target, 9 dB J/S in main
27-Jul	27022	Test #4B Error Signal #2	computer controlled tap with 20 ms int. time, 60 MHz f0, .02MHz/pel
27-Jul	27023	Test #4B O-scope output #1	
27-Jul	27024	Test #4B O-scope output #2	The correlator was giving better results this time.
27-Jul	27025	Test #4B O-scope output #3	
27-Jul	27026	Test #4B O-scope output #4	These tests were also run with an extra splitter to split the main channel AO correlator inp
27-Jul	27027	Test #8A Main Channel Signal	Measured as input to AO correlator
27-Jul	27028	Test #8A Error Signal #1	Noise jammer, tone target,-11 dB J/S in main
27-Jul	27029	Test #8A Error Signal #2	computer controlled tap with 20 ms int. time, 66.7 MHz f0, 0 MHz/pel
27-Jul	27030	Test #8A Aux Signal	Measured at input to AO correlator
27-Jul	27031	Test #8A O-scope output #1	
27-Jul	27032	Test #8B Error Signal #1	Noise jammer, tone target, -11 dB J/S in main
27-Jul	27033	Test #8B Error Signal #2	computer controlled tap with 20 ms int. time, 60 MHz f0, .02MHz/pel
27-Jul	27034	Test #8B O-scope output #1	
27-Jul	27035	Test #8B O-scope output #2	The correlator was giving better results this time.
27-Jul	27036	Test #8B O-scope output #3	
27-Jul	27037	Test #8B O-scope output #4	These tests were also run with an extra splitter to split the main channel AO correlator inp
	27038	AOTDL/Electronic Canceller Frequency Resp.	Tap frequency = 66.7 MHz, P = 25 dBm. The network analyzer was configured to run
			a -10 dBm source through a splitter to provide
			a main and aux channel input. Attenuators are 0, 2, 6.5, and 4.5 dB on the 5 µs BAW
			output, the 6.1 µs BAW output, the aux input, and the main input, respectively.
			The main channel input to the AO Correlator (the other side of a splitter that provides the

			main channel signal into the electronic canceller) is input to R1 as representative of the
			reference we would like to measure frequency response relative to.
			The network analyzer was corrected using the AOTDL input signal (directly input into the
			AOTDL) as an input to T1. The error signal from the canceller is then used as the T1
			input after correction. The scan was made slow by keeping a narrow resolution BW so
			that the electronic canceller response time was fast enough.
	27039	AOTDL/Electronic Canceller Frequency Resp.	Tap frequency = 75 MHz, P = 25 dBm. Note reference level change to 30 dBm.
	27040	AOTDL/Electronic Canceller Frequency Resp.	Tap frequency = 66.6 MHz, P = 25 dBm.
	27041	Main Channel Tone	Measured at input to AO Correlator for Main Channel. Tap frequency = 66.7 MHz, P = 25 d
	27042	Cancelled Signal	See Back for multiple single-trigger readings of peak powers.
	27043	Another Cancelled Signal	
	27044	Main Channel Tone	Same as 27041 with narrower RBW.
	27045	Cancelled Signal	
	27046	Cancelled Signal	
	27047	Input to AO TDL	This was used to normalize the earlier network analyzer plot. Note 5 dB Jam to Noise
			loss relative to 27044.
	27048	Tone source (IntraAction DE)	Note that noise floor is set by network analyzer (50 dB attn setting in all of the above plo
	27049	Tone source (IntraAction DE)	Reduction to 10 dB attn setting, same as 27048.
	27050	Input to AOTDL	Reduction to 40 dB attn setting, same as 27047.
	27051	Target source (IntraAction ME)	Note ME source bleeding through. We are regularly checking noise floor with termination
			on input port to ensure that we are seeing system noise floor.
	27052	Main Channel Jammer and Target	J/S ratio = 38 dB.
	27053	Cancelled Signal	J/S gain = 38 - 12 dB = 26 dB gain.
	27054	Cancelled Signal	J/S gain = 38 - 20 dB = 18 dB gain.
	27055	Main Channel Jammer and Target	J/S ratio = 0 dB.
	27056	Cancelled Signal	J/S gain = 0 + 22 dB = 22 dB gain.
	27057	Cancelled Signal	J/S gain = 0 + 29 dB = 29 dB gain. Note intermods are actually higher than jammer.
	27058	Cancelled Signal	J/S gain = 0 + 10 dB = 10 dB gain.
			We verified that the extra tones are intermods by tuning the IntraAction DE source.

See Figure 7/24-1 for the definition of the parameters																		
Plot Number	**P1**	**P2**	**P3**	**P4**	**P5**	**P6**	**P7**	α1	α2	α3	α4	Θ	**f j**	**f t**	αA	αM		
27005	10.6	10.8	16.9		19.4			0	8	0	20				21.5	5		
27016	10.4	8.3	16.8		17						30							
27027	10.5	11.7	16.9		20.2						10					11		

DATE	PLOT NUMBER	DESCRIPTION OF TEST	COMMENTS
28-Jul			
28-Jul	28001	Input to AO SLM	HP83623A frequency = 66 MHz, P = 22 dBm. IntraAction DE provided other source.
28-Jul	28002	AO TDL frequency response	Measured input to AO TDL through detector.
28-Jul	28003	Input to AO SLM	Another tap combination.
28-Jul	28004	AO TDL frequency response	
28-Jul	28005	Input to AO SLM	3 taps. Third tap at 80MHz provided by IntraAction ME.
28-Jul	28006	AO TDL frequency response	
28-Jul	28007	O-scope for multipath cancellation.	The Lecroy was set at 200-µs, 1-µs width/period, with a 400 mV amplitude driving the
28-Jul			IntraAction ME. This signal was used to provide an aux of 5.0 µs and two replicas in the
28-Jul			main having 6.0 µs and 6.1 µs. Taps were set with the hp 83623A and the IntraAction DE
28-Jul			Power and frequency of the taps were varied to achieve this cancellation.
			HP83623A was 65.13 MHz, 24 dBm.
28-Jul	28008	Main channel	measured at AO correlator input.
28-Jul	28009	Cancelled Signal	for 28007
28-Jul	28010	Tap Frequency Input	
28-Jul	28011	O-scope for multipath cancellation.	HP83623A was 65.154 MHz, 21.9 dBm.
28-Jul	28012	O-scope for multipath cancellation.	HP83623A was 65.153 MHz, 22.1 dBm.
28-Jul	28013	Cancelled Signal	for 28012
28-Jul	28014	Frequency Response of ZSCJ-2-1 Subtactor	See Figure 7/28-2.

APPENDIX B

ON-SITE SUPPORT PERIOD TWO TEST MATRICES

DATE	PLOT NUMBER	DESCRIPTION OF TEST	COMMENTS	
1-May	51001	Electronic Canceller Frequency Response	Vector Modulator not powered	
	51002		Vector Modulator powered (dashed plot is 51001)	
	51003		Vector Modulator powered (dashed) and not powered (solid), extended scale	
	51004		Vector Modulator not powered (dashed) and with 5-ft cable between vector modulator and	
			PA-4 amplifier (solid). Vector modulator remains unpowered for rest of tests.	
			Vector modulator remains unpowered for rest of tests.	
	51005		5-ft cable removed. PA-4 amplifier (dashed) vs. Amp Rsch TW-1000 amplifier (solid)	
			Amp Rsch TW-1000 amplifier used for rest of tests.	
	51006		100-MHz low-pass filter removed in error feedback path	
	51007		10-dB and 3-dB attenuators removed from error feedback path (solid). Dashed is 51006.	
	51008		Same as 51007 solid plot, but on a smaller scale	
			Note: the 100-MHz low-pass filter was placed after the AOTDL photodetector, and the	
			13 dB of attenuation was completely removed. This was used previously to limit max power	
			into the phase comparator to 10 dBm. When the attenuators are removed, care must be	
			taken to not overdrive phase comparator. This was done by attenuating the main channel	
			reference signal into the electronic canceller to a 0-dBm level, which led to a 7 dBm power	
			in the error channel input to the phase comparator when the system was unstable (not	
			cancelling). The plots do not reflect this 0-dBm level, but rather a stronger input.	
3-May	53001	10-dBm limiter frequency response	10-dBm limiter S11 plot, 0-dBm source (-6 dBm into device)	
	53002		10-dBm limiter S11 plot, 15-dBm source (9 dBm into device)	
	53003		10-dBm limiter S21 plot, 0-dBm source (-3 dBm into device)	
	53004		10-dBm limiter S21 plot, 12-dBm source (9 dBm into device)	
			Two of these limiters are placed at each input to the phase comparator to allow stronger	
			drive signal inputs to the electronic canceller without damage.	
	53005	Electronic Canceller Frequency Response	15-dBm source power split to reference and AOTDL inputs. Limiters in place.	
	53006	AOTDL/Elect. Canceller Frequency Response	15-dBm source power split to reference and AOTDL AO cell. Limiters in place. Tap was	
			80 MHz with 20 dBm power. N.A. scan time was 20 sec (as in above plots).	
	53007		15-dBm source power split to reference and AOTDL AO cell. Limiters in place. Tap was	
			80 MHz with 20 dBm power. Reference signal (dashed) and cancelled signal (solid).	
			APPROXIMATELY 45 dB CANCELLATION ACHIEVED !!!!	
	53008		Same as 52007 but with smaller span (20 sec scan still), and with a scanning tap	
			frequency from 75 to 85 MHz with 20 sec scan time. Tap scan begins when N.A. at	
			approximately 74.5 MHz (note transient).	
	53009	Cancelled 500-ns pulse	Cancelled pulse (solid) and reference pulse (dashed). 500-ns PW, 5-µs PRI, 23 dBm	
			into splitter that drives AOTDL AO cell, 14 dBm into splitter that drives reference.	
			Tap at 77.3 MHz, 20 dBm.	
	53010	Cancelled 200-ns pulse	Cancelled pulse (solid) and reference pulse (dashed). 200-ns PW, 2-µs PRI, 23 dBm	
			into splitter that drives AOTDL AO cell, 14 dBm into splitter that drives reference.	
	53011	Cancelled 100-ns pulse	Cancelled pulse (solid) and reference pulse (dashed). 100-ns PW, 1-µs PRI, 23 dBm	
			into splitter that drives AOTDL AO cell, 14 dBm into splitter that drives reference.	
			Power meter / 10-MHz BPF measurement of main channel was 13.8 dBm, and of error	
			signal was -3.6 dBm. Total 17.4-dBm cancellation as measured by power meter in	
			10-MHz system band.	
	53012	C-band array sum beam	Center and right jammer poles, 20-kHz separation, main beam pointed to right of right pole.	
			We use this waveform as our "auxiliary input" giving low S/J ratio ("jammer" to right).	
	53013	C-band array auxiliary beam	Center and right jammer poles, 20-kHz separation, approximately omnidirectional.	

			We use this waveform as our "main input" giving a significant S/J ratio.	
6-May	56001	Cancellation of tone with tone signal	Early test, before jammers reconfigured. Main channel (dashed) and cancelled signal (solid)	
			with about 13-dB S/J improvement. Note that aux channel had about a 15-dB J/S ratio,	
			which implies some of signal will be cancelled from main channel as well as jammer.	
			T/R switching was on for this plot, but turned off thereafter.	
	56002	Cancellation of tone with tone signal	Jammers reconfigured. Main channel (dashed) and cancelled signal (solid) with 20 dB S/J	
			improvement. Aux channel has 15-dB J/S ratio and 20.9 dBm input power. Main channel	
			has 12.7 dBm input power. T/R switched turned off.	
	56003	Total System Frequency Response	Includes RF electronics / BAW delay lines, AO tapped delay line filter, and electronic	
			canceller. Frequency response (solid) and reference signal power (dashed). In preparing	
			this plot, realized that AO tapped delay line filter was misaligned at pinhole filter. This	
			plot is after realignment.	
	56004	Total System Frequency Response	Same as 56003 except correlator output used to control tap frequency. Main effect is to	
			generate transients at each tap frequency change.	
7-May	57001	System Pulse Cancellation	System pulse cancellation performance. Carrier frequency of 80 MHz,	
			1.0 µsec pulse period, 100 nsec pulsewidth.	
			Tap frequency of 72.81 MHz and tap power of 11 dBm.	
			Power levels of +18.6 dBm AOTDL input, +19.6-9 dBm reference channel input.	
	57002	System CW tone cancellation from radar	System CW signal cancellation performance. Main channel is dashed line.	
			Cancelled channel is solid curve. Aux channel S/J is -15 dB. AOTDL input power +22 dBm.	
			Reference channel input power is 20 - 9 dBm.	
			Tap frequency of 72.81 MHz and tap power of 11 dBm.	
	57003	System CW Cancellation from radar	System CW signal cancellation performance. Main channel is dashed line.	
			Cancelled channel is solid curve. Aux channel S/J is -3 dB. AOTDL input power + 22 dBm.	
			Reference channel input power is 15.3 - 9 dBm.	
			Tap frequency of 73.5 MHz and tap power of 11 dBm.	
	57004	System CW Cancellation from radar	System CW signal cancellation performance. Same as 57003, except of the range	
			cancellations observed, a lesser cancellation was plotted.	
	57005	System CW Cancellation from radar	System CW signal cancellation performance. Main channel is dashed line.	
			Cancelled channel is solid curve. Aux channel S/J is -23 dB. AOTDL input power + 21.7 dBm.	
			Reference channel input power is 14.1 - 9 dBm.	
			Tap frequency of 73.5 MHz and tap power of 11 dBm.	
	57006	System CW Cancellation from radar	System CW signal cancellation performance. Main channel is dashed line.	
			Cancelled channel is solid curve. Aux channel S/J is -23 dB. AOTDL input power + 21.7 dBm.	
			Reference channel input power is 14.1 - 9 dBm.	
			Tap frequency of 73.5 MHz and tap power of 15 dBm.	
	57007	System Pulse Tone Cancellation from Radar	System Pulsed tone cancellation performance. Pulsed target (500 µsec pulse at 50% duty cycle).	
			CW jammer. Cancelled channel is solid line. Main channel is dashed line.	
			Aux channel S/J = -10 dB. AOTDL input power = +21.9 dBm.	
			Reference channel input power is +19.9 - 9 dBm.	
			Tap frequency of 73.5 MHz and tap power of +15 dBm.	
	57008	System Pulse Tone Cancellation from Radar	System Pulsed tone cancellation performance. Pulsed target (500 µsec pulse at 50% duty cycle).	
			CW jammer. Cancelled channel is solid line. Main channel is dashed line.	
			Aux channel S/J = -20 dB. AOTDL input power = +21.9 dBm.	
			Reference channel input power is +19.9 - 9 dBm.	
			Tap frequency of 73.5 MHz and tap power of +15 dBm.	
			Of the range of cancellations observed, this was the worst.	

	57009	System Pulse Tone Cancellation from Radar	System Pulsed tone cancellation performance. Pulsed target (500 µsec pulse at 50% duty cycle).	
			CW jammer. Cancelled channel is solid line. Main channel is dashed line.	
			Aux channel S/J = -20 dB. AOTDL input power = +21.9 dBm.	
			Reference channel input power is +19.9 - 9 dBm.	
			Tap frequency of 73.5 MHz and tap power of +15 dBm.	
			Of the range of cancellations observed, this was the best.	
	57010	System Pulse Tone Cancellation from Radar	System Pulsed tone cancellation performance. Pulsed target (500 µsec pulse at 50% duty cycle).	
			CW jammer. Cancelled channel is solid line. Main channel is dashed line.	
			Aux channel S/J = -30 dB. AOTDL input power = +21.9 dBm.	
			Reference channel input power is +19.9 - 9 dBm.	
			Tap frequency of 73.5 MHz and tap power of +15 dBm.	
			Of the range of cancellations observed, this was the best.	
	57011	System CW Tone Cancellation from Radar	System CW tone cancellation performance. Pulsed jammer (500 µsec pulse at 50% duty cycle).	
			CW target. Cancelled channel is solid line. Main channel is dashed line.	
			Aux channel S/J = -30 dB. AOTDL input power = >+30 dBm.	
			Reference channel input power is +25 to +30 dBm.	
			Tap frequency of 72.81 MHz and tap power of +15 dBm.	
			Changed Antenna pointing angle from 96.72° to 94.6°	
	57012	System CW Tone Cancellation from Radar	System CW tone cancellation performance. Pulsed jammer (500 µsec pulse at 50% duty cycle).	
			CW target. Cancelled channel is solid line. Main channel is dashed line.	
			Aux channel S/J = -30 dB. AOTDL input power = +21.8 dBm.	
			Reference channel input power is +19.5 - 9 dBm.	
			Tap frequency of 72.81 MHz and tap power of +15 dBm.	
	57013	Aux Channel Signal Levels	Signal levels from the Aux channel. CW target, pulsed target	
			(500 µsec pulse at 50% duty cycle).	
			Antenna pointed at 94.6°.	
8-May	58001	System Noise Cancellation	System noise cancellation performance.	
			Tap frequency of 77.106 MHz and tap power of +19 dBm.	
			Power levels of +19.5 dBm AOTDL input, +18.1 - 9 dBm reference channel input.	
	58002	System Noise Cancellation	System noise cancellation performance.	
			Tap frequency of 77.106 MHz and tap power of +19 dBm.	
			Power levels of +19.5 dBm AOTDL input, +18.1 - 9 dBm reference channel input.	
			Video filter of HP4195A was turned on.	
	58003	System Pulsed Multipath Cancellation	System pulse multipath cancellation performance.	
			Two pulsed waveforms: 100 nsec pulsewidth, 100 nsec separation of pulse start times.	
			Tap frequencies of 75.227 MHz and 77.518 MHz. Tap powers of +16 dBm and +14.8 dBm.	
			Video filter of HP4195A was turned off.	
	58004	System Pulsed Multipath Cancellation	System pulse multipath cancellation performance.	
			Two pulsed waveforms: 50 nsec pulsewidth, 100 nsec separation of pulse start times.	
			Tap frequencies of 75.227 MHz and MHz. Tap powers of +16 dBm and + dBm.	
			Power levels of +13.5 dBm AOTDL input, +10.4 - 9 dBm reference channel input.	
			Video filter of HP4195A was turned off.	
	58005	System Pulsed Multipath Cancellation	System pulse multipath cancellation performance.	
			Two pulsed waveforms: 50 nsec pulsewidth, 100 nsec separation of pulse start times.	
			Tap frequencies of 75.227 MHz and 77.308 MHz. Tap powers of +16 dBm and +13.5 dBm.	
			Power levels of +15.5 dBm AOTDL input, +0.4 - 9 dBm reference channel input.	
	58006	System Noise Multipath Cancellation	System multipath noise cancellation performance.	

			Two noise waveforms:100 nsec separation of noise waveforms.	
			Tap frequencies of 75.227 MHz and 77.308 MHz. Tap powers of +16 dBm and +13.5 dBm.	
			Power levels of +15.5 dBm AOTDL input, +4.3 - 9 dBm reference channel input.	
	58007	System Noise Cancellation from Radar	System noise cancellation performance. CW target and noise jammer.	
			Cancelled channel is solid line. Main channel is dashed line.	
			Tap frequency of 77.106 MHz. Tap power of +15 dBm.	
			Aux channel S/J = -14 dB. AOTDL input power = +11.5 dBm.	
			Reference channel input power is +21.5 - 9 dBm.	
			Video filter of HP4195A was turned off.	
	58008	System Noise Cancellation from Radar	System noise cancellation performance. CW target and noise jammer.	
			Cancelled channel is solid line. Main channel is dashed line.	
			Tap frequency of 77.106 MHz. Tap power of +15 dBm.	
			Aux channel S/J = -14 dB. AOTDL input power = +12.5 dBm.	
			Reference channel input power is +21.4 - 9 dBm.	
			Video filter of HP4195A was turned on.	
	58009	Aux Channel from Radar	Auxilliary channel spectrum containing CW signal and noise jammer sources.	
			Video filter of HP4195A was turned on.	
9-May	59001	System Noise Cancellation from Radar	System noise cancellation performance. CW target and noise jammer.	
			Cancelled channel is solid line. Main channel is dashed line.	
			Tap frequency of 77.106 MHz. Tap power of +16 dBm.	
			Aux channel S/J = -26 dB. Main channel S/J = -30 dB. AOTDL input power = +14.4 dBm.	
			Flip Polarization: Sum channel: Signal = -55 dBm, Jammer = -22 dBm.	
			Flip Polarization: Subarray channel: Signal = -41 dBm, Jammer = -14 dBm.	
			Reference channel input power is +22.7 - 9 dBm.	
			Video filter of HP4195A was turned on.	
	59002	System Noise Cancellation from Radar	System noise cancellation performance with jammer multipath. CW target and noise jammer.	
		with Multipath	Cancelled channel is solid line. Main channel is dashed line.	
			Tap frequency of 77.106 MHz and 84.606 MHz. Tap power of +16 dBm and +14 dBm.	
			Aux channel S = -52 dBm. Main channel S = -42 dB. AOTDL input power = +19.5 dBm.	
			Original transmitter antenna polarization.	
			Reference channel input power is +18.5 - 9 dBm.	
			Video filter of HP4195A was turned on.	
	59003	Main (Subarray) Channel Input	Main (Subarray) channel input waveform to RF subsystem.	
	59004	Aux (Sum) Channel Input	Auxilliary (Sum) channel input waveform to RF subsystem.	
	59005	Main Channel Relative to Reference Channel.	Main channel and reference channel waveforms (O-Scope channels 1 and 3).	
			Estimate channel is solid line. Reference channel is dashed line.	
			All other conditions are the same.	
			Tap frequency of 77.106 MHz and 84.606 MHz. Tap power of +16 dBm and +14 dBm.	
	59006	System Noise Cancellation from Radar	System noise cancellation performance with jammer multipath. CW target and noise jammer.	
		with Multipath	Cancelled channel is solid line. Main channel is dashed line.	
			Tap frequency of 77.106 MHz and MHz. Tap power of +16 dBm and + dBm.	
			Aux channel S = - dBm. Main channel S = - dB. AOTDL input power = + dBm.	
			Original transmitter antenna polarization.	
			Reference channel input power is + - 9 dBm.	
			Video filter of HP4195A was turned on.	
			Antenna at 94.3° azimuth.	

REFERENCES

1. Berinato, R. J., M. C. Zari, M. C. Budge, and K. O. Williams, "Optimization and Testing of the Multichannel Adaptive Optical Processor," Dynetics, Inc., TR-94-RL-0020-206, February 1995.

2. Berinato, R. J., M. C. Zari, and M. C. Budge, "Alternate Optical Architectures for Multichannel Adaptive Optical Processing," Dynetics, Inc., Final Technical Report, RL-TR-93-34, April 1993.

3. Budge, M. C., R. J. Berinato, and M. C. Zari, "Acousto-Optic Applications for Multichannel Optical Processor," Dynetics, Inc., Final Technical Report, RL-TR-92-160, June 1992.

4. Zari, M. C., R. J. Berinato, M. J. Ward, and H. G. Andrews, "Multichannel Optical Time-Integrating Correlator for Adaptive Jamming Cancellation," Advances in Optical Information Processing V, SPIE Proceedings Vol. 1704, Orlando, 1992.

5. 5Lutsko, J., M. Turbyfill, E. K. Walge, and M. A. Rudd, "The Anti-Jamming Optical Beamforming System," The Rome Laboratory Technical Journal, Vol. 1, No. 2, December 1995.

6. Ward, M. J., C. W. Keefer, and S. T. Welstead, "Adaptive Optical Processor," In-house Report, RL-TR-91-270, August 1991.

7. Welstead, S. T. and M. J. Ward, "Hybrid Electro-Optic Processor," Final Technical Report, RL-TR-91-164, July 1991.

8. Welstead, S. T., "Optical Processor Evaluation," Final Technical Report, RL-TR-91-34, March 1991.

9. Ward, M. J. , C. W. Keefer, and S. T. Welstead, "Spatial Light Modulation Techniques for System Application to Multipath Delay Estimation," Applied Optics, Vol. 31, No. 20, 1992.

10. Keefer, C. W., M. E. Turbyfill, and H. G. Andrews II, "Multichannel acousto-optic correlator for time-delay computation," Proc. SPIE, Vol. 2240, April 1994.

11. Mansour, D., and A. H. Gray, Jr., "Unconstrained Frequency Domain Adaptive Filter," IEEE Trans. Acoustics, Speech, and Signal Processing, Vol. ASSP-30, No. 5, October 1982.

12. Cioffi, J. M., "The Block-Processing FTF Adaptive Algorithm," IEEE Trans. Acoustics, Speech, and Signal Processing, Vol. ASSP-34, No. 1, February 1986.

13. Shynk, J. J., "Frequency Domain and Multirate Adaptive Filtering," IEEE Signal Processing Magazine, p. 14, January 1992.

14. Keefer, C. W. and M. J. Ward, "Modified interferometric in-line time-integrating correlator," Proc. SPIE, Vol. 2026, 1993.

15. Riza, N. A., "In-line interferometric time-integrating acousto-optic correlator," Applied Optics, Vol. 33, No. 14, 1994.

16. Berinato, R. J., "Acousto-optic tapped delay line filter," Applied Optics, Vol. 32, No. 29, 1993.

17. Anderson, C. S. and M. C. Zari, "Variable Delay Lines Offer Continuously Variable Range Selection for Radar Target Simulators," Microwave Journal, April 1994.

18. Anderson, C. S. and M. C. Zari, "Design and Characterization of a Long Time Aperture Acousto-Optic Delay Line," Optical Engineering, Vol. 34, No. 1, January 1995.

*U.S. GOVERNMENT PRINTING OFFICE: 1997-509-127-47135

MISSION OF ROME LABORATORY

Mission. The mission of Rome Laboratory is to advance the science and technologies of command, control, communications and intelligence and to transition them into systems to meet customer needs. To achieve this, Rome Lab:

a. Conducts vigorous research, development and test programs in all applicable technologies;

b. Transitions technology to current and future systems to improve operational capability, readiness, and supportability;

c. Provides a full range of technical support to Air Force Material Command product centers and other Air Force organizations;

d. Promotes transfer of technology to the private sector;

e. Maintains leading edge technological expertise in the areas of surveillance, communications, command and control, intelligence, reliability science, electro-magnetic technology, photonics, signal processing, and computational science.

The thrust areas of technical competence include: Surveillance, Communications, Command and Control, Intelligence, Signal Processing, Computer Science and Technology, Electromagnetic Technology, Photonics and Reliability Sciences.